TENMAK BOREN BOR ARAŞTIRMA ENSTİTÜSÜ
TENMAK BOREN BORON RESEARCH INSTITUTE

ISSN: 2149-9020
e-ISSN: 2667-8438

BOR DERGİSİ
JOURNAL OF BORON

CİLT/VOL 08 | SAYI/ISSUE 04 | YIL/YEAR 2023

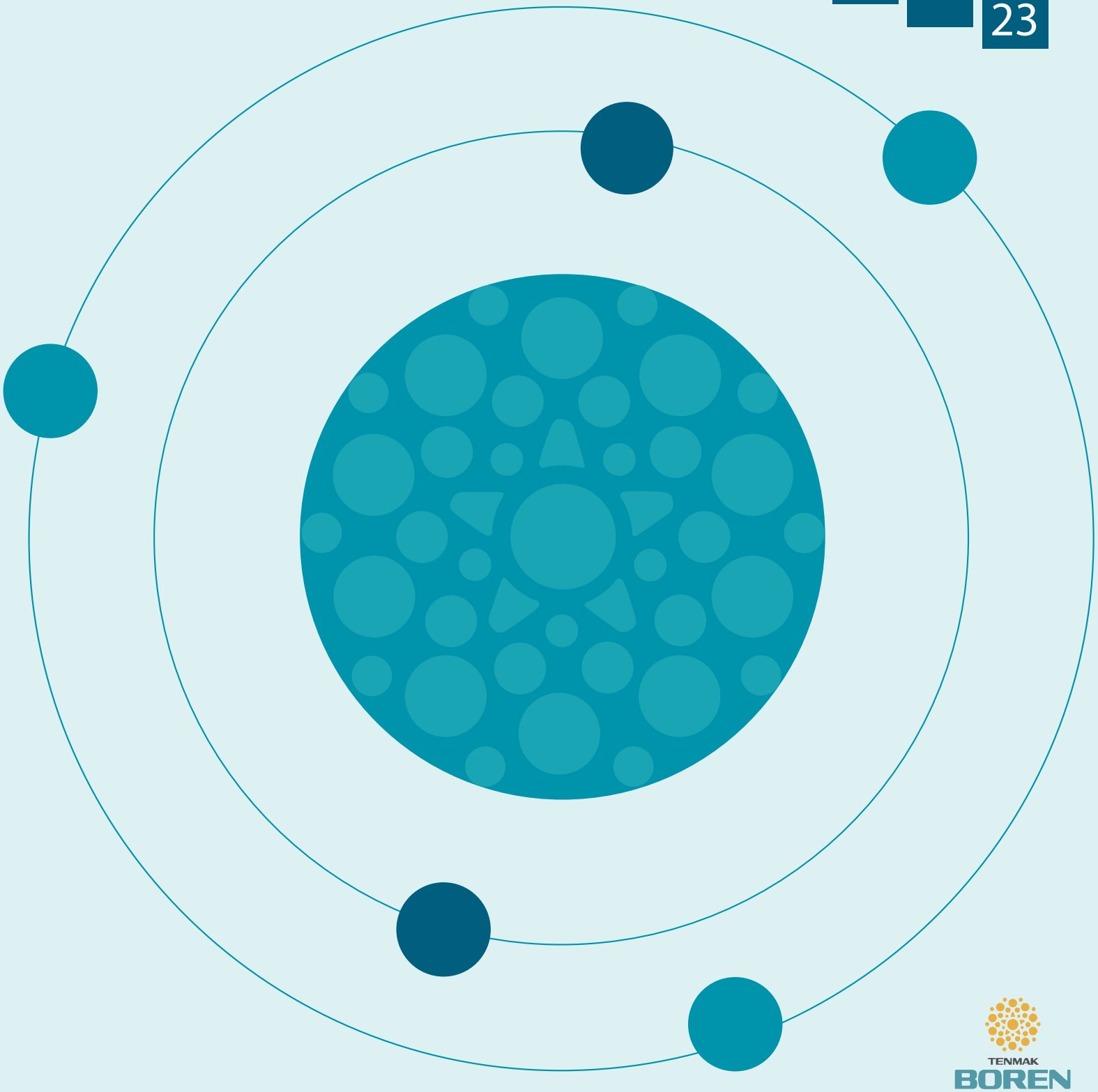

TENMAK BOREN

ISSN: 2149-9020
e-ISSN: 2667-8438

BOR DERGİSİ

JOURNAL OF BORON

CİLT VOL **08** **SAYI** ISSUE **04** **YIL** YEAR **2023**

Yayıncı/Publisher
TENMAK BOREN Bor Araştırma Enstitüsü

Yayın İdare Adresi/Adress of Publication Manager
Dumlupınar Bulvarı (Eskişehir Yolu 7. km), No:166, D Blok,
Ankara, 06530, Türkiye
Tel: (0312) 201 36 00
Fax: (0312) 219 80 55
E-posta: journalofboron@tenmak.gov.tr
Web: https://dergipark.org.tr/tr/pub/boron

Yayın Türü/Type of Publication: Yaygın süreli yayın
Yayın Aralığı/Range of Publication: 3 Aylık
Yayın Tarihi/Publication Date: 29/12/2023

Bor Dergisi uluslararası hakemli bir dergidir. Dergi, ULAKBİM TR Dizin, EBSCO ve Google Scholar tarafından indekslenmekte olup yılda dört defa yayımlanmaktadır. Derginin yazım kılavuzuna, telif hakkı devir formuna ve yayınlanan makalelere https://dergipark.org.tr/boron adresinden ulaşılabilir. / Journal of Boron is International refereed journal. Journal of Boron is indexed by ULAKBIM TR, EBSCO Indexed and Google Scholar, published quarterly a year. Please visit the Journal website https://dergipark.org.tr/boron for writing rules, copyright form and published articles.

ANKARA
ARALIK 2023 / DECEMBER 2023

TENMAK BOREN
BOR ARAŞTIRMA ENSTİTÜSÜ

BOR DERGİSİ
JOURNAL OF BORON
https://dergipark.org.tr/boron

İÇİNDEKİLER/CONTENTS

BOR DERGİSİ
JOURNAL OF BORON
https://dergipark.org.tr/boron

Borik asitin sementoblast hücrelerinde nikotin kaynaklı biyoaktivite kaybı üzerindeki etkisi

Melike Ünlütürk [1], **Abdullah Emre Hasırcı** [1], **Şerife Buket Bozkurt Polat** [2,*]

[1]*Niğde Ömer Halisdemir Üniversitesi, Tıp Fakültesi, Niğde, 51240, Türkiye*
[2]*Niğde Ömer Halisdemir Üniversitesi, Tıp Fakültesi, Tıbbi Biyokimya ABD, Niğde, 51240, Türkiye*

MAKALE BİLGİSİ

Makale Geçmişi:
İlk gönderi 19 Haziran 2023
Kabul 1 Ekim 2023
Online 29 Aralık 2023

Araştırma Makalesi

DOI: 10.30728/boron.1316579

Anahtar kelimeler:
Borik asid
Nikotin
Sementoblast

ÖZET

Borik asit (BA), dental fizyolojide mineral kompozisyonu ile ilişkili alveolar kemik yoğunluğunu etkiler ve nikotin (N) maruziyeti periodontal hastalığın patofizyolojisinde önemli bir risk faktörüdür. Bu çalışmanın amacı, BA'in sementoblast hücrelerinde N maruziyeti sonrası biyoaktivite kaybı üzerindeki etkisini araştırmaktır. Bu amaçla, sementoblast hücreleri farklı konsantrasyonlarda (10^{-1}, 10^{-2}, 10^{-3}, 10^{-4}, 10^{-5}, 10^{-6} mM) N ve 10 ng/mL konsantrasyonda BA ile muamele edilmiş ve hücre canlılığı 24 ve 72. saatlerde MTT testi ile değerlendirilmiştir. Hücrelerin yara alanına göç potansiyeli, hücre göçü yara iyileşmesi deneyi ile görüntülenmiştir. Total RNA 3, 6 ve 9. günlerde hücrelerden izole edilmiş ve mineralize doku ile ilişkili belirteçlerin gen ekspresyonu gerçek zamanlı polimeraz zincir reaksiyonu kullanılarak analiz edilmiştir. Elde edilen sonuçlar, N'in sementoblast hücrelerinin canlılığı, migrasyona dayalı yara iyileşmesi ve özellikle mineralize doku ile ilgili genlerin ekspresyonu üzerinde önemli bir etkiye sahip olduğunu göstermektedir ($p<0,01$). Ayrıca, N maruziyetinin gün bazında artmasıyla birlikte hedef gen ifade paternlerinin olumsuz etkilendiği ($p<0,01$) ve BA uygulamasının ise sementoblast hücre fonksiyonlarının korunmasında güçlü bir prevantif terapötik ajan olabileceği belirlenmiştir.

Effect of boric acid and quercetin combination on oxidative stress/cognitive function in parkinson model

ARTICLE INFO

Article History:
Received June 13, 2023
Accepted October 1, 2023
Available online December 29, 2023

Research Article

DOI: 10.30728/boron.1316579

Keywords:
Boric acid
Nicotin
Cementoblast

ABSTRACT

Boric acid (BA) affects alveolar bone density related to mineral composition in dental physiology and nicotine (N) exposure is an important risk factor in the pathophysiology of periodontal disease. The aim of this study was to investigate the effect of BA on the deprive of bioactivity in cementoblast cells after N exposure. For this purpose, cementoblast cells were treated with different concentrations (10^{-1}, 10^{-2}, 10^{-3}, 10^{-4}, 10^{-5}, 10^{-6} mM) of N and BA at a concentration of 10 ng/mL and cell viability was evaluated at 24 and 72 h by MTT assay. The migration potential of cells into the wound area was visualized by cell migration wound healing assay. Total RNA was isolated from cells on days 3, 6 and 9 and gene expression of mineralized tissue-associated markers was analyzed using real-time polymerase chain reaction. The results showed that N had a significant effect on the viability of cementoblast cells, migration-based wound healing, especially on the expression of mineralized tissue-related genes ($p<0.01$). In addition, it was determined that target gene expression patterns were negatively affected with the increase in N exposure on a daily basis ($p<0.01$), and BA application may be a powerful preventive therapeutic agent in the protection of cementoblast cell functions.

1. Giriş (Introduction)

Bor (B), kaya, toprak ve suda bulunan ve organizmada önemli fizyolojik görevler üstlenen bir elementtir [1]. Bu element doğada daha çok sodyum ve oksijenle birleşerek borik asit, boraks gibi bor tuzları halinde bulunmaktadır [2]. Çeşitli deney modelleri kullanılarak yapılan birçok araştırma sonucu, B'un yüksek yapılı organizmalar ve insanlar için önemli bir element olduğunu ortaya çıkarmıştır [3]. Özellikle B'un kemik oluşumu ve tamir mekanizmasında trabeküler ve alveoler kemik üzerinde etkin rol oynadığı belirlenmiştir [4]. Hakki ve ark. tarafından yapılan çalışma; B'un farklı konsantrasyonlarının (0, 0,1, 1, 10, 100, 1000, 2000, 4000, 8000, 10.000 ng/mL) osteoblast hücrelerinin canlılığı, proliferasyonu, mineralizasyonu ve mineralize

*Corresponding author: buketbozkurt@ohu.edu.tr

doku ilişkili genlerin ekspresyonunu farklı seviyelerde etkileyerek moleküler düzeyde kemik yapım sürecine dahil olduğunu ve bu sebeple terapötik odaklı rejeneratif tıp alanında uygulama alanı bulabileceğini göstermiştir [5]. Ayrıca B'un kemik metabolizması üzerindeki etkilerini destekleyen bir diğer çalışmada da düşük ve yüksek B içerikli diyetle beslenen tavşanların femur ve tibia analizlerininin farklı olduğu özellikle yüksek B içerikli beslenme ile femur dayanıklılığının arttığı bununla birlikte tibiada kalsiyum, magnezyum ve fosfor konsantrasyonunun yükselişine sebep olarak osteogenezi pozitif yönde desteklediği belirlenmiştir [3]. Aynı araştırma grubunun yüksek ve düşük B içerikli diyetle beslenen tavşanların diş analizleri üzerindeki sonuçları ise yüksek B alımının dişlerin yapısını, direncini, mineral yoğunluğunu etkilemezken dişlerin mineral kompozisyonunu değiştirdiği olarak raporlanmıştır [6]. Literatürde yer alan başka bir araştırmada, sıçanların diyetlerine günlük 0,1 mg/kg ve 3 mg/kg B eklenmesi sonrası 0,1 mg/kg B ile beslenen sıçanlarda kemik hacmi fraksiyonunun ve trabeküler kalınlığın azaldığı ve bununla birlikte trabeküler boşlukların da arttığı gösterilmiştir [7]. Aynı araştırmacı devam eden deneyleri sonucunda B'un, kemik metabolizmasını osteoblast ve osteoklast hücrelerinin magnezyum, potasyum, bakır ve çinko ilişkili mineraller üzerinden etkileyebileceğini ortaya koymaktadır [8,9].

Sigara dumanı içeriğinde bulunan yaklaşık 4000'den fazla kimyasal bileşik (benzen, nikotin, kotin, nitrik oksit, karbon monoksit, asetaldehit vb.) ile hem sistemik sağlık üzerinde zararlı etkilere sahip olup hem de kardiyovasküler hastalık, solunum sistemi hastalıkları ve periodontal hastalık gibi kronik enflamatuar süreçler için önemli bir risk faktörü oluşturmaktadır [10-12].

Özellikle nikotin (N) periodontal hastalık patofizyolojisinde etkili olan önemli bir bileşiktir [13-15]. Nikotin maruziyeti sonucunda konak immün cevabında T lenfosit ve B lenfosit düzeylerinde görülen azalmayla [16] birlikte oral dokunun hücrelerinde anjiyogenez, osteogenez, fibroblast proliferasyonu, adhezyon ve kollajen sentezi ile hücresel metabolizmada hasar meydana gelmektedir [17-20]. Bununla birlikte periodontal doku rejenerasyonunda önemli olan sert ve yumuşak doku iyileşmesi proseslerinde de N, negatif etki oluşturur [10,21]. İnsan gingival fibroblast hücreleri ile yapılan *in vitro* bir çalışma sonucu N'nin Rac sinyal yolağı tarafından organize edilen hücre migrasyonunu önemli seviyede hasara uğrattığını göstermiştir [22]. Ayrıca N'in insan gingival fibroblast hücrelerinin sadece migrasyonunu bozmakla kalmayıp aynı zamanda ekstraselüler matriksin yeniden şekillenmesini etkileyerek hücresel dejeneratif değişikliklere sebep olabileceği belirlenmiştir [23]. Hem cerrahi hem de klinik periodontal tedavi uygulamalarında N maruziyetinin oluşturabileceği olumsuz etkiler halen aşılması gereken önemli parametreler arasında yer almaktadır. Özellikle periodontal cerrahi uygulama sonrası yara iyileşmesi, doku rejenerasyonu bakımından kritik bir aşamadır.

Periodontal doku hasarı sonrası yara iyileşmesi sementoblast, osteoblast, periodontal ligament fibroblast hücrelerinin dâhil olduğu bir süreçtir [24]. Özellikle yürütülen periodontal tedavi prosesinde kök sement dokusunun yeniden modellenmesi, yara iyileşmesi ve rejeneratif tedavinin niteliğini belirlemesi açısından kritiktir [25]. Dişin kök kısmının formasyonu sırasında sementoblast hücreleri tarafından sentezlenen sementum dokusu, mineralize avasküler bir dokudur [26,27]. Sementum dokusu, fiziksel ve biyokimyasal özellikleri bakımından kemik doku ile benzerlik göstermektedir [26]. Dental folikül içerisinde ektomezenkim orijinli olan sementoblast hücreleri, kollajen sentezi, osteokalsin ve bonesialoprotein ekspresyonu ile periodontal dokuların idamesi/rejenerasyonu ve periodonsiyumun homeostazı bakımından önemlidir [28,29]. Daha önceki araştırmamızda farklı konsantrasyonlarda (0, 10^{-1}, 10^{-2}, 10^{-3}, 10^{-4}, 10^{-5}, 10^{-6}, 1, 2.5, 5, 10 mM) N maruziyetinin sementoblast (OCCM-30) hücrelerinin proliferasyon, migrasyon ve mineralize doku ilişkili genlerin mRNA ekspresyon düzeyleri üzerindeki etkisini değerlendirilmiştir. Araştırma sonucu, N uygulamasının sementoblast hücrelerinin proliferasyon, migrasyon ve mineralize doku belirteçleri gen ekspresyon düzeylerini negatif etkilediğini ve bu fonksiyon kaybının yeni sement dokusu oluşumu için olumsuz olabileceğini göstermiştir [30].

Bu çalışmada, sementoblast hücrelerinin, farklı konsantrasyonlarda (10^{-1}, 10^{-2}, 10^{-3}, 10^{-4}, 10^{-5}, 10^{-6} mM) N maruziyeti ile sürekli sigara kullanan bir bireyin tükürük ve kan seviyelerindeki N miktarı üzerinden *in vitro* koşullarda deney modeli oluşturulmuştur. Oluşturulan bu deney modeli üzerine 10 ng/mL BA uygulanarak sementoblast hücrelerinin canlılığı, hücrelerinin yara alanına migrasyon potansiyelleri ile mineralize doku ilişkili gen [Bonesialoprotein (BSP), Osteopontin (OPN), Osteocalcin (OCN), Alkaline phosphatase (ALP), Osteoprotegerin (OPG), Runt Related Transcription Factor 2 (Runx2), tip I kollajen (COL-I)] mRNA ekspresyonları üzerine etkisi belirlenmiştir.

2. Malzemeler ve Yöntemler (Materials and Methods)

2.1. Sementoblast Hücreleri (Cementoblast Cells)

Deneylerde kullanılan 18. pasaj fare sementoblast (OCCM-30) hücreleri 100 mm^2'lik 2 adet hücre kültürü kabı içerisinde %10 fetal sığır serumu (FBS) içeren hücre kültürü vasatı (Dulbecco's Modified Minimal Essential Medium (DMEM)) ile çözülerek %5 CO_2'li inkübatöre yerleştirildi. Ertesi gün inverted hücre kültürü mikroskobu altında incelenen hücrelerin kabın tabanına yapıştıkları ve mitoz bölünmeyle sayılarını artırmaya başladıkları gözlendi. Gün aşırı hücrelerin ortamları %10 FBS içeren DMEM ile değiştirilerek yeterli sayıya ulaşmaları beklendi. Yeterli sayıya ulaşan ve morfolojik olarak sağlıklı görünen OCCM-30'lar tripsin enzimiyle kabın tabanından ve birbirlerinden ayrılmaları sağlanarak 4 adet 100 mm^2'lik hücre kültürü kabına pasajlandı. Sementoblastlar, prolifere olup

kabın tabanını tamamen kaplamasıyla deneylerde kullanıma hazır hale geldiler [31].

2.2. Borik Asit Deney Konsantrasyonlarının Hazırlanması (Preparation of Boric Acid Experiment Concentrations)

Borik asit (H_3BO_3, Merck, Darmstadt, Germany) stok solüsyonu (10.000 µg/mL) distile su ile hazırlandıktan sonra biyogüvenlik kabini içerisinde 0,20 µm'lik filtreden geçirilerek steril hale getirildi. Sonrasında bu stok solüsyondan seri dilüsyonlarla 1000 µg/mL, 100 µg/mL, 10 µg/mL ve ideal stok konsantrasyon olan 1 µg/mL'ye ulaşıldı. Daha önceki deneylerimizde osteoblast (MC3T3-E1) hücrelerinin mineralize-doku ilişkili gen ekspresyon düzeylerini artıran 10 ng/mL etkin dozu [5] her deney uygulaması öncesinde olmak şartıyla 1 µg/mL borik asit konsantrasyonundan %5 FBS içeren DMEM içerisinde çalışma konsantrasyonu olarak hazırlandı.

2.3. Nikotin Deney Konsantrasyonlarının Hazırlanması (Preparation of Nicotine Experiment Concentrations)

Literatürde yer alan araştırma sonuçları, sigara içen bireylerin tükürükteki nikotin konsantrasyonunu 1-9 mM [32] ve kan değerlerini ise 0,06-1,2 mM [33] konsantrasyon olarak belirtmiştir. Daha önceki çalışmamızda sementoblast hücrelerine 10^{-1}, 10^{-2}, 10^{-3}, 10^{-4}, 10^{-5}, 10^{-6} , 1, 2,5, 5 ve 10 mM nikotin uygulaması sonrasında 1 mM üzerindeki konsantrasyonlarda (1, 2,5, 5, 10 mM) hücre proliferasyonu, mineralizasyonu ve mineralize doku belirteçleri gen ekspresyonlarında önemli seviyelerde azalmaya sebep olduğu tespit edildi [30]. Bu çalışmada sementoblast hücrelerine 1 mM'dan daha düşük olan 10^{-6}, 10^{-5}, 10^{-4}, 10^{-3}, 10^{-2}, 10^{-1} mM nikotin konsantrasyonları kullanıldı. Bu amaçla ticari olarak satın alınan nikotin (Merck, Darmstadt, Germany) solüsyonundan %5 FBS içeren DMEM kullanılarak her bir deney uygulaması öncesinde hazırlanmak kaydıyla 10^{-6}, 10^{-5}, 10^{-4}, 10^{-3}, 10^{-2}, 10^{-1} mM N konsantrasyonları elde edildi.

2.4. Hücre Canlılık Deneyi (Cell Viability Assay)

Borik asit ve farklı konsantrasyonlarda N uygulamasının, sementoblast hücrelerinin canlılığı üzerindeki etkisi hücrelerin tetrazolium tuzunu, formazan boyasına dönüştürebilmesine dayalı olarak yapılan 3-(4,5-Dimethylthiazol-2-yl)-2,5-Diphenyltetrazolium Bromide (MTT) analizi ile 24 ve 72. saatlerde değerlendirildi. Hücreler 96 kuyulu hücre kültürü kapları içerisine $2x10^4$ hücre/cm^2 olacak şekilde inkübe edildikten 24 saat sonra her bir kuyu üzerine 10^{-1}, 10^{-2}, 10^{-3}, 10^{-4}, 10^{-5}, 10^{-6} mM konsantrasyonda N ve 10 ng/mL konsantrasyonda BA %5 FBS içeren DMEM içerisinde aynı anda uygulandı (n=8). Bu işlemi takip eden 24. saatte sementoblast hücrelerinin canlılığının tespit edebilmek için hücre kültürü kabının kuyularındaki 10^{-1}, 10^{-2}, 10^{-3}, 10^{-4}, 10^{-5}, 10^{-6} mM konsantrasyonda N ve 10 ng/mL konsantrasyonda BA içeren %5 FBS içeren DMEM aspire edilip hücrelerin fosfat tampon çözeltisi (PBS) ile yıkanması sonrasında her bir kuyuya hazırlanan MTT solüsyonundan 200 µL (0,55 mg/mL MTT) eklendi. Devamında hücre kültür kabı alüminyum folyoya sarılarak sonraki 2 saat için tekrar inkübatöre yerleştirildi. 96 kuyulu hücre kültür kabının 2 saatlik MTT inkübasyonundan sonra, MTT içeren kültür ortamı çıkarılarak her bir kuyu 200 µL PBS ile yıkanıp bu işlem iki kez tekrar edildi. Devamında kuyulardan PBS'in uzaklaştırılmasının ardından petri kabı kurulanarak, her bir kuyuya 200 µL dimetil sülfoksit eklenip çözünen formazon'ın analizi için kültür kabı 30 dakika oda sıcaklığında çalkalanıp ve absorbansı 450 nm'de spektrofotometrede okundu. Hazırlanmış olan ikinci 96 kuyulu deney kabı inkübatörde bekletilerek deneyin 2. zaman periyodu olan 72. saatin sonunda da aynı işlemler uygulanarak tekrarlandı.

2.5. Hücre Migrasyonu: Yara İyileşmesi Modeli (Cell Migration: A Wound Healing Model)

Hücre migrasyonu: yara iyileşmesi deneyi, 60 mm'lik hücre kültürü kaplarında yapıldı. Her bir petri kabı içerisine 5x104 sementoblast hücresi 4 mL %10 FBS içeren DMEM içerisinde eklenip 24 saat inkübe edildi. Hücre yoğunluğu %90 üzerine ulaştıktan sonra 1000 µL steril pipet ucu kullanılarak vertikal yara alanı oluşturuldu. Her bir petri kabında başlangıçta oluşturulan yara alanı tersmikroskop altında fotoğraflanıp deneyin başlangıç saati (0. saat) olarak kabul edildi. Daha sonra sementoblast hücrelerine sadece 10^{-1}, 10^{-2}, 10^{-3}, 10^{-4} mM N konsantrasyonları, sadece BA konsantrasyonu (10 ng/mL), N ve BA konsantrasyonlarını birlikte (BA+10^{-1}, BA+10^{-2}, BA+10^{-3}, BA+10^{-4}) içeren %5 FBS içeren DMEM uygulamaları yapılıp ters mikroskop altında 0, 2, 4, 6 ve 24. saatlerde fotoğrafları çekildi.

2.6. mRNA Ekspresyon Deneyleri (mRNA Expression Assays)

2.6.1. Sementoblast hücrelerinden RNA izolasyonu (RNA ısolation from cementoblast cells)

Sementoblast hücrelerinin, sadece N konsantrasyonları (10^{-1}, 10^{-2}, 10^{-3}, 10^{-4} mM), sadece BA (10 ng/mL) ile BA ve N konsantrasyonlarının birlikte (BA+10^{-1}, BA+10^{-2}, BA+10^{-3}, BA+10^{-4} N) uygulaması sonrasında mineralize doku belirteçleri (BSP, OPN, OCN, ALP, OPG, Runx2, COLI) mRNA ekspresyon düzeylerini belirlemek için deneyin 3, 6 ve 9. günlerinde total RNA izolasyonları gerçekleştirildi. Bu amaçla tasarlanan deney modeli kullanılarak sementoblast hücreleri 25.000/cm^2 olacak şekilde 60 mm'lik hücre kültür kaplarına dağıtılıp %10 FBS içeren DMEM ile 24 saat inkübe edildi. Devamında hücreler sadece N konsantrasyonları (10^{-1}, 10^{-2}, 10^{-3}, 10^{-4} mM), sadece BA (10 ng/mL), BA ve N konsantrasyonlarının birlikte (BA+10^{-1}, BA+10^{-2}, BA+10^{-3}, BA+10^{-4} N) içeren %5 FBS içeren DMEM ile muamele edilip deneyin 3, 6 ve 9. günlerinde total RNA izolasyonu yapıldı. Bu deney kapsamında RNA izolasyonları için hücreler üzerindeki

Tablo 1. mRNA ekspresyonları incelenen primerler (Primers analysed for mRNA expression).

Primerler	Forward (5'-3')	Reverse (3'-5')
BSP	GAGACGGCGATAGTTCC	AGTGCCGCTAACTCAA
OPN	TTTACAGCCTGCACCC	CTAGCAGTGACGGTCT
OCN	TGAACAGACTCCGGCG	GATACCGTAGATGCGTTTG
ALP	ATTGCCCTGAAACTCCAAAACC	CCTCTGGTGGCATCTCGTTATC
OPG	CCGTTTTATCCTCTCTACACT	TCAGAAAGGAAATGCAACACA
RunX2	CTTCATTCGCCTCACAAAC	GTCACTGCGCTGAAGA
COLI	GCAACATTGGATTCCCTGGACC	GTTCACCCTTTTCTCCCTTGCC
GAPDH	TGCACCACCAACTGCTTAG	GATGCAGGGATGATGTTCTG

sadece N konsantrasyonları (10^{-1}, 10^{-2}, 10^{-3}, 10^{-4} mM), sadece BA (10 ng/mL), BA ve N konsantrasyonlarının birlikte (BA+10^{-1}, BA+10^{-2}, BA+10^{-3}, BA+10^{-4} N) içeren %5 FBS içeren DMEM aspire edilip hücreler PBS ile yıkanması sonrasında kullanılan RNA izolasyon kitinin (In vitrogen, Camarillo, CA) bileşenlerinden EZ-RNA A solüsyonu 500 µL olarak ilave edilip hücre zarlarının parçalanıp nükleik asitlerin açığa çıkması sağlandı. Bu işlem sonrasında hücre lizatları toplanarak üzerine izolasyon kitinin diğer bileşeni olan EZ-RNA B solusyonundan 500 µL ilave edilip hücre-lizat karışımı 4°C 12.000 rpm'de 15 dakika santrifüj edildi. Böylece tüpler içerisindeki karışımın protein-DNA-RNA fazlarına ayrılması sağlanıp RNA fazı başka bir tüpe aktarılıp üzerine 500 µL izopropanol ilavesi yapıldı. Devamında örneklerin yeniden 4°C 12.000 rpm'de 15 dakika santrifüj edilmesiyle RNA peletleri elde edilip RT-PCR deneyleri yapılıncaya kadar -80°C'de saklandı.

2.6.2. RNA örneklerinin absorbanslarının ölçülmesi (Measuring the absorbance of RNA samples)

Elde edilen total RNA örnekleri muhafaza edildikleri -80°C'den çıkarıldıktan sonra 4°C 12000 rpm'de 15 dakika santrifüj edilip dipteki RNA peletleri hareket ettirilmeden etanol (EtOH)-dietil pirokarbonat (DEPC)-distile su(dH_2O) karışımı pipetör ile toplandı. Örneklerin ağzı açık bırakılarak içlerindeki alkol karışımın tamamen uçması sağlandı. Sonrasında RNA peletlerinin bulunduğu tüpler kapakları açık olarak 65°C'de 5 dakika ısıtma işlemine tabi tutuldu. Bu işlemin ardından RNA peletleri 25 µL DEPC dH_2O karışımında çözülerek ısıtıcı blok cihazında 5 dakika ısıyla muamele edildi ve DEPC-dH_2O'da homojenize edilen RNA örneklerinin 1 µL'si spektrofotometrede 260 nm'de okunarak her bir gruptan elde edilen total RNA miktarları ve saflık oranları belirlendi.

2.6.3. Tamamlayıcı DNA sentezi (Complementary DNA (cDNA) synthesis)

Tamamlayıcı DNA sentezi, cDNA sentez kitinin (RevertAid First Strand cDNA Synthesis Kit, Thermo Scientific, USA) protokolüne uygun olarak gerçekleştirildi. RNA örneklerinin her birinden, içerisinde 1 µg RNA bulunacak miktar, 1 µl 20XRT Enzym Mix, 10 µl 2XRT Buffer Solution ve dH_2O eklenerek reaksiyon hacmi 20 µl'ye tamamlandı. Örnekler, Polymerase chain reaction (PCR) cihazında 37°C'de 60 dakika, 95°C'de 50 dakika ve 4°C'de inkübe edilip, işlem sonunda elde edilen cDNA'lar RT-PCR deneylerinde kullanılacakları zamana kadar -20°C'de muhafaza edildi.

2.6.4. RT-PCR deneyleri (RT-PCR experiments)

Sementoblast hücrelerinin sadece N konsantrasyonları (10^{-1}, 10^{-2}, 10^{-3}, 10^{-4} mM), sadece BA (10 ng/mL) ile BA ve N konsantrasyonlarının birlikte (BA+10^{-1}, BA+10^{-2}, BA+10^{-3}, BA+10^{-4} N) uygulaması sonrasında mineralize doku belirteçleri (BSP, OPN, OCN, ALP, OPG, Runx2, COLI) genlerinin ifade düzeyleri RT-PCR ile belirlendi (Tablo 1). Normalizasyon amacı ile GAPDH kontrol geni kullanıldı. mRNA ekspresyonları Maxima SYBR Green/ROX qPCR Master Mix (Maxima SYBR Green qPCR Master Mix (2X), Thermo Scientific) ile çalışıldı. Mineralize doku belirteçleri olan BSP, OCN, ALP, COL-I, RunX2 ve GAPDH için BIORAD-CFX Connect cihazı ile 94/180; 94/45, 55/45, 95/54, 55/30 ve 95/30 °C)/sn, amplifikasyon protokolü kullanılarak 35-40 siklus aralığında döngü gerçekleştirildi. Bununla birlikte OPG ve GAPDH içinse 94/180; 94/45, 57/45; 95/60, 55/30 ve 95/30 °C)/sn amplifikasyon protokolü BIORAD-CFX Connect cihazı ile 35-40 döngü olarak yapıldı.

2.7. İstatistiksel analiz (Statistical analysis)

Hücre canlılığının tespit edilmesi için yapılan MTT deney sonuçlarının analizinde günler/saatler arasında farklılık olup olmadığı tek yönlü varyans analizi (ANOVA) ile değerlendirildi. Aritmetik ortalama ve standart sapmalar alınmıştır. Yapılan değerlendirme sonucunda aynı gün/saat içerisinde gruplar arasındaki değişiklik Tukey HSD Testi ile analiz edildi. Real-time PCR ile elde edilen sonuçların değerlendirmesinde karşılaştırmalı Ct yöntemi kullanıldı [34-36]. Normalize edilmiş ekspresyon değerleri tek yönlü varyans analizi yapılarak karşılaştırılacak ve gruplardaki gen ekspresyonunun GAPDH'e göre artış ya da azalışları α=0,05 önem seviyesine göre gösterildi.

3. Sonuçlar ve Tartışma (Results and Discussion)

3.1. Sonuçlar (Results)

3.1.1. Hücre canlılık deney sonucu (Cell viability experiment result)

Sementoblastların farklı konsantrasyonlarda N (10^{-1}, 10^{-2}, 10^{-3}, 10^{-4}, 10^{-5}, 10^{-6} mM) ve BA (10 ng/mL) uygulanması sonrası hücre canlılık oranları 24. ve 72. saatlerde MTT deneyi ile belirlenerek aritmetik ortalama ve standart sapmaları alınmıştır. Elde edilen sonuçlara göre; sadece N (10^{-1}, 10^{-2}, 10^{-3}, 10^{-4}, 10^{-5}, 10^{-6} mM) uygulanan hücre gruplarında kontrol grubuna kıyasla 24 ve 72. saatlerde doza bağımlı olarak hücre canlılığında istatistiksel olarak anlamlı bir azalma tespit edildi ($p<0,01$) (Şekil 1). Bununla birlikte sadece BA (10 ng/mL) uygulanan grubun hem 24 hem de 72. saatte elde edilen hücre canlılık değerlerinin kontrol grubu ile aynı olduğu belirlendi ($p>0,05$). Farklı N (10^{-1}, 10^{-2}, 10^{-3}, 10^{-4}, 10^{-5}, 10^{-6} mM) konsantrasyonlarının BA (10 ng/mL) ile birlikte uygulandığı deney gruplarında ise hücre canlılığı kontrol grubuna göre 24 ve 72. saatlerde istatistiksel olarak anlamlı düzeyde az olmakla birlikte bu değerin sadece N uygulanan gruplara göre hücre canlılığı bakımından istatistiksel olarak daha fazla olduğu tespit edildi $p<0,05$).

3.1.2. Hücre migrasyonu: yara iyileşmesi modeli (Cell migration: a wound healing model)

Hücre migrasyonu: yara iyileşmesi deneyi, 60 mm'lik hücre kültürü kaplarında yapıldı. Her bir petri kabı içerisine $5x10^4$ sementoblast hücresi 4 mL %10 FBS içeren DMEM içerisinde eklenip 24 saat inkübe edildi. Hücre yoğunluğu %90 üzerine ulaştıktan sonra 1000 µL steril pipet ucu kullanılarak vertikal yara alanı oluşturuldu. Her bir petri kabında başlangıçta oluşturulan yara alanı ters mikroskop altında fotoğraflanıp deneyin başlangıç saati (0. saat) olarak kabul edildi. Daha sonra sementoblast hücrelerine sadece 10^{-1}, 10^{-2}, 10^{-3}, 10^{-4} mM N konsantrasyonları, sadece BA konsantrasyonu (10 ng/mL), N ve BA konsantrasyonlarını birlikte (BA+10^{-1}, BA+10^{-2}, BA+10^{-3}, BA+10^{-4}) içeren %5 FBS içeren DMEM uygulamaları yapılıp ters mikroskop altında 0, 2, 4, 6 ve 24. saatlerde fotoğrafları çekildi (Şekil 2 a,c). Hücrelerin yara alanına migrasyon potansiyelleri ImageJ programı kullanılarak değerlendirilerek aritmetik ortalama ve standart sapmaları alınmıştır (Şekil 2 b,d). Yara iyileşmesi deneyi sonuçlarına göre tüm N konsantrasyonları (10^{-1}, 10^{-2}, 10^{-3}, 10^{-4} mM) kontrol grubuna göre tüm zaman dilimlerinde (2, 4, 6 ve 24 saat) istatistiksel olarak anlamlı seviyede hücrelerin migrasyon potansiyellerini azalttı ($p<0,05$) (Şekil 2 a,b). Bununla birlikte bu azalmanın 10^{-3} ve 10^{-4} mM N konsantrasyonlarında 10^{-1} ve 10^{-2} mM N konsantrasyonlarına göre kontrol grubuna kıyasla 2, 4 ve 6. saatlerde istatistiksel olarak daha az olduğu belirlendi ($p<0,05$). Devamında N grupları arasındaki bu farklılık 24. saatte eşitlendi ($p<0,05$) (Şekil 2 a,b). Sadece BA (10 ng/mL) uygulanan grup ise sementoblastların migrasyon kapasitesini deneyin 4, 6 ve 24. saatinde kontrol grubuna göre anlamlı seviyede artırdı ($p<0,05$) (Şekil 2 c,d). Ayrıca N konsantrasyonları ile birlikte BA uygulanan gruplar (BA+10^{-1}, BA+10^{-2}, BA+10^{-3}, BA+10^{-4} N) hücrelerin migrasyon süreçlerini kontrol grubuna göre istatistiksel olarak anlamlı seviyede 2, 4, 6 ve 24. saatlerde azaltmış olmalarına rağmen bu etki sadece N uygulanan gruplara göre daha az olarak tespit edildi ($p<0,05$) (Şekil 2 c,d). Bu sonuçlar BA'in, sementoblastların N maruziyeti sonrasında azalan migrasyonuna zaman bağımlı olarak pozitif yönde desteklediğini ortaya koydu.

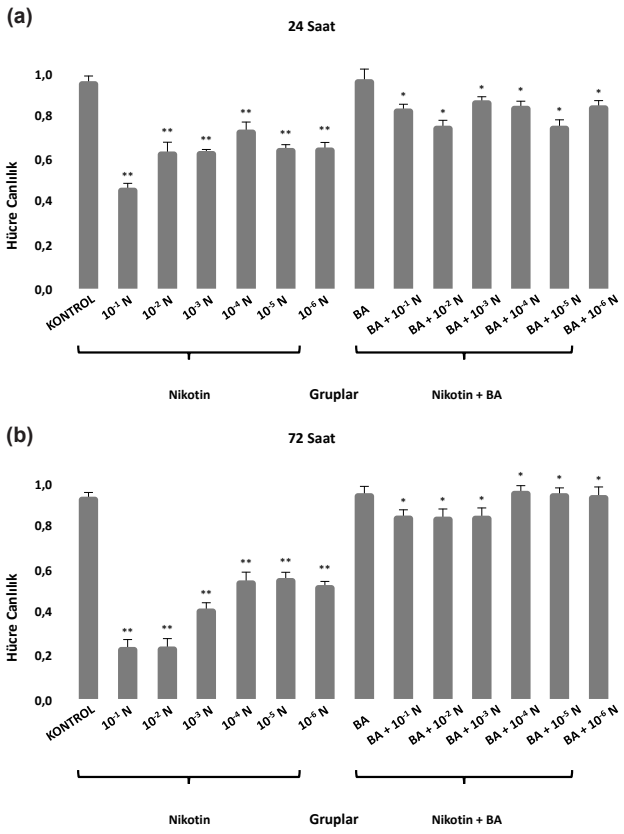

Şekil 1. BA'in N ile indüklenen sementoblast hücre canlılığı üzerindeki etkisi. Sementoblast hücrelerinin canlılığı sadece N konsantrasyonları (10^{-1}, 10^{-2}, 10^{-3}, 10^{-4}, 10^{-5}, 10^{-6} mM), sadece BA (10 ng/mL) ile BA ve N konsantrasyonlarının birlikte (BA+10^{-1} N, BA+10^{-2} N, BA+10^{-3} N, BA+10^{-4} N, BA+10^{-5} N, BA+10^{-6} N) uygulanması sonucunda 24 saat sonuçları a). Sementoblast hücrelerinin canlılığı sadece N konsantrasyonları (10^{-1}, 10^{-2}, 10^{-3}, 10^{-4}, 10^{-5}, 10^{-6} mM), sadece BA (10 ng/mL) ile BA ve N konsantrasyonlarının birlikte (BA+10^{-1} N, BA+10^{-2} N, BA+10^{-3} N, BA+10^{-4} N, BA+10^{-5} N, BA+10^{-6} N) uygulanması sonucunda 72 saat sonuçları b). *p<0,05, **p<0,001. (Effect of BA on N-induced cementoblast cell viability. The viability of cementoblast cells only at N concentrations (10^{-1}, 10^{-2}, 10^{-3}, 10^{-4}, 10^{-5}, 10^{-6} mM), only BA (10 ng/mL) with BA and N concentrations together (BA+10^{-1} N, BA+10^{-2} N, BA+10^{-3} N, BA+10^{-4} N, BA+10^{-5} N, BA+10^{-6} N) results after 24 hours of application a). the viability of cementoblast cells only at N concentrations (10^{-1}, 10^{-2}, 10^{-3}, 10^{-4}, 10^{-5}, 10^{-6} mM), only BA (10 ng/mL) and N concentrations together (BA+10^{-1} N, BA+10^{-2} N, BA+10^{-3} N, BA+10^{-4} N, BA+10^{-5} N, BA+10^{-6} N) results after 72 hours of application b). *p<0.05, **p<0.001).

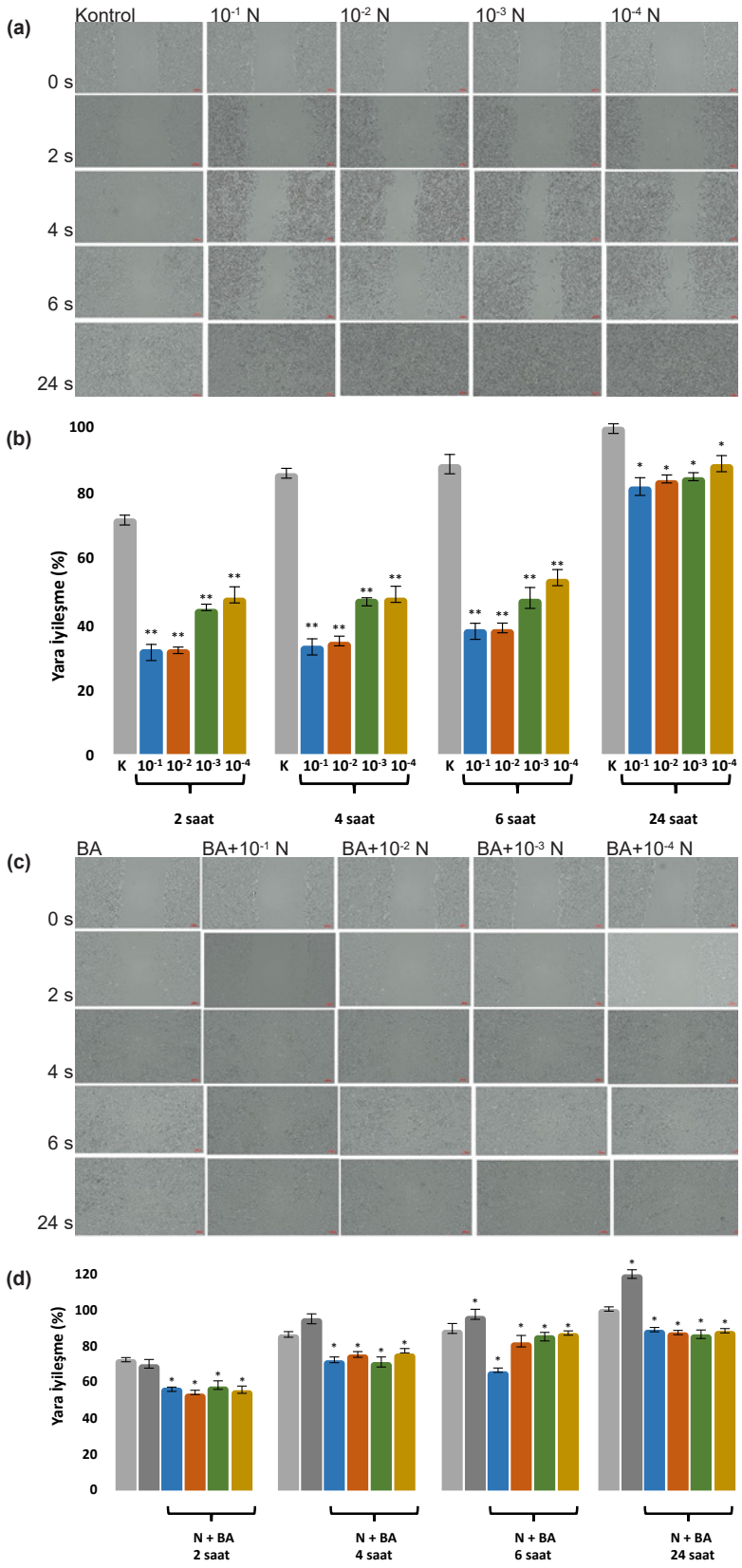

Şekil 2. Sementoblast hücrelerine N uygulaması sonrası migrasyon potansiyelinin BA ile module edilmesi. Sementoblast hücreleri kontrol (sadece DMEM), sadece N konsantrasyonları (10^{-1}, 10^{-2}, 10^{-3}, 10^{-4} mM), sadece BA (10 ng/mL) ile BA ve N konsantrasyonlarının birlikte (BA+10^{-1} N, BA+10^{-2} N, BA+10^{-3} N, BA+10^{-4} N) uygulanması sonucunda migrasyon potansiyelleri belirlendi (0, 2, 4, 6, 24 saat) a,c). Yara kapanma oranının belirlenmesi b,d). *p<0,05; **p<0,01. (Modulation of migration potential by BA after N treatment of cementoblast cells. Migration potentials were determined (0, 2, 4, 6, 24 h) after treatment of cementoblast cells with control (DMEM only), N concentrations only (10^{-1}, 10^{-2}, 10^{-3}, 10^{-4} mM), BA only (10 ng/mL) and BA and N concentrations together (BA+10^{-1} N, BA+10^{-2} N, BA+10^{-3} N, BA+10^{-4} N) a,c). Determination of wound closure rate b,d). *p<0.05, **p<0.01).

3.1.3. Borik asit nikotin ile indüklenen sementoblastlarda mineralize dokuyla ilişkili belirteçleri düzenler (Boric acid regulates markers associated with mineralized tissue in nicotine-ınduced cementoblasts)

Real-time PCR deney sonuçlarının aritmetik ortalama ve standart sapmaları alınmış ve buna göre BSP ifadesi sadece N konsantrasyonları (10^{-1}, 10^{-2}, 10^{-3}, 10^{-4} mM) uygulanan sementoblast hücrelerinde doza ve zamana bağlı şekilde kontrol grubuna kıyasla istatistiksel olarak anlamlı şekilde azaldı ($p<0,01$). Bununla birlikte sadece BA (10 ng/mL) uygulaması sonrası ise en fazla deneyin 6. gününde olmak üzere BSP mRNA ifadesi kontrol grubuna göre istatistiksel olarak anlamlı seviyede arttı ($p<0,01$). Ayrıca BA ve N konsantrasyonlarının birlikte (BA+10^{-1}, BA+10^{-2}, BA+10^{-3}, BA+10^{-4} N) uygulandığı gruplarda ise BSP ifadesi kontrol grubuna göre düşük olmakla birlikte sadece N konsantrasyonlarına göre bu düşüklüğün istatistiksel olarak anlamlı seviyede daha az olduğu tespit edildi ($p<0,05$) (Şekil 3a). OPN ifadesi de benzer bir grafik sergilemekle birlikte sadece BA (10 ng/mL) uygulamasının zaman bağlı olarak kontrol grubuna göre istatistiksel olarak anlamlı seviyede arttığı belirlendi ($p<0,01$). Aynı zamanda, BA ve N konsantrasyonlarının birlikte (BA+10^{-1}, BA+10^{-2}, BA+10^{-3}, BA+10^{-4} N) uygulanmasının da hücrelerin OPN ifadelerinin tek başına aynı N konsantrasyonlarına (10^{-1}, 10^{-2}, 10^{-3}, 10^{-4} mM) göre kontrol grubuna göre istatistiksel olarak daha az baskıladığını gösterdi ($p<0,05$) (Şekil 3b). COL-I mRNA ifadesi sadece N konsantrasyonları (10^{-1}, 10^{-2}, 10^{-3}, 10^{-4} mM) uygulaması sonrasında deneyin 3, 6 ve 9. günlerinde kontrol grubuna göre istatistiksel olarak anlamlı seviyede azaldı ($p<0,01$). Sadece BA (10 ng/mL) uygulaması ise sementoblastların COL-I ifadesini kontrol grubuna kıyasla istatistiksel olarak anlamlı seviyede zamana bağlı olarak artırdı ($p<0,01$). Özellikle BA ve N konsantrasyonlarının birlikte (BA+10^{-1}, BA+10^{-2}, BA+10^{-3}, BA+10^{-4} N) uygulandığı gruplarda, BA'in sadece N maruziyeti sonrası oluşan COL-I ifade eksikliğini kontrol grubuna göre istatistiksel olarak anlamlı seviyede artırdığı bu durumun deneyin 6. gününden itibaren olmak üzere 9. günde daha belirgin olduğu tespit edildi ($p<0,01$) (Şekil 3c). OCN mRNA ifadesi de sadece N konsantrasyonları (10^{-1}, 10^{-2}, 10^{-3}, 10^{-4} mM) uygulamasından zamana ve doza bağlı olarak kontrol grubuna göre istatistiksel olarak anlamlı seviyede azalma yönünde etkilendi ($p<0,01$). Sadece BA (10 ng/mL) uygulaması hücrelerde OCN mRNA ifadesini kontrol grubuna göre anlamlı seviyede artırmakla birlikte deneyin 9. gününde BA ve N konsantrasyonlarının birlikte (BA+10^{-1}, BA+10^{-2}, BA+10^{-3}, BA+10^{-4} N) uygulamasının da sementoblastlarda OCN ifadesini sadece BA ile aynı seviyede istatistiksel olarak anlamlı seviyede artırdığını gösterdi ($p<0,01$) (Şekil 3d). ALP mRNA ifadesi sadece N konsantrasyonları (10^{-1}, 10^{-2}, 10^{-3}, 10^{-4} mM) uyarısı sonrasında kontrol grubuna göre istatistiksel olarak anlamlı seviyede azaldı ($p<0,01$). Sadece BA (10 ng/mL) uygulamasının kontrol grubuna göre ALP ifadesini istatistiksel olarak anlamlı seviyede artırdığı bununla birlikte BA ve N konsantrasyonlarının birlikte (BA+10^{-1}, BA+10^{-2}, BA+10^{-3}, BA+10^{-4} N) hücrelere uygulanmasının da aynı N konsantrasyonları maruziyetine göre ALP ifadesini kontrol grubuna göre istatistiksel olarak anlamlı seviyede daha az azalttığı belirlendi ($p<0,05$) (Şekil 3e). OPG ifadesi ise sadece N konsantrasyonları (10^{-1}, 10^{-2}, 10^{-3}, 10^{-4} mM) sonrasında kontrol grubuna göre istatistiksel olarak anlamlı seviyede azalırken ($p<0,01$), sadece BA (10 ng/mL) uygulaması ise kontrol grubuna göre zamana bağımlı şekilde OPG ifadesini istatistiksel olarak anlamlı seviyede artırdı ($p<0,01$) (Şekil 3f). Bununla birlikte BA ve N konsantrasyonlarının birlikte (BA+10^{-1}, BA+10^{-2}, BA+10^{-3}, BA+10^{-4} N) hücrelere uygulanması sonrasında OPG ifade düzeyleri deneyin 3 ve 6. günlerinde sadece BA (10 ng/mL) uygulanan grupla yakın seviyelere ulaşmakla birlikte deneyin 9. gününde BA ve N konsantrasyonlarının birlikte (BA+10^{-1}, BA+10^{-2}, BA+10^{-3}, BA+10^{-4} N) uygulanmasının OPG düzeyini daha az ifade ettiğini gösterdi ($p<0,01$) (Şekil 3f). RunX2 düzeyi de sadece N konsantrasyonları (10^{-1}, 10^{-2}, 10^{-3}, 10^{-4} mM) sonrasında kontrol grubuna göre istatistiksel olarak anlamlı seviyede azalırken ($p<0,01$), bu durum hem sadece BA (10 ng/mL) hem de BA ve N konsantrasyonlarının birlikte (BA+10^{-1}, BA+10^{-2}, BA+10^{-3}, BA+10^{-4} N) uygulanması sonrasında kontrol grubuna göre istatistiksel olarak anlamlı seviyede artış olarak tespit edilmiştir ($p<0,01$) (Şekil 3g).

3.2. Tartışma (Discussion)

Periodonsiyumun nikotin ile olan direkt teması sonucunda hücre proliferasyonu, konak cevabı ve immün sistem etkilenerek periodontal hastalık patogenezine yatkın hale gelmektedir [37-39]. Dişin sement dokusunun ana hücreleri olan sementoblastlar, kök yapısının yeniden şekillenmesi, periodontal rejenerasyon ve sağlıklı periodonsiyum için kritik öneme sahip olup fizyolojik olarak eksprese ettikleri ALP, BSP, OCN, COL-I, OPN gibi mineralize doku belirteçlerinin N maruziyeti sonrasında önemli derecede azaldığı bilinmektedir [30,40,41]. Bununla birlikte BA'in ise osteoblast hücrelerinin kemik morfogenetik protein (BMP)-4, BMP-6, BMP-7 düzeyleri ile BSP, OPN, OCN, COL-I mRNA ekspresyon seviyelerini önemli düzeyde artırdığı böylece kemik yapısının direnci ve mineral kompozisyonu ile dişin mineral içeriği yanında alveoler kemik yoğunluğunun farklılaşmasına da olumlu katkı sağladığı belirlendi [3,5,6]. Bu çalışmada BA'in, sementoblast hücrelerinde N maruziyeti sonrası biyoaktivite kaybı üzerindeki etkisini sementoblast hücrelerinin canlılığı, migrasyon: yara iyileşmesi, mineralize doku belirteçlerinin mRNA ifade düzeyleri üzerinden değerlendirildi. MTT analiz sonuçları deneyin her iki zaman periyodunda da sadece N konsantrasyonları (10^{-1}, 10^{-2}, 10^{-3}, 10^{-4}, 10^{-5}, 10^{-6} mM) uygulanan gruplarda hücre canlılığının kontrol grubuna (sadece DMEM) göre istatistiksel olarak anlamlı seviyede azaldığını ($p<0,01$) bununla birlikte sadece BA (10 ng/mL) uygulamasının ise kontrol grubu ile benzer hücre canlılık düzeyi sergilediğini gösterdi. Ayrıca BA ve N konsantrasyonlarının (BA+10^{-1} N, BA+10^{-2} N, BA+10^{-3} N, BA+10^{-4} N, BA+10^{-5} N, BA+10^{-6}

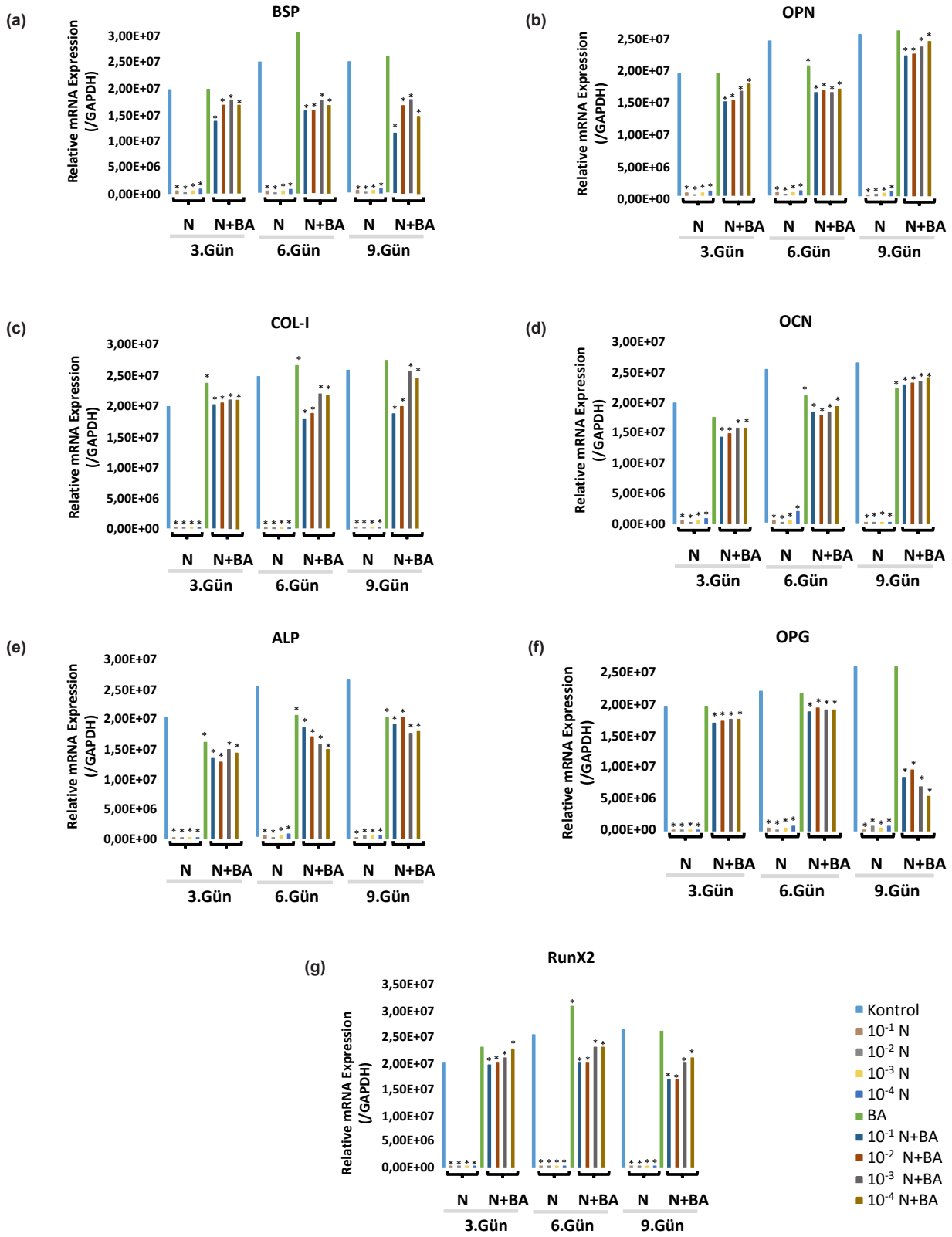

Şekil 3. BA'in N ile indüklenen sementoblastlarda mineralize dokuyla ilişkili gen ekspresyon sonuçları. Sementoblast hücreleri sadece N konsantrasyonları (10^{-1}, 10^{-2}, 10^{-3}, 10^{-4} mM), sadece BA (10 ng/mL) ile BA ve N konsantrasyonlarının birlikte (BA+10^{-1} N, BA+10^{-2} N, BA+10^{-3} N, BA+10^{-4} N) uygulanması sonucunda 3, 6 ve 9. gün; BSP mRNA ifadesi a). OPN mRNA ifadesi b). COL-I mRNA ifadesi c). OCN mRNA ifadesi d). ALP mRNA ifadesi e). OPG mRNA ifadesi f). RunX2 mRNA ifadesi g). *p<0,05, **p<0,001. (Mineralised tissue-related gene expression results of BA in N-induced cementoblasts. Cementoblast cells were treated with N concentrations only (10^{-1}, 10^{-2}, 10^{-3}, 10^{-4} mM), BA only (10 ng/mL) and BA and N concentrations together (BA+10^{-1} N, BA+10^{-2} N, BA+10^{-3} N, BA+10^{-4} N) on day 3, 6 and 9; BSP mRNA expression a). OPN mRNA expression b). COL-I mRNA expression c), OCN mRNA expression d). ALP mRNA expression e). OPG mRNA expression f). RunX2 mRNA expression g). *p<0.05, **p<0.001).

N) birlikte uygulanmasının ise kontrol grubuna (sadece DMEM) göre hücre canlılık seviyesini sadece N konsantrasyonlarına göre istatistiksel olarak daha az azalttığı belirlendi ($p<0,05$). Daha önceki araştırma sonucumuz ile 1, 2,5, 5 ve 10 mM N konsantrasyonları dramatik düzeyde hücre proliferasyonunu azalttığını 10^{-1}, 10^{-2}, 10^{-3}, 10^{-4}, 10^{-5}, 10^{-6} mM N konsantrasyonlarının ise sementoblast proliferasyonunda anlamlı bir değişiklik oluşturmadığını belirlemiştik [30]. Şimdiki çalışmamızda hücre canlılığını MTT yöntemiyle daha önceki çalışmamızda [30] ise hücre proliferasyonunu gerçek zamanlı hücre analizörü (xCELLigence) ile test etmiştik. Proliferasyonda eş zamanlı olarak sonuçlara yansıyan stabil durum hücre canlılığının azalması kaynaklı olabilir. Bununla birlikte literatürde yeralan N'nin sementoblast hücrelerine uygulamasının 1,5 mM'dan daha yüksek konsantrasyonlarının toksik olduğu [28], insan periodontal ligament hücrelerine 100 ng/mL üzerinde N ilavesi sonrası hücre proliferasyonunun inhibe edildiği [42,43], 1 ve 100 mM N'nin ise insan gingival fibroblastlarının proliferasyonunu suprese ettiği [32] yönünde çalışma sonuçları yer almaktadır. Orafasiyal alandan izole edilen farklı doku orijinli hücrelerin *in vitro* sonuçlarında N konsantrasyonuna bağlı farklılıklar olmakla birlikte literatürde yer alan çalışma sonuçlarının ortak noktası N periodontal hücre canlılığı ve proliferasyonunu negatif olarak etkilediği yönündedir. Yara iyileşmesi deneyi sonuçlarına göre tüm N konsantrasyonları (10^{-1}, 10^{-2}, 10^{-3}, 10^{-4} mM) kontrol grubuna göre tüm zaman dilimlerinde (2, 4, 6 ve 24 saat) istatistiksel olarak anlamlı seviyede hücrelerin migrasyon potansiyellerini azalttı. Sadece BA (10 ng/mL) uygulanan grup ise sementoblastların migrasyon kapasitesini deneyin 4, 6 ve 24. saatinde kontrol grubuna göre anlamlı seviyede artırdı. Ayrıca N konsantrasyonları ile birlikte BA uygulanan gruplar (BA+10^{-1} N, BA+10^{-2} N, BA+10^{-3} N, BA+10^{-4} N) hücrelerin migrasyon süreçlerini kontrol grubuna göre istatistiksel olarak anlamlı seviyede 2, 4, 6 ve 24. saatlerde azaltmış olmalarına rağmen bu etki sadece N uygulanan gruplara göre daha az olarak tespit edildi. Böylece elde edilen sonuçlar BA'in, sementoblastların N maruziyeti sonrasında azalan migrasyonuna zaman bağımlı olarak pozitif yönde katkı sağladığını gösterdi. Kaymaz ve ark.'ları iyileşmesi uzun süre alan tendon yaralanmalarında, oral olarak BA uygulamasının ekstraselüler matriks bileşenlerinin sentezi ile anjiyogenez indüklenmesi üzerinden tendon hasarını iyileştirmede güvenli ve etkili bir tedavi bileşeni olabileceğini *in vivo* rat deney modelinde gösterdiler [44]. Biyolojik veya kimyasal birçok ajan indüklemesi sonucunda gelişen periodontal hastalık etiyolojisinde sık karşılaşılan diş kayıplarının önlenebilmesi için yeni kemik, yeni periodontal ligament ve yeni sement dokusu oluşumunu hedefleyen tedavi yöntemleri amaçlanmaktadır. Rejeneratif odaklı tedavi yaklaşımlarının ana hedef hücresi periodontal ligament hücreleri olup bu hücrelerin uygun uyaranlarla osteoblast veya sementoblast hücrelerine farklılaşması yeni kemik ve yeni sement doku oluşumu için elzemdir. Özellikle periodonsiyumda doku yıkımına sebep olan ajanın uzun dönem ve kısa dönemde oluşturduğu hasarı ortadan kaldıracak ve yeni doku oluşumunu indükleyecek biyo-uyumlu moleküllerin, etkinliklerinin ortaya konması ve mevcut tedavi planlarına katılması önemlidir. Dolayısıyla periodonsiyumun N ile olan direkt teması sonucunda hücre proliferasyonu, konak cevabı ve immün sistem etkilenerek periodontal hastalık patogenezine yatkın hale gelmektedir [30]. Sementoblastlar, dişin sement dokusunun ana hücreleri olup kök yapısının yeniden şekillenmesi, periodontal rejenerasyon ve sağlıklı periodonsiyum için kritik öneme sahiptir [27,45]. Literatürde yer alan daha önceki araştırma sonuçları, sementoblast hücrelerinin mineralize doku belirteçleri arasında yer alan ALP, BSP ve OCN eksprese ettiğini [40,41] bununla birlikte N maruziyeti sonrasında COL, OCN, OPN düzeylerinin periodonsiyumun farklı hücrelerinde azaldığı ve araştırma grubumuzun da bir önceki çalışmasında sementoblast hücrelerinde de N bağımlı mineralize doku belirteçlerinin mRNA seviyelerinin önemli derecede azaldığı belirlendi [30]. Bununla birlikte daha önceki araştırma sonuçlarımız, 0,1, 1, 10, 100 ng/mL bor konsantrasyonlarının osteoblast (MC3T3-E1) hücrelerinin bone morphogenetic protein (BMP)-4, BMP-6, BMP-7 düzeyleri ile BSP, OPN, OCN, COL-I mRNA ekspresyon seviyelerini önemli derecede artırdığını gösterdi [5]. Araştırma grubumuzun yapmış olduğu başka bir araştırmada, BMP-7 uygulaması sonrasında sementoblast hücrelerinin COL-I, BSP, OCN seviyelerinin dramatik düzeyde arttığı belirlendi [46]. Her iki araştırma sonucumuza bakarak borik asit-BMP-7 indüklemesi sonucunda sementoblast fonksiyonuna bağlı periodontal hastalık sonucu gelişen doku kaybının önüne geçilebileceği öngörülmüştür. Araştırma ekibimizn bir diğer *in vivo* çalışmasında BA içeren diyetle beslenen tavşanların kemik yapısının direnci ve mineral kompozisyonunun değiştiği belirlenirken [3] diş yapısında ise mineral kompozisyonu ile alveoler kemik yoğunluğunun farklılaştığı görüldü [6]. Borik asitin, osteoblast hücreleri üzerindeki etkinliğini araştırdığımız başka bir çalışma sonucumuzda da farklılaşma faktörü olan Tuftelin düzeyinin BA uygulaması ile önemli düzeyde artış sergilediği belirlendi [47].

4. Sonuçlar (Conclusions)

Elde edilen sonuçlar BA'in, N maruziyetine uğramış sementoblast hücrelerinin biyoaktivite kaybı üzerinde pozitif regülatör rol oynayabileceğini göstermektedir. Bununla birlikte N uygulamasının sementoblast hücrelerinin canlılığı, migrasyon temelli yara iyileşmesi özellikle de mineralize doku ilişkili genlerin ekspresyonunda önemli bir etkisi olduğu, N maruziyetinin gün bazında artmasıyla birlikte hedef gen ifade paternlerinin olumsuz etkilendiği, BA uygulamasının ise sementoblast hücre fonksiyonlarının korunmasında aktif bir rol alabileceği sonucuna varılmıştır. Proje kapsamında *in vivo* deney modeli uygulamasının olmaması çalışmanın limitasyonu olup bundan sonraki aşamalarda BA'in, N maruziyetinin olası sonuçları üzerindeki etkisinin *in vivo* deney modeli üzerinde değerlendirmeye yönelik ilave analizler ve çalışmalar yapılması gerekmektedir. Sementoblastların N maruziyeti sebebiyle

karşılaştıkları biyoaktivite kaybınının BA uygulaması ile hücre canlılığı, yara iyileşmesi ve mineralize doku belirteçleri açısından konsantrasyon ve zaman bazlı kıyaslanması sonucu elde edilen bulguların hayvan modelleri/klinik uygulamalara geçişte kritik bilgiler sağlayıp prevantif terapötik ajan olarak kullanıma yönelik aday olabileceğini düşünmekteyiz.

Yazar Katkısı Beyanı (Author Contribution Statement)

Şerife Buket Bozkurt Polat (ŞBBP) makalenin kavramsallaştırmasında; ŞBBP, Melike Ünlütürk (MÜ) ve Abdullah Emre Hasırcı (AEH) veri analizinde; ŞBBP proje yönetiminde; ŞBBP, MÜ, AEH görselleştirme, orijinal taslak yazma aşamalarında katkı sağlamıştır.

Teşekkürler (Acknowledgements)

Bu çalışma TÜBİTAK tarafından desteklenmiştir (TÜBİTAK-2209-A Üniversite Öğrencileri Araştırma Projeleri Destek Programı-No:1919B012104849)

Kaynaklar (References)

[1] Bolt, H. M., Duydu, Y., Başaran, N., & Golka, K. (2017). Boron and its compounds: Cur-rent biological research activities. *Archives of Toxicology*, *91*(8),2719-2722. https://doi.org/10.1007/s00204-017-2010-1

[2] Uluisik, I., Karakaya, H.C., & Koc, A. (2018) The importance of boron in biological sys-tems. *Journal of Trace Elements in Medicine and Biology*, *45*,156-162. https://doi.org/10.1016/j.jtemb.2017.10.008

[3] Hakki, S. S., Dundar, N., Kayis, S. A., Hakki, E. E., Hamurcu, M., Kerimoglu, U., … & Nielsen, F. H. (2013) Boron enhances strength and alters mineral composition of bone in rabbits fed a high energy diet. *Journal of Trace Elements in Medicine and Biology*, *27*(2),148-153. https://doi.org/10.1016/j.jtemb.2012.07.001

[4] Sağlam, M., Arslan, U., Bozkurt, Ş. B., & Hakki, S. S. (2013). Boric acid irrigation as an adjunct to mechanical periodontal therapy in patients with chronic periodontitis: A randomized clinical trial. *Journal of Periodontology*, *84*(9),1297-1308.https://doi.org/10.1902/jop.2012.120467

[5] Hakki, S. S., Bozkurt, B. S., & Hakki, E. E. (2010). Boron regulates mineralized tissue-associated proteins in osteoblasts (MC3T3-E1). *Journal of Trace Elements in Medicine and Biology*, *24*(4), 243-250. https://doi.org/10.1016/j.jtemb.2010.03.003

[6] Hakki, S. S., Malkoc, S., Dundar, N., Kayis, S. A., Hakki, E. E., Hamurcu, M., … & Götz, W. (2015) Dietary boron does not affect tooth strength, micro-hardness, and density, but affects tooth mineral composition and alve-olar bone mineral density in rabbits fed a high-energy diet. *Journal of Trace Elements in Medicine and Biology*, *29*, 208-215. https://doi.org/10.1016/j.jtemb.2014.10.007

[7] Nielsen, F. H. (1994) Biochemical and physiologic consequences of boron deprivation in humans. *Environmental Health Perspectives*, *102*, 59-63. https://doi.org/10.1289/ehp.94102s759.

[8] Nielsen, F. H. (2004) The alteration of magnesium, calcium and phosphorus metabolism by dietary magnesium deprivation in postmenopausal women is not affected by dietary boron deprivation. *Magnesium Research*, *17*,197-210. PMID: 15724868.

[9] Nielsen, F. H., Stoecker, B. J., & Penland, J. G. (2007) Boron as a dietary factor for bone microarchitecture and central nervous system function. In: F. Xu, H. E. Goldbach, P. H. Brown, R. W. Bell, T. Fujiwara, Hunt C. D., S. Goldberg, & L. Shi (Eds.), *Advances in plant and animal boron butrition* (pp. 227-290). Springer, Dordrecht. https://doi.org/10.1007/978-1-4020-5382-5_27.

[10] Malhotra, R., Kapoor, A., Grover, V., & Kaushal, S. (2010) Nicotine and periodontal tissues. *Journal of Indian Society of Periodontology*, *14*,72-79. https://doi.org/10.4103/0972-124X.65442.

[11] Meenawat, A., Govila, V., Goel, S., Verma, S., Punn, K., Srivastava, V., & Dolas, R. S. (2015). Evaluation of the effect of nicotine and metabolites on the periodontal status and the mRNA expression of interleukin-1 in smokers with chronic periodontitis. *Journal of Indian Society of Periodontology*, *19*, 381-387. https://doi.org/10.4103/0972-124X.157879.

[12] Lahdentausta, L., Paju, S., Mäntylä, P., Buhlin, K., Pietiäinen, M., Tervahartiala, T., … & Pussinen, P. J. (2019) Smoking confounds the periodontal diagnostics using saliva biomarkers. *Journal of Periodontology*, *90*, 475-483. https://doi.org/10.1002/JPER.18-0545.

[13] Nogueira-Filho G., R., Rosa, B. T., Cesar-Neto, J. B., Tunes, R. S., & Tunes U., R. (2007) Low- and high-yield cigarette smoke inhalation potentiates bone loss during ligature-induced periodontitis. *Journal of Periodontology*, *78*, 730-735. https://doi.org/10.1902/jop.2007.060323.

[14] Talhout, R., Schulz, T., Florek, E., van Benthem, J., Wester, P., & Opperhuizen, A. (2011) Hazardous compounds in tobacco smoke. *International Journal of Environmental Research and Public Health*, *8*, 613-628. https://doi.org/10.3390/ijerph8020613.

[15] Wu, L. Z., Duan, D. M., Liu, Y. F., Ge, X., Zhou, Z. F., & Wang, X. J. (2013) Nicotine favors osteoclastogenesis in human periodontal ligament cells co-cultured with CD4(+) T cells by upregulating IL-1. *International Journal of Molecular Medicine*, *31*, 938-942. https://doi.org/10.3892/ijmm.2013.1259.

[16] Barbour, S. E., Nakashima, K., Zhang, J. B., Tangada, S., Hahn, C. L., Schenkein, H. A., & Tew, J. G. (1997) Tobacco and smoking: Environmental factors that modify the host response (immune system) and have an impact on periodontal health. *Critical Reviews in Oral Biology & Medicine*, *8*, 437-460. https://doi.org/10.1177/10454411970080040501.

[17] Theiss, S. M., Boden, S. D., Hair, G., Titus, L., Morone, M. A., & Ugbo, J. (2000) The effect of nicotine on gene expression during spine fusion. *Spine*, *25*(20),2588-2594. https://doi.org/10.1097/00007632-200010150-00008.

[18] Pinto, J. R., Bosco, A. F., Okamoto, T., Guerra, J. B., & Piza, I. G. (2002) Effects of nicotine on the healing of extraction sockets in rats. A histological study. *Brazilian Dental Journal*, *13*(1), 3-9. PMID: 11870959.

[19] Zhou, J., Olson, B. L., & Windsor, L. J. (2007) Nicotine increases the collagen degrading ability of human gingival fibroblasts. *Journal of Periodontal Research*, *42*, 228-235. https://doi.org/10.1111/j.1600-0765.2006.00937.x.

[20] Zheng, L. W., Ma, L., & Cheung, L. K. (2008) Changes in blood perfusion and bone healing induced by nicotine during distraction osteogenesis. *Bone*, *43*, 355-361. https://doi.org/10.1016/j.bone.2008.04.002.

[21] Riebel, G. D., Boden, S. D., Whitesides, T. E., & Hutton, W. C. (1995) The effect of nicotine on in-corporation of cancellous bone graft in an animal model. *Spine*, *20*, 2198-2202. https://doi.org/10.1097/00007632-199510001-00004.

[22] Fang, Y., & Svoboda, K. K. (2005) Nicotine inhibits human gingival fibroblast migration via modulation of Rac signalling pathways. *Journal of Clinical Periodontology*, *32*, 1200-1207. https://doi.org/10.1111/j.1600-051X.2005.00845.x.

[23] Takeuchi-Igarashi, H., Kubota, S., Tachibana, T., Murakashi, E., Takigawa, M., Okabe, M., & Numabe, Y. (2016) Matrix remodeling response of human periodontal tissue cells toward fibrosis upon nicotine exposure. *Odontology*, *104*, 35-43. https://doi.org/10.1007/s10266-014-0177-y.

[24] Sculean, A., Gruber, R., & Bosshardt, D. D. (2014) Soft tissue wound healing around teeth and dental implants. *Journal of Clinical Periodontology*, *41*, 6-22. https://doi.org/10.1111/jcpe.12206.

[25] Bosshardt, D. D., Stadlinger, B., & Terheyden, H. (2015) Cell-to-cell communication-periodontal regeneration. *Clinical Oral Implants Research*, 26, 229-239. https://doi.org/10.1111/clr.12543.

[26] Moon, J. S., Kim, S. D., Ko, H. M., Kim, Y. J., Kim, S. H., & Kim, M. S. (2018) Twist1 suppresses cementoblast differentiation. *Dentistry Journal*, *6*, E57. https://doi.org/10.3390/dj6040057.

[27] Bozkurt, S. B., Hakki, E. E., Kayis, S. A., Dundar, N., & Hakki, S. S. (2017) Biostimulation with diode laser positively regulates cementoblast functions, in vitro. *Lasers in Medical Science*, *32*, 911-919. https://doi.org/10.1007/s10103-017-2192-z.

[28] Chen, C. S., Lee, S. S., Yu, H. C., Huang, F. M., & Chang, Y. C. (2015) Effects of nicotine https://doi.org/ species by cementoblasts. *Journal of Dental Sciences*, *10*, 154-160. https://doi.org/10.1016/j.jds.2014.04.002.

[29] Hakki, S. S., Bozkurt, S. B., Türkay, E., Dard, M., Purali, N., & Götz, W. (2018) Recombinant amelogenin regulates the bioactivity of mouse cementoblasts in vitro. *International Journal of Oral Science*, *10*, 15. https://doi.org/10.1038/s41368-018-0010-5.

[30] Bozkurt, S. B., & Hakki, S. S. (2020) Nicotine suppresses proliferation and mineralized tissue-associated gene expressions of cementoblasts. *Journal of Periodontology*, 91, 800-808. https://doi.org/10.1002/JPER.19-0256.

[31] D'Errico, J. A., Ouyang, H., Berry, J. E., MacNeil, R. L., Strayhorn, C., Imperiale, M. J., … & H., Somerman, M. J. (1999) Immortalized cementoblasts and periodontal ligament cells in culture. *Bone*, *25*,39-47. https://doi.org/10.1016/s8756-3282(99)00096-4.

[32] Torshabi, M., Rezaei Esfahrood, Z., Jamshidi, M., Mansuri Torshizi, A., & Sotoudeh, S. (2017) Efficacy of vitamins E and C for reversing the cytotoxic effects of nicotine and cotinine. *European Journal of Oral Sciences*, *125*, 426-437. https://doi.org/10.1111/eos.12375.

[33] Kim, B. S., Kim, S. J., Kim, H. J., Lee, S., Park, Y. J., Lee, J., & You, H. K. (2012) Effects of nicotine on proliferation and osteoblast differentiation in human alveolar bone marrow derived mesenchymal stem cells. *Life Science Journal*, *90*, 109-115. https://doi.org/10.1016/j.lfs.2011.10.019.

[34] Giulietti, A., Overbergh, L., Valckx, D., Decallonne, B., Bouillon, R., & Mathieu, C. (2001) An overwiew of real-time quantitative PCR: Applications to quantify cytokine gene expression. *Methods*, *25*, 386-401. https://doi.org/10.1006/meth.2001.1261.

[35] Livak, K. J., & Schmittgen, T. D. (2001) Analysis of relative gene expression data using real-time quantitative PCR and the 2-Delta Ct method. *Methods*, *25*, 402-408. https://doi.org/10.1006/meth.2001.1262.

[36] Pfaffl, M. (2001) A new mathematical model for relative quantification in real-time RT-PCR. *Nucleic Acids Research*, *29*, 900. https://doi.org/10.1093/nar/29.9.e45.

[37] de Almeida, J. M., Bosco, A. F., Bonfante, S., Theodoro, L. H., Nagata, M. J., & Garcia, V. G. (2011) Nicotine-induced damage affects gingival fibroblasts in the gingival tissue of rats. *Journal of Periodontology*, *82*, 1206-1211. https://doi.org/10.1902/jop.2010.100549.

[38] Chang, Y. C., Lii, C. K., Tai, K. W., & Chou, M. Y. (2001) Adverse effects of arecoline and nicotine on human periodontal ligament fibroblasts in vitro. *Journal of Periodontology*, *28*, 277-282. https://doi.org/10.1034/j.1600-051x.2001.028003277.x.

[39] Bergström, J. (2004) Tobacco smoking and chronic destructive periodontal disease. *Odontology*, *92*, 1-8. https://doi.org/10.1007/s10266-004-0043-4.

[40] Nakayama, Y., Mezawa, M., Araki, S., Sasaki, Y., Wang, S., Han, J., … & Ogata, Y. (2009) Nicotine suppresses bone sialoprotein gene expression. *Journal of Periodontal Research*, *44*, 657-663. https://doi.org/10.1111/j.1600-0765.2008.01171.x.

[41] Rothem, D. E., Rothem, L., Soudry, M., Dahan, A., & Eliakim, R. (2009) Nicotine modulates bone metabolism-associated gene expression in osteoblast cells. *Journal of Bone and Mineral Metabolism*, *27*(5), 555-561. https://doi.org/10.1007/s00774-009-0075-5.

[42] Giannopoulou, C., Geinoz, A., & Cimasoni, G. (1999) Effects of nicotine on periodontal ligament fibroblasts in vitro. *Journal of Clinical Periodontology*, *26*(1), 49-55. https://doi.org/10.1034/j.1600-0765.2002.01612.x.

[43] Chang, Y. C., Huang, F. M., Tai, K. W., Yang, L. C., & Chou, M. Y. (2002) Mechanisms of cytotoxicity of nicotine in human periodontal ligament fibroblast cultures in vitro. *Journal of Periodontal Research*, *37*(4), 279-285. https://doi.org/10.1034/j.1600-0765.2002.01612.x.

[44] Kaymaz, B., Gölge, U. H., Ozyalvaclı, G., Kömürcü, E., Goksel, F., Mermerkaya, M. U., & Doral, M. N. (2016) Effects of boric acid on the healing of Achilles tendons of rats. Knee Surgery, *Sports Traumatology, Arthroscopy*, *24*(12), 3738-3744. https://doi.org/10.1007/s00167-015-3617-5.

[45] Bosshardt, D. D. (2005) Are cementoblasts a subpopulation of osteoblasts or a unique phenotype?. *Journal of Dental Research*, *84*, 390-406. https://doi.org/10.1177/154405910508400501.

[46] Hakki, S. S., Foster, B. L., Nagatomo, K. J., Bozkurt, S. B., Hakki, E. E., Somerman, M. J., & Nohutcu, R. M. (2010) Bone morphogenetic protein-7 enhances cementoblast function in vitro. *Journal of Periodontology*, *81*(11), 1663-1674. https://doi.org/10.1902/jop.2010.100074.

[47] Hakki, S. S., Bozkurt, S. B., Hakki, E. E., & Nielsen, F. H. (2021) Boron as boric acid induces mRNA expression of the differentiation factor tuftelin in pre-osteoblastic MC3T3-E1 cells. *Biological Trace Element Research*, *199*(4),1534-1543. https://doi.org/10.1007/s12011-020-02257-x.

BOR DERGİSİ
JOURNAL OF BORON
https://dergipark.org.tr/boron

Isolation and stabilization of aryldiazonium cations with boron clusters

Ozan Unver [1], **Akin Akdag** [1,*]

[1]*Middle East Technical University, Department of Chemistry, Ankara, 06800, Türkiye*

ARTICLE INFO

Article history:
Received September 8, 2023
Accepted October 15, 2023
Available online December 29, 2023

Research Article

DOI: 10.30728/boron.1338235

Keywords:
Aryl diazonium
Boron clusters
Carborone
Reactive intermediate

ABSTRACT

Diazonium salts were found to be useful intermediates for many applications. Although few salts were isolated, they were found to be short-lived. Charged boron cages have been known to be weakly coordinating anions. The cages were used to isolate short lived cations for characterizations and further reactions. In this study, we have facilitated dodecaborate dianion and carborate anion to isolate and characterize diazonium cations. With these cages, it was found that diazonium cation was stable more than a month at ambient conditions.

1. Introduction

Since the discovery of aryl diazonium salts by Griefs in 1858 [1], they have been used in numerous application areas. The most common one is dyeing. When diazonium salts undergo diazo-coupling reactions, diazo compounds are produced with great coloring features [2,3], and some of the important diazo dyes are shown in Figure 1a. Other than dyeing, some of the diazo compounds have antimicrobial, anticancer, antibacterial, antioxidant, antibiotic, antifungal and anti-HIV activity (Figure 1b) [4-7]. Moreover, some diazo compounds are known to be used in photoelectronics, optical recording and gas storage [8,9]. Also, aryl diazonium salts which have strong electrophilic character arising from the reactivity of diazonium group, can be used in Sandmeyer reactions, Balz-Schiemann reaction, Pschorr reaction, Meerwein reaction, Gomberg-Bachmann reaction and palladium catalyzed cross-coupling reactions [10-18].

The syntheses of aryl diazonium salts are straightforward. Starting with acidifying an aniline derivative and proceeding through addition of a nitrite resulting an aryl diazonium salt (Figure 2) [19,20]. Due to the high reactivity of diazonium cation, they must be kept at low temperature [21]. In the literature, there are many incidents reported coming from the unstable nature of aryl diazonium cations such as wild decomposition or explosion [22]. In order to use aryl diazonium cations in further reactions, they should be treated with the nucleophile in the same environment where they were formed [17,23-28]. Meanwhile, these cations can be stabilized by tosylates, disulfonamides,

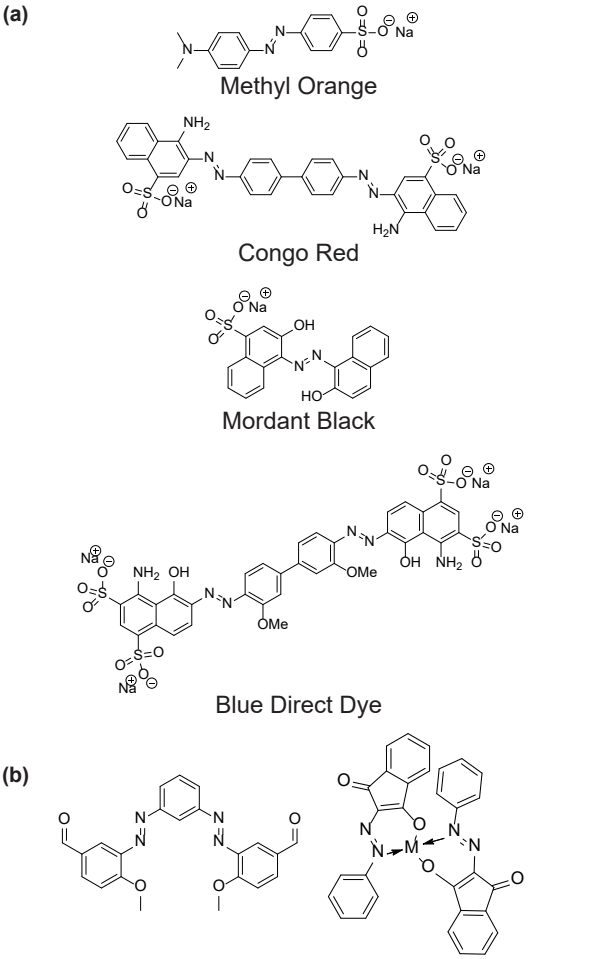

Figure 1. Examples of diazo compounds produced from diazonium salts a). used as dyes and b). that have biological activity.

*Corresponding author: aakdag@metu.edu.tr

hexafluorophosphates and tetrafluoroborates which are considered as the most effective anions to stabilize aryl diazonium cations but not as good as expected [22,29].

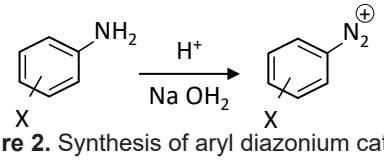

Figure 2. Synthesis of aryl diazonium cations.

The famous stabilized diazonium salt is the salt of tetrafluoroborate anion. However, this salt could lead to fluoroaryl compounds upon heating. (Figure 3a) [11]. Besides, this compound is not as stable as it is advertised. A new stabilizing anion is needed. Charged boron clusters are known to stabilize cationic intermediates [30,31]. For this purpose, dodecahydro-*closo*-dodecaborate, dodecachloro-*closo*-dodecaborate and mono-carba-*closo*-dodecaborate (Figure 3b-d) could be used which are synthesized in our laboratory according to the literature [32-35]. These boron clusters are accepted as weakly coordinating anions which have low affinity for coordination to their counter cations [36]. Also, these anions have high thermal stability and high chemical stability [37].

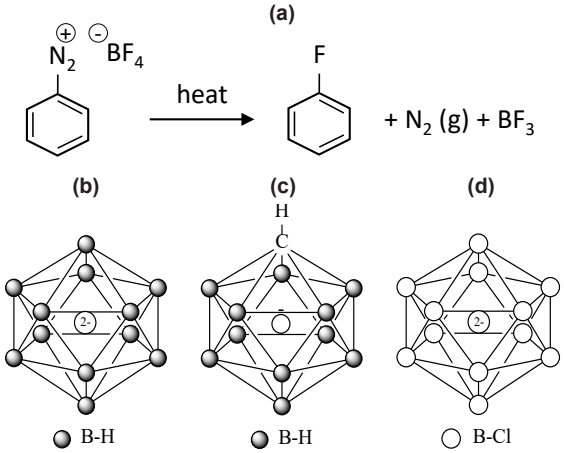

Figure 3. a). Conversion of benzenediazonium tetrafluoroborate into fluorobenzene upon heating. b). dodecahydro-*closo*-dodecaborate, c). mono-carba-*closo*-deodecaborate and d). dodecachloro-*closo*-dodecaborate.

2. Materials and Methods

2.1. Materials

All chemicals were purchased from Sigma-Aldrich (USA). IR spectrums were measured with Thermo Scientific Nicolet iS10 Atr-IR (USA).

2.2. Synthesis of Boron Clusters

2.2.1. Synthesis of triethylammonium salt of dodecahydro-closo-dodecaborate

A 3-necked round bottom flask equipped with a condenser (connected to an acetone trap), a dropping funnel and a stopper was charged with 30 g (0.793 mol) $NaBH_4$ and 150 mL of diglyme under Ar atmosphere. The silicon oil bath was heated to 120ºC to dissolve the sodium borohydride in the reaction mixture. 62.5 g (0.246 mol) I_2 was dissolved in 200 mL of diglyme and added to the dropping funnel. The solution of iodine in diglyme was added to the solution containing sodium borohydride dropwise in 6 hours. After the addition, the solution was stirred overnight at 120ºC. Temperature of the oil bath was increased to 185ºC and the solution was stirred for 1 day. The solvent was removed with distillation. 143 mL of distilled water was added to the residue and 84 mL 37% HCl was added to the reaction mixture slowly. The reaction vessel was stored in refrigerator overnight for completion of the formation of boric acid. The reaction mixture was filtered and boric acid was collected. To the filtrate, 150 mL Et_3N was added and white crystals of triethylammonium salt of dodecahydro-*closo*-dodecaborate were started to form immediately. The expected product was collected by filtering the reaction mixture. (15.728 g, 0.046 mol, 68.9%) IR: 2473 cm^{-1} (B-H str.), 3125 cm^{-1} (N-H str.)

2.2.2. Synthesis of sodium salt of dodecahydro-closo-dodecaborate

2.2 equivalent of NaOH was dissolved in distilled water and 1 equivalent of triethylammonium salt of dodecaborate was added into the solution. The solution was heated and stirred until it became clear. Then, the solvent was removed and the obtained solid was the expected sodium salt of dodecaborate.

2.2.3. Synthesis of sodium salt of dodecachloro-closo-dodecaborate

0.51 g (12.7 mmol, 2.2 eqv.) NaOH was dissolved in water and 2 g (5.8 mmol, 1 eqv.) $(Et_3NH)_2B_{12}H_{12}$ was added to the solution. The solution was heated and stirred until it became clear. Solvent was removed and Na salt of $B_{12}H_{12}^{2-}$ was obtained. Obtained $Na_2B_{12}H_{12}$ was mixed with MeCN (~60 mL) and SO_2Cl_2 (~60 mL) was added to the suspension dropwise and the solution became yellow. The solution was stirred for 20 minutes without applying heat and then, refluxed for 1 day. Solvent was removed and the residue was the expected compound. IR: 1031 cm^{-1} (B-Cl str.) Also, disappearance of the belonging to B-H stretching proved the product formation.

2.2.4. Synthesis of trimethylammonium salt of tetradecahydro-nido-undecaborate

30 g (0.793 mol) NaBH4 and 150 mL of diglyme were charged into a 3-necked round bottom flask equipped with a dropping funnel, a condenser (connected to an acetone trap) and a stopper under Ar atmosphere. Temperature of the silicon oil bath was raised to 120ºC for complete dissolution of sodium borohydride. 125 mL (0.995 mol) $BF_3.OEt_2$ was added to the solution dropwise with dropping funnel in 5 hours. Then, the reaction mixture was cooled to room temperature

(RT) and suction filtration was applied. During the filtration process, both the reaction flask and the solid were washed with diglyme until the solid becomes white. To the filtrate, solvent exchange procedure was applied with portions of 150 mL distilled water (total 1050 mL) and the evaporated liquid was nearly 1060 mL. Resulting solution was cooled to RT and 6.5 g (0.068 mol) trimethylammonium chloride was added to the solution. The solution was stored in refrigerator overnight and filtered. Obtained solid was dissolved in acetone and heated to reflux. Distilled water was added to the solution until cloudiness was observed. The solution was cooled to RT and stored in refrigerator overnight. The solution was filtered and the collected solid was dried yielding 5.8 g (0.03 mol, 41.7%) $(CH_3)_3NHB_{11}H_{14}$. IR: 2501 cm^{-1} (B-H str.), 3169 cm^{-1} (N-H str.).

2.2.5. Synthesis of trimethylammonium salt of mono-carba-closo-dodecaborate

5.0 g (0.026 mol) trimethylammonium salt of tetradecahydro-*nido*-undecaborate was dissolved in freshly distiled THF under Ar atmosphere and cooled to 0ºC in an ice bath. 17.5 g (0.648 mol) NaH was washed with hexane and added to the solution slowly. The solution was stirred for 1 hour at RT and solvent was removed. After evaporation, freshly distilled THF was added to the flask to dissolve the solid. Then, 12.5 mL (0.156 mol) $CHCl_3$ was added slowly at 0ºC. The solution was stirred for 1 hour at RT and EtOH was added to the solution dropwise at 0ºC and allowed to stir overnight. Next day, the solvent was removed and distilled water was added to the residue. The solution was acidified with 40 mL of 37% HCl + 80 mL of distilled water. After the acidification process, trimethylammonium chloride was added to the solution and filtered. Obtained solid was dissolved with minimum amount of MeOH with heating and after all the solid was dissolved, distilled water was added to the solution and filtered. To the filtrate, trimethylammonium chloride was added and some precipitation occurred. The desired product was collected with filtration yielding 0.18 g (0.9 mmol, 3.41%). IR: 3172 cm^{-1} (N-H str.), 3037 cm^{-1} (C-H str.), 2525 cm^{-1} (B-H str.).

2.2.6. Synthesis of sodium salt of mono-carba-closo-dodecaborate

2.2 equivalent of NaOH was dissolved in distilled water and 1 equivalent of triethylammonium salt dodecahydro-*closo*-dodecaborate was added into the solution. The solution was heated and stirred until it became clear. Then, the solvent was removed and the obtained solid was the expected sodium salt of dodecahydro-*closo*-dodecaborate.

2.3. General Synthesis of Different Benzenediazonium Salts of Boron Clusters

2.3.1. Synthesis of diazonium salts of dodecahydro-closo-dodecaborate, dodecachloro-closo-dodecaborate

2 equivalent of an aniline derivative was mixed with 2 M HCl solution. 2.5 equivalent of $NaNO_2$ was dissolved in distilled water and added to the solution slowly at 0ºC. The solution was stirred for 1 hour. 1 equivalent of sodium salt of dodecaborate was dissolved in distilled water and added to the solution slowly at 0ºC. The solution was stirred for 2 hours and after the filtration, expected compound was obtained by filtration. IR: *ca*. 2200 cm^{-1} (-N≡N str.), *ca*. 2400 cm^{-1} (B-H str.), *ca*. 1030 cm^{-1} (B-Cl str.)

2.3.2. Synthesis of diazonium salts of mono-carba-closo-dodecaborate

1 equivalent of an aniline derivative was mixed with 2 M HCl solution. 1.25 equivalent of $NaNO_2$ was dissolved in distilled water and added to the solution slowly at 0ºC. The solution was stirred for 1 hour. 1 equivalent of sodium salt of dodecaborate was dissolved in distilled water and added to the solution slowly at 0ºC. The solution was stirred for 2 hours and after the filtration, expected compound was obtained by filtration. IR: *ca*. 2200 cm^{-1} (-N≡N str.), *ca*. 2520 cm^{-1} (B-H str.), *ca*. 3030 cm^{-1} (C-H str.).

3. Results and Discussion

Dodecahydro-*closo*-dodecaborate was synthesized according to the reported literature with modifications (Figure 4a) [32]. The procedure starts with ensuring the reaction setup was under inert atmosphere by flushing Argon through setup. Sodium borohydride was suspended in diglyme. Before addition of iodine to the borohydride, the complete dissolution of $NaBH_4$ was attained at 105-110ºC. Then, iodine in diglyme was added dropwise at this temperature. Faster addition resulted in lower yields for the dodecaborate. With the iodine addition over, the reaction mixture was stirred for 12 hours at this temperature to ensure that the conversion of all BH_3 to $B_3H_8^-$. Then, the reaction mixture was brought to reflux temperature and kept at that temperature for 24 hours. The cooled reaction mixture was added water to quench the reaction. With solvents removed, the formed $B(OH)_3$ was separated, and $B_{12}H_{12}^{2-}$ was precipitated as triethylammonium salt. The IR spectrum of triethylammonium salt of dodecahydro-*closo*-dodecaborate (Figure 4b) shows the characteristic peaks as 2475 cm^{-1} for B-H stretching and 3125 cm^{-1} for N-H stretching in the cation.

With dodecaborate in hand, perchlorination of the dodecaborate was performed with refluxing the dodecaborate with sulfuryl chloride (Figure 5a). The perchlorinated dodecaborate was separated as sodium salt. This salt was characterized with IR spectroscopy. The IR spectrum of the obtained compound (Figure 5b) shows B-Cl stretching at 1030 cm^{-1}. Also, disappearance of the peak belonging to B-H stretching proves the product formation.

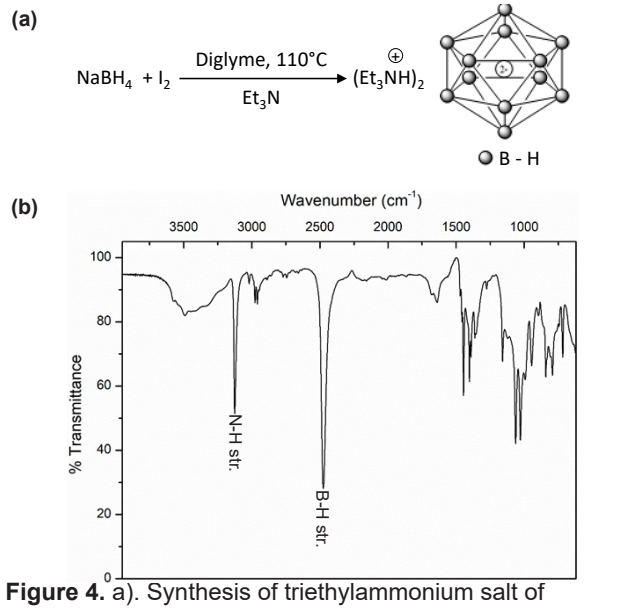

Figure 4. a). Synthesis of triethylammonium salt of dodecahydro-*closo*-dodecaborate, b). IR Spectrum of triethylammonium salt of dodecahydro-*closo*-dodecaborate.

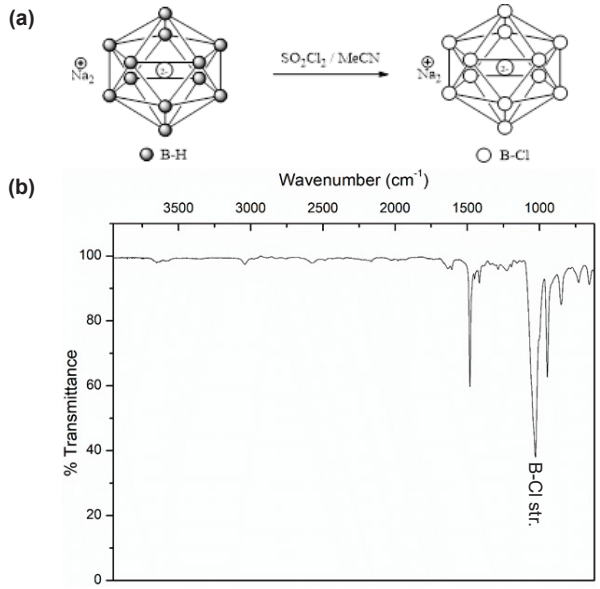

Figure 5. a). Synthesis of dodecahloro-*closo*-dodecaborate, b). IR Spectrum of dodecachloro-*closo*-dodecaborate.

For the synthesis of mono-carba-*closo*-dodecaborate, Michl's method was followed with modifications (Figure 6a). For that, tetradecahydro-*nido*-undecaborate was synthesized by following Dunk's method from $NaBH_4$ treated with $BF_3.OEt_2$ and characterized by IR Spectroscopy (Figure 6b). The undecaborate anion was then treated with dichlorocarbene which was generated *in situ* from chloroform yielded the carborate. The carborate was characterized by IR spectroscopy and HRMS. The characterization of the salt was done with IR Spectroscopy which shows characteristic B-H stretching at 2525 cm^{-1} and C-H stretching at 3037 cm^{-1} (Figure 6c).

It is known that the charged borate cages could be used to stabilize cationic intermediates [38].

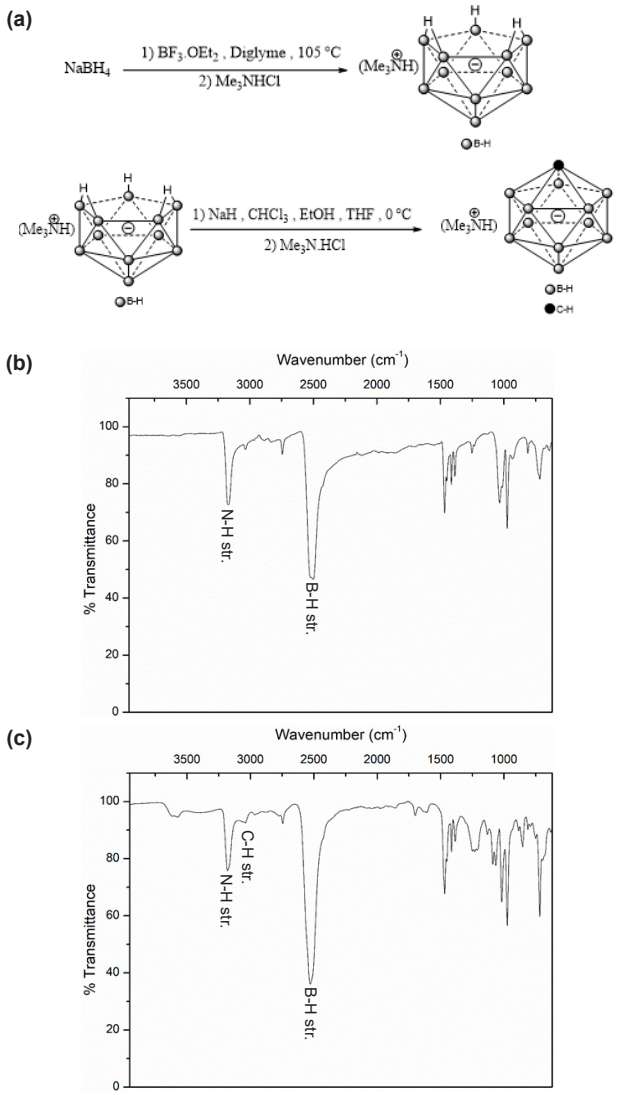

Figure 6. a). Synthesis of mono-carba-*closo*-dodecaborate, b). IR Spectrum of undecahydro-*nido*-undecaborate, c). IR Spectrum of mono-carba-*closo*-dodecaborate.

With that in mind, they could also be used to stabilize aryldiazonium cations. In order to test this hypothesis, first, aniline was converted into benzenediazonium cation by reacting with $NaNO_2$ in the presence of an acid at 0ºC. As soon as the sodium salt of dodecaborates (dodecahydro-*closo*-dodecaborate, dodecachloro-*closo*-dodecaborate and mono-carba-*closo*-dodecaborate) were added onto benzenediazonium cation, precipitates were formed (Figure 7). The precipitates were characterized with IR spectroscopy. The spectra showed characteristic peaks for diazonium cations ca. 2200 cm^{-1} and for $B_{12}H_{12}^{2-}$, B-H str., *ca*. 2480 cm^{-1}, for $B_{12}Cl_{12}^{2-}$, B-Cl str., *ca*. 1030 cm^{-1}, for $CB_{11}H_{12}^{-}$, B-H str., *ca*. 2520 cm^{-1} and C-H str., *ca*. 3000 cm^{-1}. However, in the IR spectra of 1b and 1c, peaks belonging to diazo group (-N=N-) were also observed. Figure 7 shows the IR spectra for the benzenediazonium salts (Figure 8).

After stabilizing benzenediazonium cation with dodecahydro-*closo*-dodecaborate (1a),

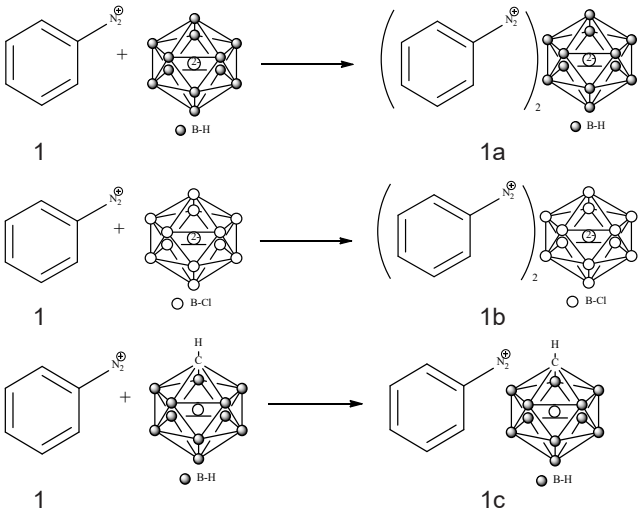

Figure 7. Stabilization of benzenediazonium cation with a). dodecahydro-*closo*-dodecaborate, b). dodecachloro-*closo*-dodecaborate and c). mono-carba-*closo*-dodecaborate

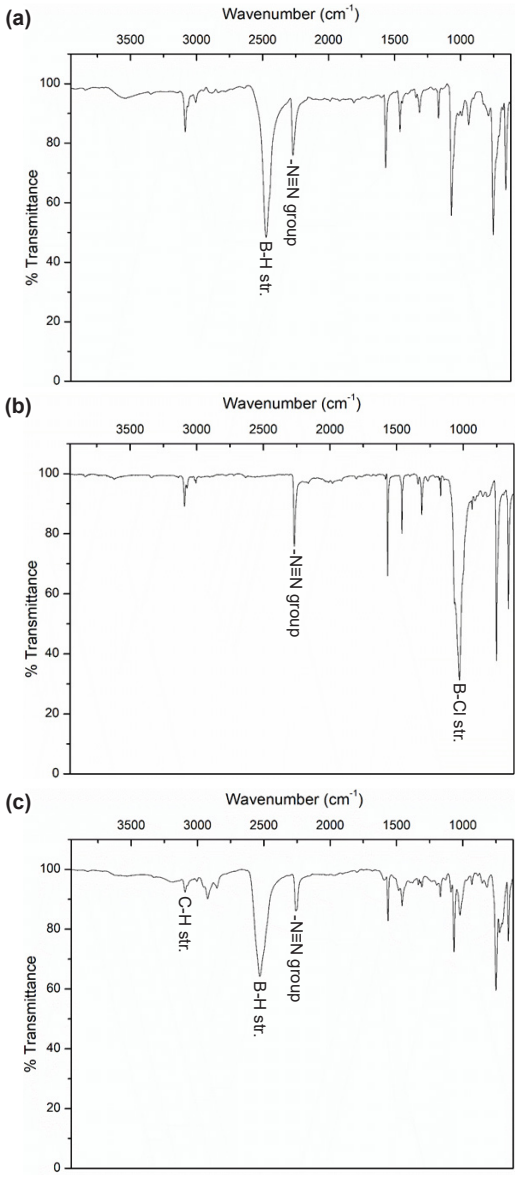

Figure 8. Benzenediazonium salts of a). dodecahydro-*closo*-dodecaborate, b). dodecachloro-*closo*-dodecaborate and c). mono-carba-*closo*-dodecaborate

dodecachloro-*closo*-dodecaborate (1b) and mono-carba-*closo*-dodecaborate (1c), some of the aniline derivatives (Figure 9) were also converted into aryldiazonium compounds and stabilized with dodecaborates.

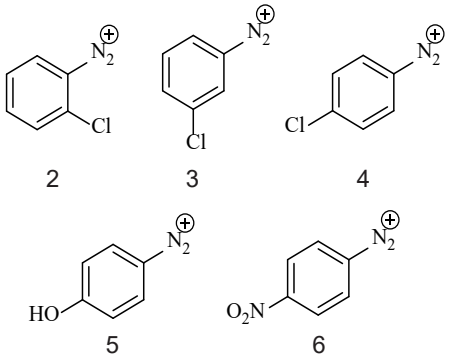

Figure 9. Some of the aniline derivatives that were stabilized with dodecaborates.

First, compounds 2,4 and 5 were stabilized with dodecahydro-*closo*-dodecaborate (the salts forms numbered as 2a,4a and 5a) with the same procedure which aniline was subjected. Then, these compounds and also compound 1a were subjected into a stability test. The tests were applied with the help of IR spectroscopy. These compounds were characterized immediately after they were synthesized. Then, for 4 weeks, they were characterized after each week ended. The results showed that dodecahydro-*closo*-dodecaborate was a good stabilizer since all the IR spectra showed the same result (Figure 10). Apart from these compounds, compound 6 was also tried to be stabilized with the same procedure with dodecahydro-*closo*-dodecaborate (6a). The compound 6a was immediately characterized with IR spectroscopy (Figure 10) but when it was fully dried under vacuum and tried to be transferred into a vial, it exploded.

After obtaining meaningful results from 4-week stability tests with dodecahydro-*closo*-dodecaborate, it was decided to stabilize *o*-chlorobenzenediazonium (2), *m*-chlorobenzenediazonium (3) and *p*-chlorobenzenediazonium (4) cations with dodecachloro-*closo*-dodecaborate (2b, 3b and 4b). Same procedure was applied for stabilization process and characterizations of these salts were performed with IR spectroscopy. In IR spectra of these compounds (Figure 12), there were peaks for both diazonium salt ca. 2200 cm^{-1} and diazo compound ca. 1500 cm^{-1} as observed in IR spectrum of 1b.

Next, these three cations were also tried to be stabilized with mono-carba-*closo*-dodecaborate (2c, 3c and 4c). Same procedure was applied for stabilization process. The resulting compounds were characterized with IR spectroscopy. IR spectra of these compounds (Figure 13) show peaks for diazonium salt *ca*. 2200 cm^{-1} and diazo compound *ca*. 1500 cm^{-1} as observed in the IR spectrum of 1c.

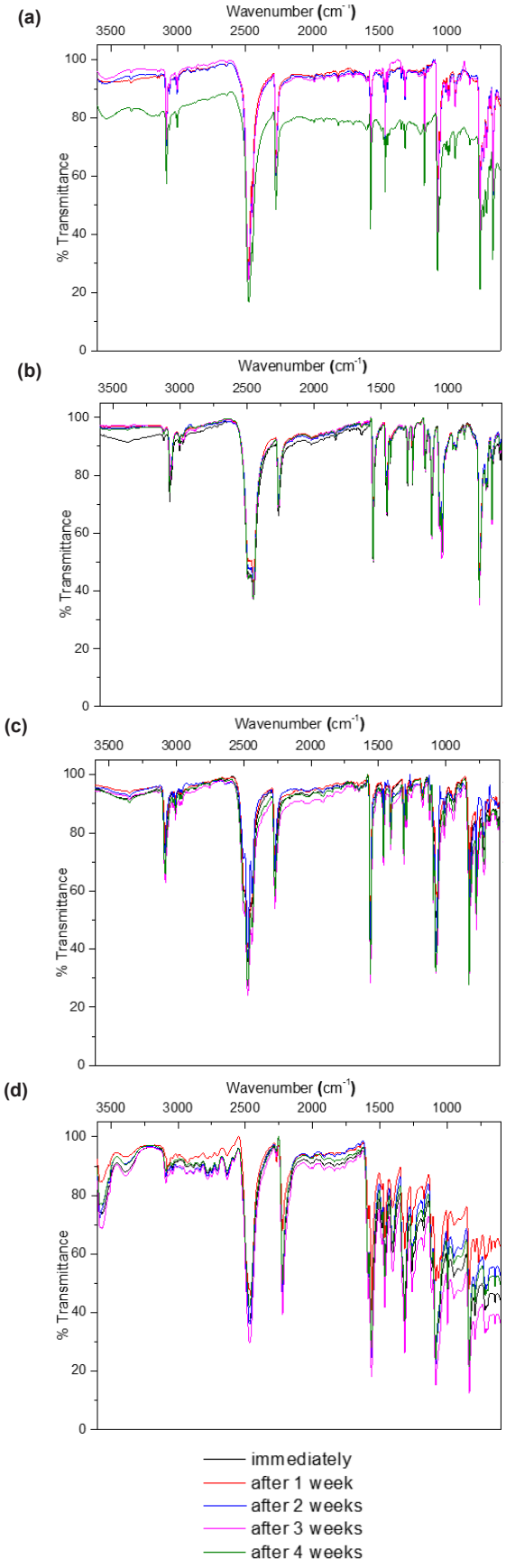

Figure 10. Stability test results of a). benzenediazonium cation, b). *o*-chlorobenzenediazonium salt, c). *p*-chlorobenzenediazonium cation and d). *p*-hydroxybenzenediazonium cation with dodecahydro-*closo*-dodecaborate

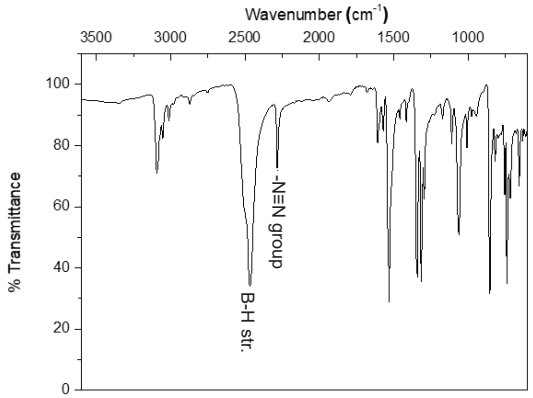

Figure 11. IR spectrum of *p*-nitrobenzenediazonium salt of dodecahydro-*closo*-dodecaborate.

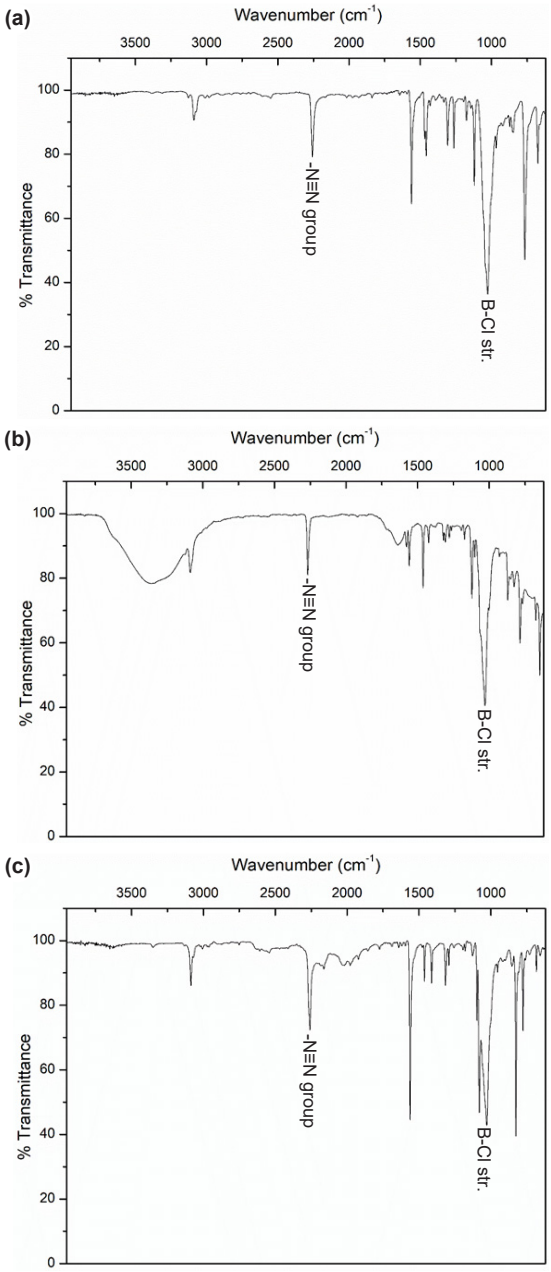

Figure 12. IR spectra of a). *o*-chlorobenzenediazonium cation, b). *m*-chlorobenzenediazonium cation and c). *p*-chlorobenzenediazonium cation stabilized with dodecachloro-*closo*-dodecaborate.

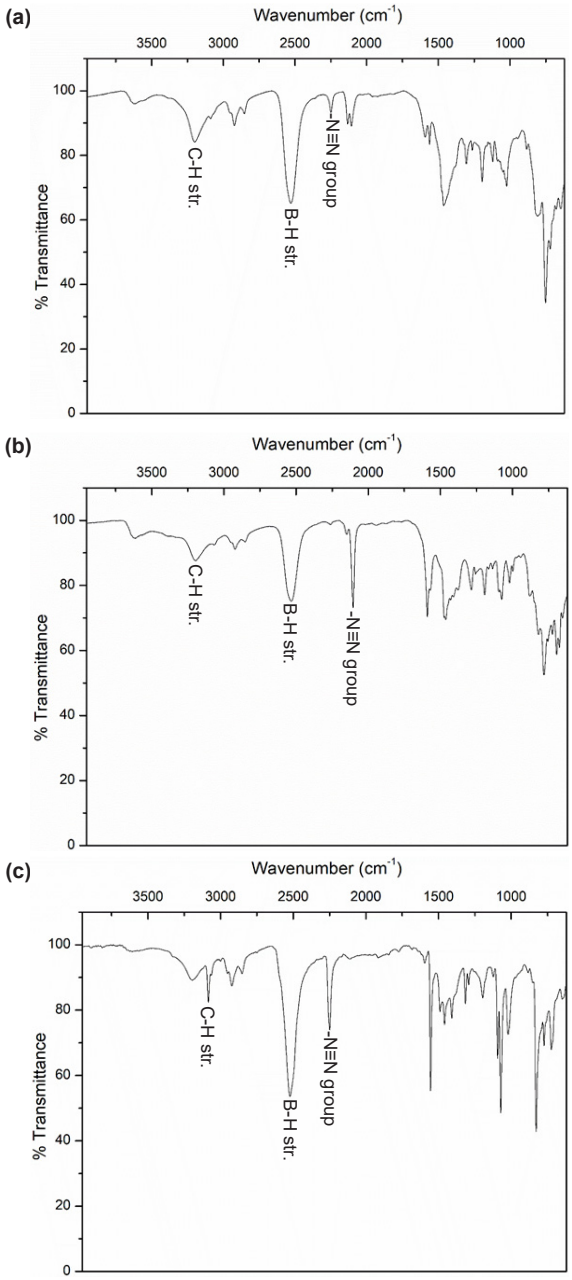

Figure 13. IR spectra of a). *o*-chlorobenzenediazonium cation, b). *m*-chlorobenzenediazonium cation and c). *p*-chlorobenzenediazonium cation stabilized with mono-carba-*closo*-dodecaborate.

4. Conclusions

In this study, dodecaborate and carborate anions are synthesized successfully in our laboratories. These anions were known to be weakly coordinating anions. With this in mind, we employed these anions to stabilize and capture aryldiazonium cations. The aryldiazonium borate salts were found to be stable for months under ambient conditions as judged by IR spectroscopy.

5. Acknowledgements

We would like to thank Fatma Nur Aydemir for initial studies. Also, Oğuzhan Albayrak and Sevban Doğan are acknowledged for helpful discussions. Turkish Energy Nuclear Mineral Research Agency (TENMAK) Boron Research Institute (BOREN) is acknowledged for partially funding this study (Project Number 2018-30-06-30-004).

Competing interests

The authors declare that they have no known competing financial interests or personal relationships that could have appeared to influence the work reported in this paper

Authors' contributions

A.A. conceived the idea. O.U. performed the experiments. O.U. and A.A. analyzed the results. O.U. and A.A. wrote and edited the manuscript together.

References

[1]. Griefs, P. (1858). Vorläufige notiz über die einwirkung von salpetriger säure auf amidinitro- und aminitrophenylsäure. *Justus Liebigs Annalen der Chemie*, *106*, 123-125. https://doi.org/10.1002/jlac.18581060114.

[2]. de Souza Ferreira, I. L., de Medeiros, J. I., Steffens, F., & Oliveira, F. R. (2020). Seawater as an alternative to dye cotton fiber with reactive dyes. *Textile Research Journal*, *91*(9-10), 1184-1193. https://doi.org/10.1177/0040517520972482.

[3]. Hanor, A. (1942). Dyes and dyeing. *Journal of Chemical Education*, *19*(10), 460. https://doi.org/10.1021/ed019p460.

[4]. Mahmoud, W. H., Omar, M. M., & Sayed, F. N. (2016). Synthesis, spectral characterization, thermal, anticancer and antimicrobial studies of bidentate azo dye metal complexes. *Journal of Thermal Analysis and Calorimetry*, *124* (2), 1071-1089. https://doi.org/10.1007/s10973-015-5172-1.

[5]. Sharma, R., Rawal, R. K., Gaba, T., Singla, N., Malhotra, M., Matharoo, S., & Bhardwaj, T. R. (2013). Design, synthesis and ex vivo evaluation of colon-specific azo based prodrugs of anticancer agents. *Bioorganic & Medicinal Chemistry Letters*, *23*(19), 5332-5338. https://doi.org/10.1016/j.bmcl.2013.07.059.

[6]. Ahmad, K., Naseem, H. A., Parveen, S., Shah, H.-R., Shah, S. S. A., Shaheen, S., … & Ashfaq, M. (2019). Synthesis and spectroscopic characterization of medicinal azo derivatives and metal complexes of Indandion. *Journal of Molecular Structure*, *1198*, 126885. https://doi.org/10.1016/j.molstruc.2019.126885.

[7]. Mutlu, H., Geiselhart, C. M., & Barner-Kowollik, C. (2018). Untapped potential for debonding on demand: the wonderful world of azo-compounds. *Materials Horizons*, *5*(2), 162-183. https://doi.org/10.1039/C7MH00920H.

[8]. Li, X., Wu, Y., Gu, D., & Gan, F. (2010). Spectral, thermal and optical properties of metal(II)-azo complexes for optical recording media. *Dyes and Pigments*, *86*(2), 182-189. https://doi.org/10.1016/j.dyepig.2010.01.002.

[9]. Arab, P., Rabbani, M. G., Sekizkardes, A. K., İslamoğlu, T., & El-Kaderi, H. M. (2014). Copper(I)-catalyzed

synthesis of nanoporous azo-linked polymers: Impact of textural properties on gas storage and selective carbon dioxide capture. *Chemistry of Materials*, *26*(3), 1385-1392. https://doi.org/10.1021/cm403161e

[10]. Hodgson, H. H. (1947). The sandmeyer reaction. *Chemical Reviews*, *40*(2), 251-277. https://doi.org/10.1021/cr60126a003.

[11]. Balz, G., & Schiemann, G. (1927). Über aromatische fluorverbindungen, I.: Ein neues verfahren zu ihrer darstellung. *Berichte der Deutschen Chemischen Gesellschaft (A and B Series)*, *60*(5), 1186-1190. https://doi.org/10.1002/cber.19270600539.

[12]. Pschorr, R. (1896). Neue synthese des phenanthrens und seiner derivate. *Berichte der Deutschen Chemischen Gesellschaft*, *29*(1), 496-501. https://doi.org/10.1002/cber.18960290198.

[13]. Meerwein, H., Büchner, E., & van Emster, K. (1939). Über die einwirkung aromatischer diazoverbindungen auf α,β-ungesättigte carbonylverbindungen. *Journal für Praktische Chemie*, *152*(7-10), 237-266. https://doi.org/10.1002/prac.19391520705.

[14]. Gomberg, M., & Bachmann, W. E. (1924). The synthesis of biaryl compounds by means of the diazo reaction. *Journal of the American Chemical Society*, *46*(10), 2339-2343. https://doi.org/10.1021/ja01675a026.

[15]. Roglans, A., Pla-Quintana, A., & Moreno-Mañas, M. (2006). Diazonium salts as substrates in palladium-catalyzed cross-coupling reactions. *Chemical Reviews*, *106*(11), 4622-4643. https://doi.org/10.1021/cr0509861.

[16]. Mo, F., Dong, G., Zhang, Y., & Wang, J. (2013). Recent applications of arene diazonium salts in organic synthesis. *Organic & Biomolecular Chemistry*, *11*(10), 1582. https://doi.org/10.1039/C3OB27366K.

[17]. Oger, N., d'Halluin, M., Le Grognec, E., & Felpin, F. X. (2014). Using aryl diazonium salts in palladium-catalyzed reactions under safer conditions. *Organic Process Research & Development*, *18*(12), 1786-1801. https://doi.org/10.1021/op500299t.

[18]. Felpin, F. X., & Sengupta, S. (2019). Biaryl synthesis with arenediazonium salts: Cross-coupling, CH-arylation and annulation reactions. *Chemical Society Reviews*, *48*(4), 1150-1193. https://doi.org/10.1039/C8CS00453F.

[19]. Naseem, H. A., Aziz, T., Shah, H. R., Ahmad, K., Parveen, S., & Ashfaq, M. (2021). Rational synthesis and characterization of medicinal phenyl diazenyl-3-hydroxy-1h-inden-1-one azo derivatives and their metal complexes. *Journal of Molecular Structure*, *1227*, 129574. https://doi.org/10.1016/j.molstruc.2020.129574.

[20]. Oger, N., Le Grognec, E., & Felpin, F. X. (2015). Handling diazonium salts in flow for organic and material chemistry. *Organic Chemistry Frontiers*, *2*(5), 590-614. https://doi.org/10.1039/c5qo00037h.

[21]. Hu, T., Baxendale, I., & Baumann, M. (2016). Exploring flow procedures for diazonium formation. *Molecules*, *21*(7), 918. https://doi.org/10.3390/molecules21070918.

[22]. Firth, J. D., & Fairlamb, I. J. S. (2020). A need for caution in the preparation and application of synthetically versatile aryl diazonium tetrafluoroborate salts. *Organic Letters*, *22*(18), 7057-7059. https://doi.org/10.1021/acs.orglett.0c02685.

[23]. Filimonov, V. D., Trusova, M., Postnikov, P., Krasnokutskaya, E. A., Lee, Y. M., Hwang, H. Y., & Chi, K. W. (2008). Unusually stable, versatile, and pure arenediazonium tosylates: Their preparation, structures, and synthetic applicability. *Organic Letters*, *10*(18), 3961-3964. https://doi.org/10.1021/ol8013528.

[24]. Callonnec, F. L., Fouquet, E., & Felpin, F. X. (2021). Unprecedented substoichiometric use of hazardous aryl diazonium salts in the heck-matsuda reaction via a double catalytic. *Cycle Organic Letters*, *13*(10), 2646-2649. https://doi.org/10.1021/ol200752x.

[25]. Susperregui, N., Miqueu, K., Sotiropoulos, J. M., Le Callonnec, F., Fouquet, E., & Felpin, F. X. (2012). Sustainable heck–matsuda reaction with catalytic amounts of diazonium salts: An experimental and theoretical study. *Chemistry-A European Journal*, *18*(23), 7210-7218. https://doi.org/10.1002/chem.201200444.

[26]. Oger, N., Le Callonnec, F., Jacquemin, D., Fouquet, E., Le Grognec, E., & Felpin, F. X. (2014). Heck–matsuda arylation of olefins through a bicatalytic approach: Improved procedures and rationalization. *Advanced Synthesis & Catalysis*, *356*(5), 1065-1071. https://doi.org/10.1002/adsc.201301144.

[27]. Mihelac, M., Siljanovska, A., & Kosmrlj, J. (2021). A convenient approach to arenediazonium tosylates. *Dyes and Pigments*, *184*, 108726. https://doi.org/10.1016/j.dyepig.2020.108726.

[28]. Honraedt, A., Raux, M. A., Grognec, E. L., Jacquemin, D., & Felpin, F. X. (2014). Copper-catalyzed free-radical C-H arylation of pyrroles. *Chemical Communications*, *50*(40), 5236-5238. https://doi.org/10.1039/C3CC45240A.

[29]. Bonin, H., Fouquet, E., & Felpin, F. X. (2011). Aryl diazonium versus iodonium salts: Preparation, applications and mechanisms for the suzuki–miyaura cross-coupling reaction. *Advanced Synthesis & Catalysis*, *353*(17), 3063-3084. https://doi.org/10.1002/adsc.201100531.

[30]. Reed, C. A. (2009). H+, CH3+, and R3Si+ Carborane reagents: When triflates fail. *Accounts of Chemical Research*, *43*(1), 121-128. https://doi.org/10.1021/ar900159e.

[31]. Reed, C. A. (2000) Taming superacids: Stabilization of the fullerene cations HC60+ and C60·+. *Science*, *289*(5476), 101-104. https://doi.org/10.1126/science.289.5476.101.

[32]. Geis, V., Guttsche, K., Knapp, C., Scherer, H., & Uzun, R. (2009). Synthesis and characterization of synthetically useful salts of the weakly-coordinating dianion [B12Cl12]2-. *Dalton Transactions*, *2009*(15), 2687-2694. https://doi.org/10.1039/b821030f.

[33]. Knoth, W. H., Miller, H. C., Sauer, J. C., Balthis, J. H., Chia, Y. T., & Muetterties, E. L. (1964). Chemistry of boranes. IX. Halogenation of B10H10-2 and B12H12-2.

Inorganic Chemistry, *3*(2), 159-167. https://doi.org/10.1021/ic50012a002.

[34]. Gu, W., & Ozerov, O. V. (2011). Exhaustive chlorination of [B12H12]2- without chlorine gas and the use of [B12Cl12]2- as a supporting anion in catalytic hydrodefluorination of aliphatic C-F bonds. *Inorganic Chemistry*, *50*(7), 2726-2728. https://doi.org/10.1021/ic200024u.

[35]. Rempala, P., & Michl, J. (2003). A proposed mechanism of [closo-CB11H12]- formation by dichlorocarbene insertion into [nido-B11H14]-. A computational study by density functional theory. *Collection of Czechoslovak Chemical Communications*, *68*(3), 644-662. https://doi.org/10.1135/cccc20030644.

[36]. Mueller, L.O. (2008). *Weakly coordinating anions and lewis superacidity* [Doctoral dissertation, Albert Ludwig University of Freiburg]. Retrieved from https://d-nb.info/988804875/34.

[37]. Pecyna, J., Rončević, I., & Michl, J. (2019). Insertion of carbenes into deprotonated nido-undecaborane, B11H13(2-). *Molecules*, *24*(20), 3779. https://doi.org/10.3390/molecules24203779.

[38]. Douvris, C., & Michl, J. (2013). Update 1 of: Chemistry of the carba-closo-dodecaborate(-) Anion, CB11H12-. *Chemical Reviews*, *113*(10), PR179-PR233. https://doi.org/10.1021/cr400059k.

BOR DERGİSİ
JOURNAL OF BORON
https://dergipark.org.tr/boron

Bakır matrisli hibrit kompozitlerde krom, bor ve bor karbür takviyelerinin tribolojik özelliklere etkisinin incelenmesi

Merve Horlu[1,*], Cevher Kürşat Macit[2], Gamze İspirlioğlu Kara[3] Burak Tanyeri[4], Bünyamin Aksakal[4]

[1]*Aisin Otomotiv Sanayi Ticaret A.Ş. Tuzla, İstanbul, 34953, Türkiye*
[2]*Fırat Üniversitesi, Mühendislik Fakültesi, Makine Mühendisliği Bölümü, Elazığ, 23000, Türkiye*
[3]*Atatürk Üniversitesi, Mühendislik Fakültesi, Makine Mühendisliği Bölümü, Erzurum, 25000, Türkiye*
[4]*Fırat Üniversitesi, Sivil Havacılık Yüksekokulu, Uçak Bakım ve Onarım Bölümü, Elazığ, 23000, Türkiye*

MAKALE BİLGİSİ

Makale Geçmişi:
İlk gönderi 11 Eylül 2023
Kabul 9 Ekim 2023
Online 29 Aralık 2023

Araştırma Makalesi

DOI: 10.30728/boron.1358658

Anahtar kelimeler:
Bakır
Bor
Bor Karbür
Hibrit Kompozit
Triboloji
Toz Metalurjisi

ÖZET

Bu çalışmada saf bakır (Cu) tozuna ağırlıkça sabit oranda Krom (Cr) (%1) ve ayrı olarak belirli oranlarda Bor (B) (%1, %2, %3) ile Bor karbür (B_4C) (%1, %2, %3) tozlarının eklenmesiyle hibrit bir karışım hazırlanmıştır. Cu tozunun Cr, B ve B_4C tozları ile karıştırılmasında toz metalurjisi üretim parametrelerinden yararlanılmıştır. Hazırlanan hibrit kompozitlerin, mikroyapı (X-Işını Difraktometresi (XRD), Taramalı Elektron Mikroskobu (SEM) ve Enerji Dağılımı X-Işını (EDX)), sertlik ve kuru koşullar altında sabit kayma mesafesinde aşınma testleri gerçekleştirilmiştir. Her kompozit numune için ağırlık kaybı grafikleri oluşturulmuş ve sürtünme katsayısı değerleri hesaplanmıştır. Aşınma deneyleri sonrasında aşınma yüzeylerinde meydana gelen aşınma izleri SEM analizleri ile incelenmiştir. Sertlik ve aşınma testleri sonucunda en iyi sonuçları veren hibrit kompozit Cu-Cr-3B olurken, en düşük performans ise saf Cu numunesinde görülmüştür. Cu-Cr-3B kompozitinde Cu numunesine göre sertlik değerinde %32, aşınma ağırlığında ise %151 oranında daha iyi sonuç elde edilmiştir. Aşınma sonrası SEM görüntülerinde, B ve B_4C parçacıklarının aşınma yüzeyindeki direnci artırdığı gözlenmiştir. Çalışmada elde edilen sonuçlara göre ülkemiz için önemli bir yeri olan B ve B_4C'nin Cu matrisli kompozitlerin tribolojik özelliklerini artırdığı ve çalışmaların yeni hibrit karışımlarla devam edebileceğini göstermiştir.

Investigation of the effect of chromium, boron, and boron carbide reinforcements on tribological properties in copper matrix hybrid composites

ARTICLE INFO

Article History:
Received September 11, 2023
Accepted October, 2023
Available online December 29, 2023

Research Article

DOI: 10.30728/boron.1358658

Keywords:
Copper
Boron
Boron Carbide
Hybrid Composites
Tribology
Powder Metallurgy

ABSTRACT

In this study, a hybrid mixture was prepared by adding Chromium (Cr) (1%) in a fixed ratio by weight and Boron (B) (1%, 2%, 3%), and Boron carbide (B_4C) (1%, 2%, 3%) powders separately in certain ratios to pure copper (Cu) powder. Powder metallurgy production parameters were utilized for mixing Cu powder with Cr, B and B_4C powders. The prepared hybrid composites were tested for microstructure (X-Ray Diffraction (XRD), Scanning Electron Microscope (SEM), and Energy dispersive X-ray (EDX)), hardness, and wear at constant sliding distance under dry conditions. Weight loss plots and coefficient of friction values were generated for each composite sample. After the wear tests, the wear marks on the wear surfaces were analyzed by SEM analysis. As a result of hardness and wear tests, the hybrid composite Cu-Cr-3B gave the best results, while the pure Cu sample had the lowest performance. In Cu-Cr-3B composite, 32% better results were obtained in hardness value and 151% better results were obtained in wear weight compared to Cu sample. In the SEM images after wear, it was observed that B and B_4C particles increased the resistance on the wear surface. According to the results obtained in the study, it has shown that B and B_4C, which have an important place for our country, increase the tribological properties of Cu matrix composites and that studies can continue with new hybrid mixtures.

1. Giriş (Introduction)

Bakır (Cu) matrisli kompozitler, yüksek gerilme mukavemeti, yüksek Young modülü, aşınma direnci, iyi elektrik iletkenliği ve termal iletkenlik gibi üstün mekanik ve fiziksel özelliklerinden dolayı geniş çapta araştırılmıştır. Bu nedenle, elektronik paketler, soğutucular ve yakıt hücresi elektrotları alanlarında kullanılmak üzere potansiyel yüksek performanslı malzemeler olarak kabul edilirler [1-4].

*Corresponding author: mervehorlu@gmail.com

Cu, otomotiv, elektrik ve elektronik sektörlerinde kullanılan çeşitli mühendislik malzemeleri için önemli özellikler taşımasına rağmen, uygulama alanlarında sınırlamaları vardır. Bu kısıtların üstesinden gelmek için temel faktör olan mekanik ve tribolojik özelliklerin iyileştirilmesi amacıyla doğru takviye elemanlarını seçmek gereklidir [5]. Özellikle bakır matrisli kompozitlerin yukarıda belirtilen özellikler için endüstride kullanılabilecek en uygun malzemeler olduğu ve daha uzun ömürlü kullanılabileceği düşünülmektedir.

Cu ve alaşımları, geleneksel ve ileri şekillendirme (aralarında karıştırmalı döküm, basınçlı döküm, toz metalurjisi (TM), basınçlı sıvı metal süzdürme tekniği, derin çekme, haddeleme, sıcak ekstrüzyon gibi sıcak ve soğuk şekillendirme) teknikleri ile rahat ve hızlı bir şekilde üretilmektedir. Son zamanlarda TM ile malzeme üretimi en hızlı büyüyen üretim yöntemlerinden biri haline gelmiştir. Metal matrisli kompozitlerin kristal kafes yapıları nedeniyle haddeleme ve ekstrüzyon gibi geleneksel yöntemlerle şekillendirilebilirliğinin kısıtlı olması, bu alaşımların farklı yöntemlerle şekillendirilmesi konusunda çalışmalar yapılmasını gerekli hale getirmiştir. TM üretim yöntemi, karışık metal tozlarının oda sıcaklığında veya yüksek sıcaklıkta, yapılacak parçanın şekil ve boyutlarına göre bir kalıpta preslenip kalıplanması ve ardından belirli bir sıcaklıkta sinterlenmesiyle gerçekleştirilen bir üretim yöntemidir [6-8]. Cu bazlı toz metalurjisi işlemlerinde, sürtünme bileşenleri olarak kullanılan tekli seramik partiküller, Cu matristeki eşit olmayan dağılım ve daha düşük bağlanma ara yüzü mukavemeti nedeniyle sürtünme performansının kararlılığını önemli ölçüde iyileştirmez. İki veya daha fazla parçacığın kullanılması, yüksek sıcaklıkta mükemmel sürtünme performansı elde etmek için performans ve yapının tamamlayıcısını sağlayabilirken, metal matrisin güçlü karbür oluşturucu elementlerle (örneğin bor) alaşımlanması, Cu'nun ara yüzey yapısının iyileştirilmesine yarar sağlar [9].

Çalışmada takviye olarak kullanılan B_4C partiküllerinin, yüksek sıcaklıktaki bir ortamda kolayca oksitlenerek B_2O_3 çökelmesine neden olduğu bilinmektedir [10]. Bu durum aşınma yüzeyinde sürtünme performansını artırmak için iyi bir yağlama filmi oluşturabilen akışkanlığa sahiptir [11]. Sathiskumar ve ark., takviye olarak kullanılan B_4C partiküllerinin aşınma mekanizması üzerindeki etkisini gözlemlemiştir [12]. Aşınma üzerinde B_4C takviyesinin aşındırmaya bir direnç oluşturduğu görülmüştür. Balalan ve ark., B_4C içeriğinin (ağırlıkça %1,5-6) Cu matris kompozitlerin mikro yapısı üzerindeki etkisini araştırmış ve B_4C içeriğinin artmasıyla daha üstün aşınma direncinin oluştuğunu ortaya koymuştur [13].

Bor takviyeli Cu matrisli kompozitler yüksek sertlik, mukavemet ve termal stabilite gibi özelliklere sahip olabilir. Bor korozyona dayanıklı bir malzeme olduğundan, Cu matrisli kompozitlerde takviye malzemesi olarak kullanıldığında korozyon direncini artırabilir [12,13]. Oda sıcaklığında bor, metallerde çok düşük çözünürlüğe sahiptir. Sertleşebilirlik ve dönüşüm özellikleri üzerinde önemli bir etkiye sahip olmasısebebiyle metallerin yüksek sıcaklık direnci, yüksek mukavemet, yüksek elastikiyet, yüksek yüzey koruması, yüksek aşınma ve korozyon direnci, yüksek yapışma ve yapışma gibi özelliklerini geliştirmede büyük fayda sağlar [14].

Yapılan araştırmalarda Cu matrisli malzemelere katkılanan diğer bir takviye elemanı ise kromdur (Cr). Cr takviyeli kompozitler, farklı takviye kategorileri ile takviye edilmiş kompozitlere kıyasla üstün refrakterliği, sertleşebilirliği artırması, nispeten ucuz olması, kolayca geri dönüştürülebilir ve üstün tribolojik özellikleri olması nedeniyle diğer alaşım elementlerinden bir adım öndedir ve tercih edilmektedir [15].

Bu çalışmada ise, saf Cu tozuna ağırlıkça %1'de sabit kalacak şekilde Cr, ağırlıkça %1, %2 ve %3 oranlarında B_4C ve ağırlıkça %1, %2 ve %3 oranlarında B eklenerek yeni iki ayrı hibrit karışımı yapılmıştır. Literatür çalışmaları incelendiğinde Cu tozlarına bu çalışmadaki gibi Cr-B ve Cr-B_4C takviyeleriyle hibrit bir karışım yapılmadığı görülmüştür. Hazırlanan numunelerin mikroyapısı (SEM, EDX ve XRD), sertliği ve 10 N yük altında kuru şartlarda aşınma testleri yapılarak aşınma sonrası ağırlık kaybı miktarı, sürtünme katsayısı değişimi ve aşınma sonrası aşınma yüzey deformasyonun SEM analizleri ile incelenmiştir.

2. Malzemeler ve Yöntemler (Materials and Methods)

2.1. Hibrit Kompozit Karışımların Hazırlanması (Preparation of Hybrid Composite Mixtures)

Çalışmada kullanılan tozların isimlendirilmesi ve ağırlıkça katkı miktarları Tablo 1'de gösterilmiştir.

Tablo 1. Çalışmada kullanılan takviye elemanlarının ağırlıkça katkı miktarları ve isimlendirilmesi (Nomenclature and contribution amounts of the reinforcing elements used in the study).

Numune	Ağ. (%)			
	Cu	Cr	B_4C	B
Cu	100	-	-	-
Cu-Cr	99	1	-	-
Cu-Cr-1B	98	1	-	1
Cu-Cr-2B	97	1	-	2
Cu-Cr-3B	96	1	-	3
Cu-Cr-1B_4C	98	1	1	-
Cu-Cr-2B_4C	97	1	2	-
Cu-Cr-3B_4C	96	1	3	-

Hibrit kompozit karışımların hazırlanma aşamaları Şekil 1' de gösterilmiştir. Hazırlanan numuneler 12 mm çapa ve 5 mm et kalınlığına sahip olacak şekilde hazırlanmıştır. Matris malzeme ve takviye elemanları Nanografi (Ankara) firmasından satın alınmıştır. Kompozit malzemelerin birleştirilmesinde, tozlar ilk

olarak Şekil 1'deki karışım oranlarına göre tartımları yapılmıştır. Manyetik karıştırıcıda 750 rpm'de 75 dakika boyunca karıştırılmıştır. Karıştırma işleminden sonra karışımlar 25 ml etanol içerisinde 20 dakika boyunca ultrasonik homojenizatörde homojenize edilmiştir. Karıştırılan tozlar 24 saat boyunca 80°C'de vakumlu fırında kurutulmuştur. Birbirine yakın partikül boyutlarına sahip tozların homojen karışımı tamamlanmıştır. Karıştırma işleminden sonra kompozitler 35 MPa basınçta soğuk presleme tekniği ile preslenmiştir. Presleme sırasında tozların kalıp içerisinde daha kolay çıkması için kalıbın içi çinko stearat ($Zn(C_{18}H_{35}O_2)_2$) ile yağlanmıştır.

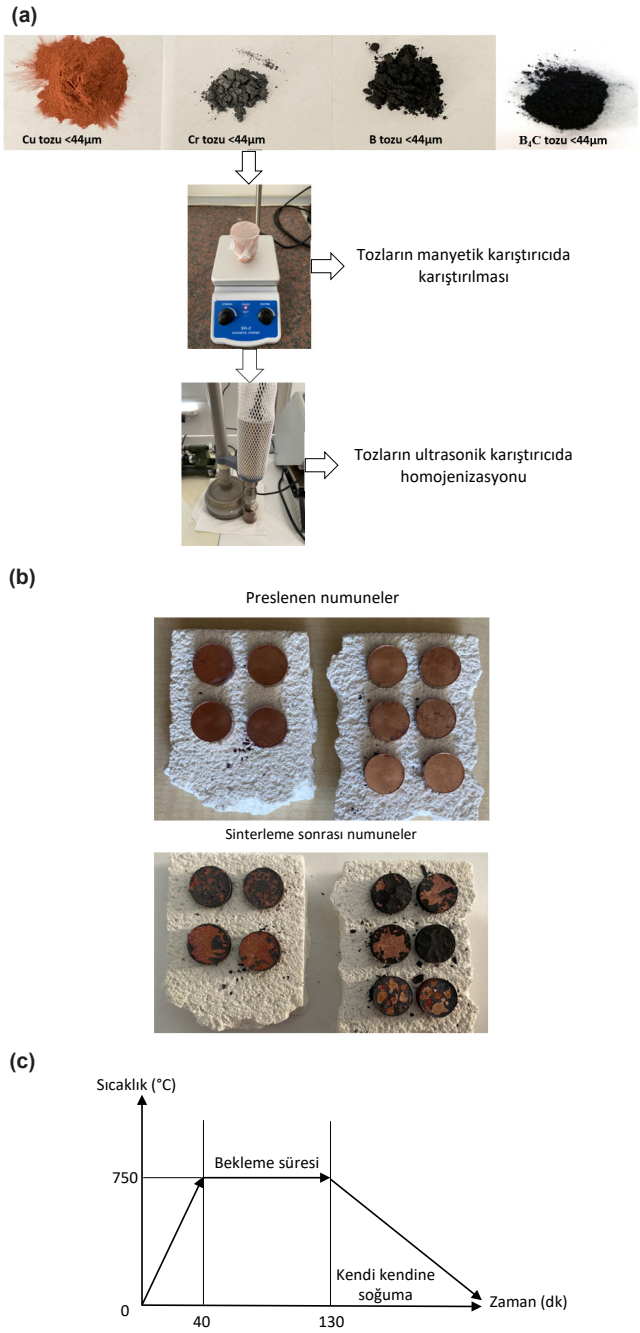

Şekil 1. a). Hibrit karışımların hazırlanması, b). Üretilen numuneler, c). Sinterleme sıcaklık-zaman grafiği (a). Preparation of hybrid mixtures, b). Produced samples, c). Sintering temperature-time graph).

Sinterleme sıcaklığı seçilirken matris malzeme ve takviye malzemeleri arasında kimyasal reaksiyonlara yol açabilen yüksek işleme sıcaklıkları benimsenir; böylece, kompozit malzeme ara yüzünün bağ kuvvetini ve özelliklerini değiştiren yeni bir intermetalik bileşik oluşur. Sinterleme işlemi Cu'nun ergime noktasından düşük olan 750°C'de argon atmosferinde 90 dakika bekleme süresinde gerçekleştirilmiş ve bu süre ile sıcaklık belirlenirken literatür çalışmalarından yararlanılmıştır [10,16,17]. Üretilen numuneler ve sinterleme zaman grafiği Şekil 1'de gösterilmiştir.

2.2. Karakterizasyon (Characterization)

Sinterlenmiş numuneler, mikroyapı ve sertlik testleri yapılmadan önce bakalite alınmıştır. Bakalit numunelerin mikroyapılarının daha net incelenebilmesi için zımparalama ve parlatma işlemleri gerçekleştirilmiştir. Numuneler sırasıyla saf su ve alkol ile yıkanmıştır. Numunelerin mikroyapılarında Cu matris yapısı içerisinde dağılmış takviye element partiküllerinin belirlenmesi ve aşınma sonrası yüzeylerin incelenmesi için SEM ve EDX (Zeiss EVO MA10) analizleri yapılmıştır. Hazırlanan numunelerin faz tanımlaması için XRD (Rigaku RINT-2000 X) 2θ=10 ila 80° tarama aralığında ve 40 kV/40 mA ile gerçekleştirilmiştir.

2.3. Sertlik ve Aşınma (Hardness and Wear)

Sertlik testlerinde HV_{30}'da 15 saniye bekleme süresinde 3 farklı noktadan alınan değerlerin ortalaması alınarak sertlik değerleri belirlenmiştir. Aşınma testleri pin-on-disk aşınma test cihazı ile 10 N yük, 50 mm/sn kayma hızı ve toplam 1000 metre kayma mesafesi altında kuru aşınma koşullarında çelik aşınma pimi kullanılarak gerçekleştirilmiştir. Toplam 1000 metre kayma mesafesinde, numunelerin ağırlık kaybı her 100 metrede bir 10^{-4} hassasiyet değerine sahip bir hassas terazide ölçülmüş, ölçülen değerler kaydedilmiş ve her numune için mesafeye göre ağırlık kaybı grafikleri oluşturulmuştur. Aşınma testlerindeki diğer işlem olan sürtünme katsayılarının belirlenmesi için her bir numune 1000 metre kayma mesafesi boyunca aşındırılmış ve kompozitlerin sürtünme katsayısı değerleri aşınma test cihazında kaydedilmiştir. Kaydedilen sürtünme katsayısı değerleri bilgisayara aktarılmış ve sürtünme katsayısı grafikleri oluşturulmuştur.

3. Sonuçlar ve Tartışma (Results and Discussion)

3.1. Mikroyapı (Microstructure)

Mikroyapı analizi için hazırlanan numuneler üzerinde ilk olarak XRD analizi gerçekleştirilmiştir. XRD analizleri Şekil 2' de gösterilmiştir. XRD analizleri bakalit alınmayan metalografik olarak hazırlanan ve sinterlenen numunelerden alınmıştır. XRD analizi sonucunda Cu matris yapısı içerisinde Cr, B ve B_4C takviye elamanlarının oluştuğu görülmüştür. XRD analizlerinde bakır (Cu), bakır oksit (CuO), bor (B), bor bakır (Cu-B), bor krom (Cr_2B), karbon (C), krom bor

karbür (Cr_7BC_4), bor krom (Cr_2B) ve krom (Cr) bileşik ve elementlerinin piklerinin oluştuğu gözlenmiştir.

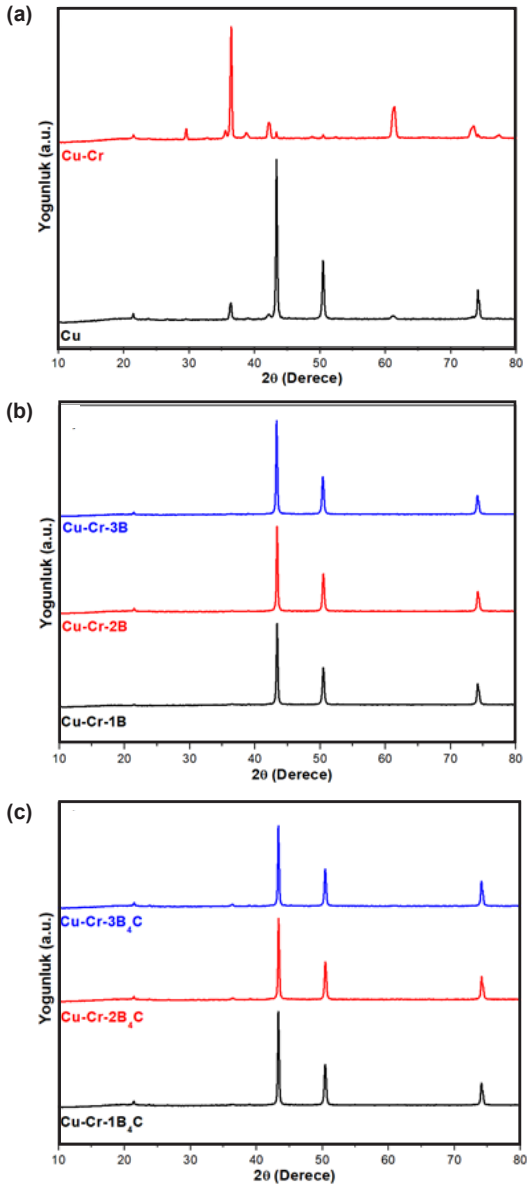

Şekil 2. Hibrit kompozitlerin XRD kırınım desenleri a). Cu, Cu-Cr, b). Cu-Cr-1B, Cu-Cr-2B, Cu-Cr-3B, c). Cu-Cr-1B_4C, Cu-Cr-2B_4C, Cu-Cr-3B_4C (XRD diffraction patterns of hybrid composites a). Cu, Cu-Cr, b). Cu-Cr-1B, Cu-Cr-2B, Cu-Cr-3B, c). Cu-Cr-1B_4C, Cu-Cr-2B_4C, Cu-Cr-3B_4C).

Kompozitlerin 10 kat magnifikasyonlu SEM görüntüleri Şekil 3'te ve numune yüzeylerinden alınan EDX analiz sonuçları Tablo 2'de gösterilmiştir. SEM görüntüleri ve EDX analiz sonuçları takviye elemanlarının matris malzeme üzerinde homojen bir şekilde dağıldığını göstermektedir.

3.2. Sertlik (Hardness)

Numunelerin 3 farklı noktasından alınan sertlik değerlerinin ortalamaları Şekil 4'te gösterilmiştir. B ve B_4C takviye miktarının artması ile kompozitlerin sertlik değerlerinde önemli artışlar gözlenmiştir. En düşük sertlik değeri saf Cu numunesinde elde edilirken diğer

Tablo 2. EDX analiz sonuçları (EDX analysis results).

Numune	Ağ. (%)			
	Cu	Cr	C	B
Cu	100	-	-	-
Cu-Cr	98,91	1,09	-	-
Cu-Cr-1B	96,58	1,34	-	1,83
Cu-Cr-2B	94,51	2,03	-	3,46
Cu-Cr-3B	92,64	1,49	-	5,87
Cu-Cr-1B_4C	94,86	1,17	2,53	1,45
Cu-Cr-2B_4C	94,84	1,42	2,32	3,42
Cu-Cr-3B_4C	88,74	1,52	4,32	5,42

bütün hibrit kompozitlerde sertlik değerlerinin saf Cu'ya göre arttığı görülmüştür. Sertlik testlerinde en yüksek sertlik değeri Cu-Cr-3B kompozitinde elde edilmiştir. B, B_4C ve Cr takviyesinin metal matrisli kompozitlerde sertlik değerini arttırdığı literatür çalışmalarında da görülmektedir [9,11-15,18,19]. B ve B_4C takviye edilmesiyle metal matrisli kompozitlerin sertlik değerleri incelendiğinde, %10; B_4C takviyesiyle bakır-nikel tozları hazırlandığında sertlik değerlerinde ise %102,5'lik yüksek bir sonuç elde edilmiştir [22]. Diğer bir çalışmada ise 316L paslanmaz çeliğine ağırlıkça %0,6'lık B katkısı ile sertlik değerinde %61,25'lik bir artış görülmüştür [14].

Şekil 5' de 10 N yük altında aşınma sonucundaki toplam aşınma ağırlık kayıpları gösterilmiştir. Aşınma testleri sonucunda en fazla ağırlık kaybı değeri saf Cu numunesinde gözlenirken, en az ağırlık kaybı Cu-Cr-3B kompozitinde gözlenmiştir. Cr ve artan B, B_4C katkıları sertlik sonuçlarına benzer şekilde hibrit kompozitlerin aşınma ağırlık kayıplarında da üstün sonuçlar elde edilmiştir [9,11-15,18,19]. Saf B kompozitlerinin B_4C kompozitlerine göre daha üstün sonuçlar vermesinde sinterleme sıcaklığı olarak seçilen 750°C'de B_4C ile Cu matris malzemenin kendi aralarında yeni bileşikler oluşturması ve B/C oranının miktarının sebep olduğu düşünülmektedir [20].

1000 metre kayma mesafesindeki aşınma testleri tamamlanan hibrit kompozitlerin sürtünme katsayısı değerleri Şekil 6'da gösterilmiştir. Sürtünme katsayısı sonuçlarında Cr, B ve B_4C katkılarının sürtünme katsayısı değerini düşürdüğü ve sürtünmeye karşı direncin arttığı gözlemlenmiştir. B ve B_4C katkısının Cu matrisine sıkı bir şekilde bağlanmasıyla köprü görevi görür ve yalnızca mekanik bağlanma yerine kimyasal bağların oluşmasına yol açar; sonuç olarak ara yüzey tabakaya aşınma esnasında zarar vermek için daha fazla enerji tüketilmesi gerekir. B ve B_4C, kırılgan Cu matrisini ve kompozitlerini belirli bir dereceye kadar kırılmaya karşı koruyabilen oldukça yüksek bir dayanıma sahiptir. Literatür çalışmaları incelendiğinde Cr, B ve B_4C katkısının aşınma özellikleri üzerinde olumlu etkisi olduğu görülmüştür [9,11-15,18,19].

Aşınma sonrası hibrit kompozitlerdeki aşınma izlerini incelemek için alınan SEM görüntüleri

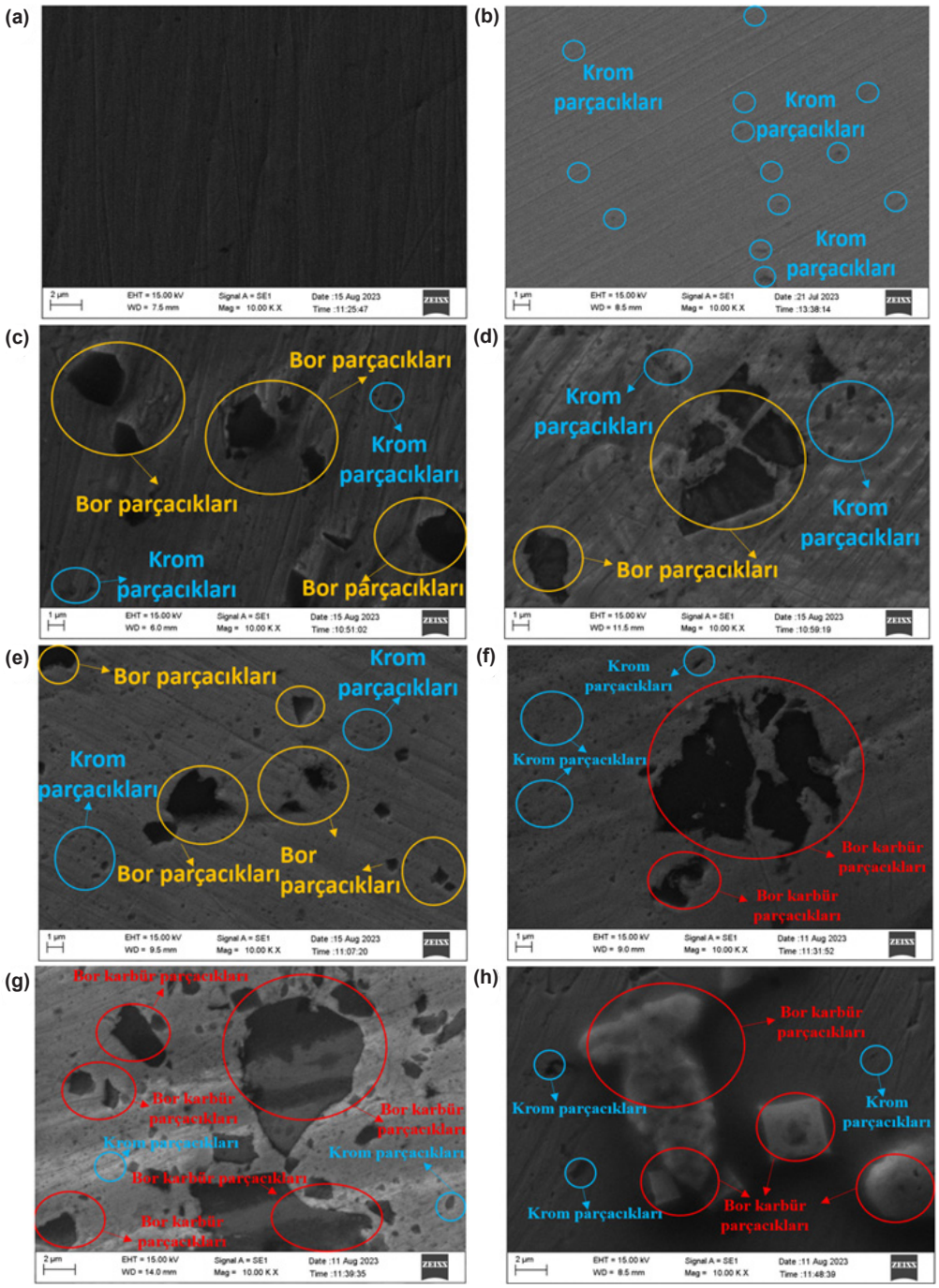

Şekil 3. Hibrit kompozitlerin SEM görüntüleri a). Cu, b). Cu-Cr, c). Cu-Cr-1B, d). Cu-Cr-2B, e). Cu-Cr-3B, f). Cu-Cr-1B_4C, g). Cu-Cr-2B_4C, h). Cu-Cr-3B_4C (SEM images of hybrid composites a). Cu, b). Cu-Cr, c). Cu-Cr-1B, d). Cu-Cr-2B, e). Cu-Cr-3B, f). Cu-Cr-1B_4C, g). Cu-Cr-2B_4C, h). Cu-Cr-3B_4C).

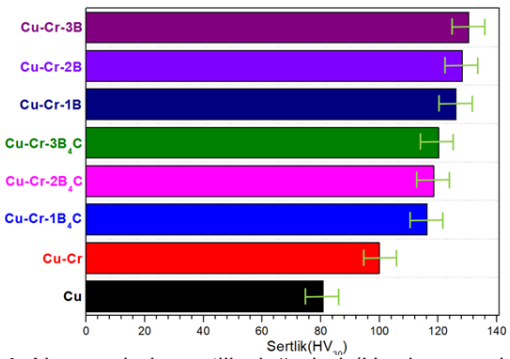

Şekil 4. Numunelerin sertlik değerleri (Hardness values of the samples

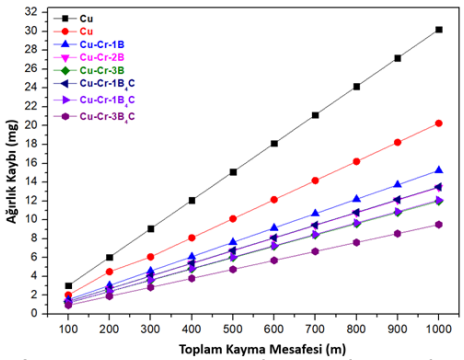

Şekil 5. Aşınma sonrası meydana gelen toplam ağırlık kayıpları (Total weight loss after wear).

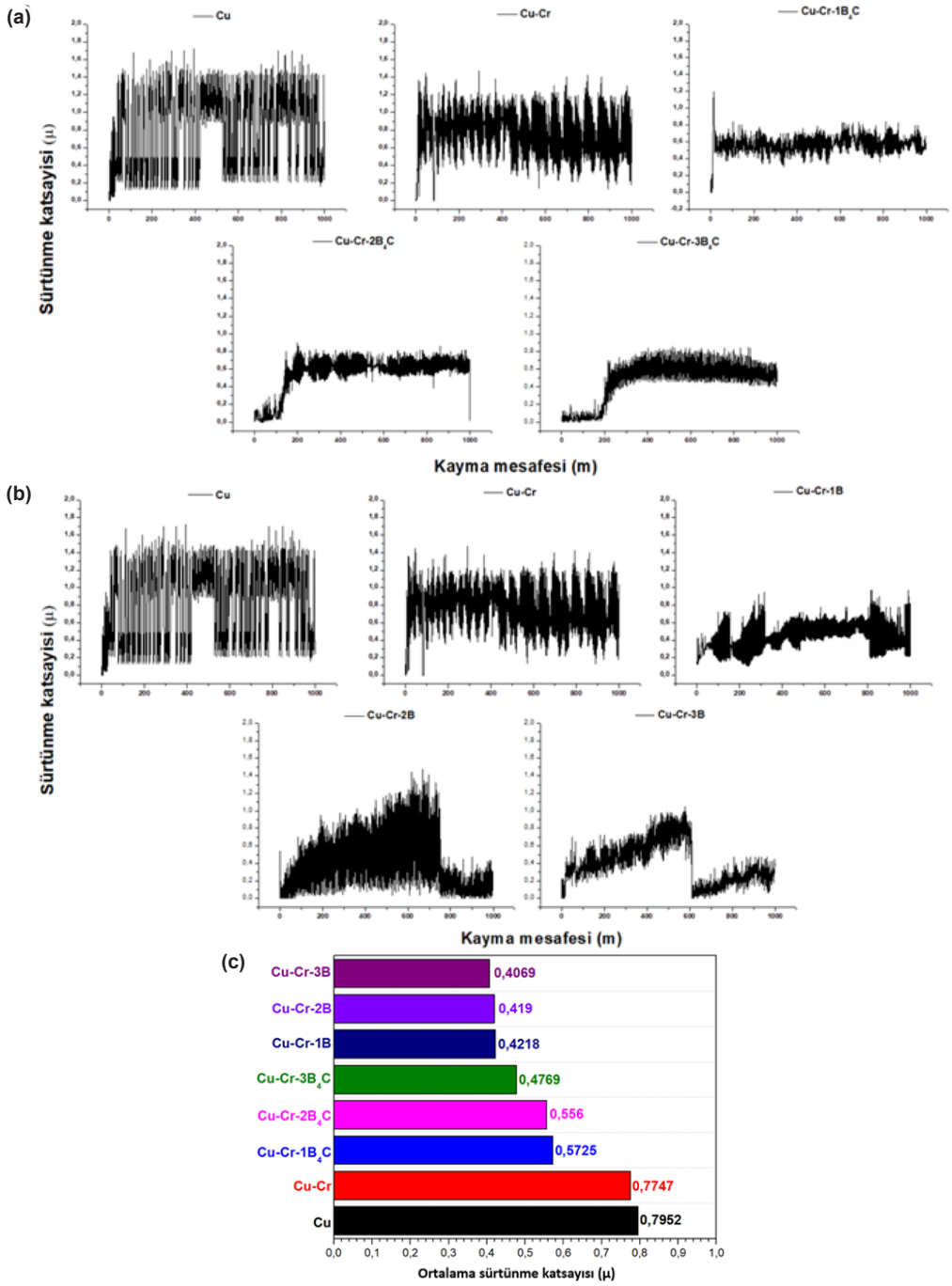

Şekil 6. a). Cr-B_4C takviyeli kompozitlerin b). Cr-B takviyeli kompozitlerin sürtünme katsayıları değerleri ve c). Üretilen bütün kompozitlerin ortalama sürtünme katsayıları (Friction coefficient values of a). Cr-B_4C reinforced composites b). Cr-B reinforced composites and c). Average friction coefficients of all composites produced).

Şekil 7' de gösterilmiştir. SEM görüntülerinde saf Cu numunesinin yüzeyinde aşınma sonrası derin çatlaklar ve izler oluştuğu gözlemlenmiştir. Bor katkısının artması ile aşınma yüzeylerinde daha yoğun B partiküllerinin oluştuğu ve aşınmaya karşı direnci arttırdığı gözlemlenmiştir. Saf Cu ve Cu-Cr numunelerinde görülen çatlakların B ve B_4C takviyeli aşınma yüzeylerinde görülmediği, numunelerin daha az deforme olduğu ve aşınma derinliğinin azaldığı gözlemlenmiştir. B_4C takviyesinin aşındırıcı uç ile Cu matris arasındaki aşınmayı artırıcı bir direnç sergilediği düşünülmektedir [11-17]. Sürtünme katsayısı değerlerindeki azalmanın temel nedeninin ise, kayma aşınması sırasında B miktarının artmasıyla kompozitlerin pim yüzeyinde ince bir yağlayıcı film oluşturması olduğu düşünülmektedir [19]. Ayrıca B, aşınma meydana gelen yüzeylerde grafit benzeri bir yapı oluşturabilir, böylece sınır yağlama rejiminde düşük sürtünmeyi kolaylaştırmıştır [21,22].

4. Sonuçlar (Conclusions)

Üretilen Cu matrisli Cr, B ve B_4C takviyeli kompozitlerin mikroyapı, sertlik, aşınma ve sürtünme katsayısı özellikleri deneysel olarak incelenmiştir. Yapısal ve morfolojik analizler sonucunda XRD analizlerinde matris

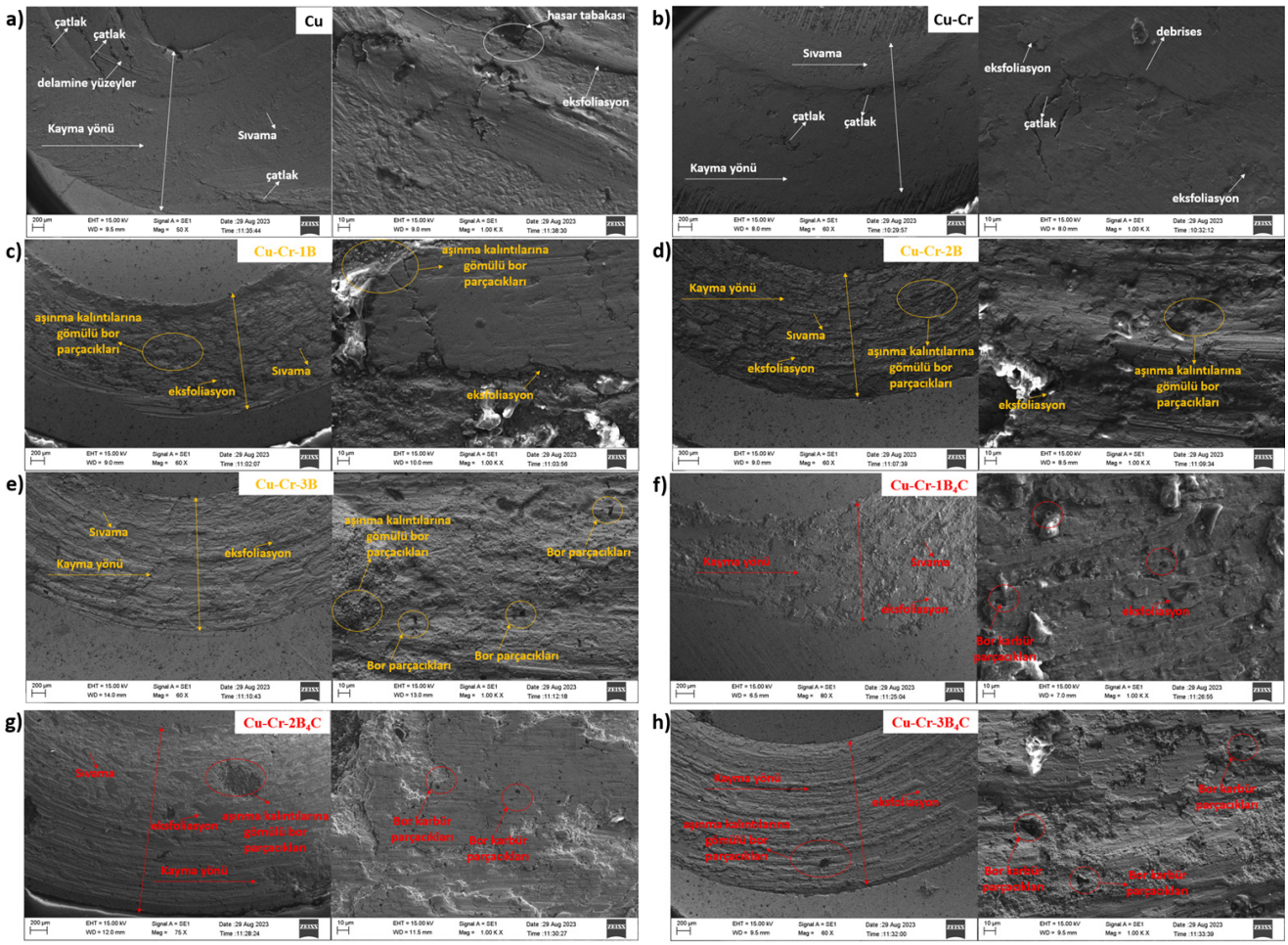

Şekil 7. Aşınma sonrası SEM görüntüleri a). Cu, b). Cu-Cr, c). Cu-Cr-1B, d). Cu-Cr-2B, e). Cu-Cr-3B, f).Cu-Cr-1B_4C, g). Cu-Cr-2B_4C, h). Cu-Cr-3B_4C (SEM images after wear a). Cu, b). Cu-Cr, c). Cu-Cr-1B, d). Cu-Cr-2B, e). Cu-Cr-3B, f).Cu-Cr-1B_4C, g). Cu-Cr-2B_4C, h). Cu-Cr-3B_4C).

malzemenin ve takviye elemanlarının karakteristik piklerini koruduğu ve her bir kompozisyonun arasında yeni bileşiklerin oluştuğu gözlemlenmiştir. SEM görüntülerinde ise takviye elemanlarının matris yapı üzerinde homojen bir şekilde dağıldığı görülmüştür. Çalışmadaki tüm takviyeli kompozitlerin sertlik değerleri saf Cu numunesine göre önemli ölçüde artmıştır. En yüksek sertlik değerine sahip Cu-Cr-3B hibrit kompozitinde saf Cu numunesine göre %61,26'lık daha yüksek bir değer elde edilmiştir. Ağırlıkça yüzde 3 B_4C takviyesinde ise saf Cu numunesine kıyasla sertlik değerinde %48,66'lık bir artış görülmüştür. Cr, B ve B_4C takviyeleri hibrit kompozitlerin aşınma direncini artırmıştır. Saf Cu numune ile karşılaştırıldığında, Cu-Cr-3B kompoziti %217 daha düşük toplam ağırlık kaybı ve %95,86 daha düşük sürtünme katsayısı değeri ile en iyi sonuçları elde etmiştir.

Kaynaklar (References)

[1]. Liu, Q., He, X. B., Ren, S. B., Zhang, C., Ting Ting, L., & Qu, X. H. (2014). Thermophysical properties and microstructure of graphite flake/copper composites processed by electroless copper coating. *Journal of Alloys and Compounds*, *587*, 255-259. https://doi.org/10.1016/j.jallcom.2013.09.207.

[2]. Tjong, S. C., & Ma, Z. Y. (2000). Microstructural and mechanical characteristics of in situ metal matrix composites. *Materials Science and Engineering: R: Reports*, *29*(3-4), 49-113. https://doi.org/10.1016/S0927-796X(00)00024-3.

[3]. Xiaosong, J., Liu, W., Li, J., Shao, Z., & Zhu, D. (2015). Microstructures and mechanical properties of Cu/Ti3SiC2/C/MWCNTs composites prepared by vacuum hot-pressing sintering. *Journal of Alloys and Compounds*, *618*, 700-706. https://doi.org/10.1016/j.jallcom.2014.08.221.

[4]. Yoo, S. J., Han, S. H., & Kim, W. J. (2013). A combination of ball milling and high-ratio differential speed rolling for synthesizing carbon nanotube/copper composites. *Carbon*, *61*, 487-500. https://doi.org/10.1016/j.carbon.2013.04.105.

[5]. Thankachan, T., & Prakash, K. S. (2017). Microstructural, mechanical and tribological behavior of aluminum nitride reinforced copper surface composites fabricated through friction stir processing route. *Materials Science and Engineering: A*, *688*, 301-308. https://doi.org/10.1016/j.msea.2017.02.010.

[6]. Kumar Bhoi, N., Singh, H., & Pratap, S. (2020). Synthesis and characterization of zinc oxide reinforced aluminum metal matrix composite produced by microwave sintering. *Journal of Composite*

Materials, *54*(24), 3625-3636. https://doi.org/10.1177/0021998320918646.

[7]. Tandon, R., & Madan, D. (2014). Emerging applications using magnesium alloy powders: a feasibility study. In Alderman, M., Manuel, M.V., Hort, N., & Neelameggham, N.R. (Eds.). *Magnesium Technology 2014* (pp. 21-25). Springer, Cham. https://doi.org/10.1007/978-3-319-48231-6_7.

[8]. Burke, P., Kipouros, Y. G., Judge, W. D., & Kipouros, G. J. (2019). Surprises and Pitfalls in the Development of Magnesium Powder Metallurgy Alloys. In Dobrzanski, L. A., Bamberger, M., & Totten, G. E. (Eds.). *Magnesium and Its Alloys* (pp. 337-373). CRC Press. https://doi.org/10.1201/9781351045476.

[9]. Weber, L., & Tavangar, R. (2007). On the influence of active element content on the thermal conductivity and thermal expansion of Cu-X (X=Cr, B) diamond composites. *Scripta Materialia*, *57*(11), 988-991. https://doi.org/10.1016/j.scriptamat.2007.08.007.

[10]. Islak, S., Kır, D., & Buytoz, S. (2014). Effect of sintering temperature on electrical and microstructure properties of hot pressed Cu-TiC composites. *Science of Sintering*, *46*(1), 15-21. https://doi.org/10.2298/SOS1401015I.

[11]. Zhang, D., He, X., Liu, Y., Bai, F., & Wang, J. (2021). The effect of in situ nano-sized particle content on the properties of TiCx/Cu composites. *Journal of Materials Research and Technology*, *10*, 453-459. https://doi.org/10.1016/j.jmrt.2020.12.037.

[12]. Uzunsoy, D. (2010). Investigation of dry sliding wear properties of boron doped powder metallurgy 316L stainless steel. *Materials & Design*, *31*(8), 3896-3900. https://doi.org/10.1016/j.matdes.2010.02.053.

[13]. Hsu, C. Y., Yeh, J. W., Chen, S. K., & Shun, T. T. (2004). Wear resistance and high-temperature compression strength of Fcc CuCoNiCrAl 0.5Fe alloy with boron addition. *Metallurgical and Materials Transactions A*, *35*, 1465-1469. https://doi.org/10.1007/s11661-004-0254-x.

[14]. Li, J., Gan, L., Liu, Y., Mateti, S., Lei, W., Chen, Y., & Yang, J. (2018). Boron nitride nanosheets reinforced waterborne polyurethane coatings for improving corrosion resistance and antifriction properties. *European Polymer Journal*, *104*, 57-63. https://doi.org/10.1016/j.eurpolymj.2018.04.042.

[15]. Sreenivasa, R., & Mallur, S. B. (2021). Sliding wear behavior of Cu+ Sn+ Cr composites by Taguchi technique. *Journal of Bio-and Tribo-Corrosion*, *7*, 1-8. https://doi.org/10.1007/s40735-020-00465-5.

[16]. Pham, V. T., Bui, H. T., Tran, B. T., Nguyen, V. T., Le, D. Q., Than, X. T., & Phan, N. M. (2011). The effect of sintering temperature on the mechanical properties of a Cu/CNT nanocomposite prepared via a powder metallurgy method. *Advances in Natural Sciences: Nanoscience and Nanotechnology*, *2*(1), 15006. https://doi.org/10.1088/2043-6262/2/1/015006.

[17]. Kumar, N., Bharti, A., Dixit, M., & Nigam, A. (2020). Effect of powder metallurgy process and its parameters on the mechanical and electrical properties of copper-based materials: Literature review. *Powder Metallurgy and Metal Ceramics*, *59*, 401-410. https://doi.org/10.1007/s11106-020-00174-1.

[18]. Sathiskumar, R., Murugan, N., Dinaharan, I., & Vijay, S. J. (2013). Characterization of boron carbide particulate reinforced in situ copper surface composites synthesized using friction stir processing. *Materials Characterization*, *84*, 16-27. https://doi.org/10.1016/j.matchar.2013.07.001.

[19]. Balalan, Z., & Gulan, F. (2019). Microstructure and mechanical properties of Cu-B4C and CuAl-B4C composites produced by hot pressing. *Rare Metals*, *38*(12), 1169-1177. https://doi.org/10.1007/s12598-019-01287-2.

[20]. Deepa, J. P., Resmi, V. G., Rajan, T. P. D., Pavithran, C., & Pai, B. C. (2011). Studies on the effect of processing parameters on electroless coating of copper on boron carbide particles. *Transactions of the Indian Institute of Metals*, *64*, 47-51. https://doi.org/10.1007/s12666-011-0009-5.

[21]. Shah, F. U., Glavatskih, S., & Antzutkin, O. N. (2013). Boron in tribology: from borates to ionic liquids. *Tribology Letters*, *51*, 281-301. https://doi.org/10.1007/s11249-013-0181-3.

[22]. Zuo, H., Wei, W., Yang, Z., Li, X., Ren, J., Xian, Y., … & Wu, G. (2021). Performance enhancement of carbon/copper composites based on boron doping. *Journal of Alloys and Compounds*, *876*, 160213. https://doi.org/10.1016/j.jallcom.2021.160213.

BOR DERGİSİ
JOURNAL OF BORON
https://dergipark.org.tr/boron

Amonyum floroborat katkılı PAN nanofiberlerin termal davranışının incelenmesi

Havva Tutar Kahraman [1,*], **Ayhan Abdullah Ceyhan** [1]

[1]*Konya Teknik Üniversitesi, Mühendislik ve Doğa Bilimleri Fakültesi, Kimya Mühendisliği Bölümü, Konya, 42250, Türkiye*

MAKALE BİLGİSİ

Makale Geçmişi:
İlk gönderi 12 Eylül 2023
Kabul 11 Ekim 2023
Online 29 Aralık 2023

Araştırma Makalesi

DOI: 10.30728/boron.1359170

Anahtar kelimeler:
Amonyum floroborat
Elektro-eğirme
Nanofiber
Poliakrilonitril

ÖZET

Bu çalışmada, amonyum floroboratın (AFB), poliakrilonitril (PAN) polimerinin termal özelliklerine olan etkisi incelenmiştir. Bu amaç için, sürekli nanofiber üretim yöntemlerinden biri olan elektro-eğirme yöntemiyle, PAN ve AFB katkılanmış PAN (PAN-AFB) nanofiber formunda üretilmiştir. Üretilen nanofiberlerin ısıl bozunma davranışı, termal gravimetrik analiz (TGA) ile incelenmiştir. Fiberlerin yapısal karakterizasyonu, Fourier Dönüşümlü Kızılötesi Spektroskopisi (FTIR) ve Taramalı Elektron Mikroskobu (SEM) teknikleri kullanılarak gerçekleştirilmiştir. Elde edilen sonuçlara göre, PAN içerisine eklenen AFB miktarının artması ile nanofiberlerin ağırlık kaybının azaldığı ve termal kararlılığının arttığı gözlenmiştir. Polimer matrisine AFB katkı oranları %0,2, %0,4 ve %0,6 olarak uygulanmıştır. Deneysel çalışmaların sonuçlarına göre, AFB'nin PAN üzerindeki olumlu etkileri gözlenmiş ve termal direncini artırdığı sonucuna varılmıştır. Bunun yanı sıra, SEM görüntüleri, AFB partiküllerinin, PAN içerisinde homojen olarak dağıldığını göstermektedir.

Investigation of thermal behavior of ammonium fluoroborate doped PAN nanofibers

ARTICLE INFO

Article History:
Received September 12, 2023
Accepted October 11, 2023
Available online December 29, 2023

Research Article

DOI: 10.30728/boron.1359170

Keywords:
Ammonium fluoroborate
Electro-spinning
Nanofiber
Polyacrylonitrile

ABSTRACT

In this study, the effect of ammonium fluoroborate (AFB) on the thermal properties of polyacrylonitrile (PAN) polymer was investigated. For this purpose, PAN and AFB doped PAN (PAN-AFB) nanofibers were produced by electro-spinning method. The thermal degradation behavior of produced nanofibers was examined by thermal gravimetric analysis (TGA). Structural characterizations of the fibers were performed using Fourier Transform Infrared Spectroscopy (FTIR) and Scanning Electron Microscopy (SEM) techniques. According to the results, it was observed that the weight loss of the nanofibers decreased and the thermal stability increased with the increase in the amount of AFB added to the PAN. AFB additive ratios of 0.2%, 0.4% ve 0.6% were applied to the polymer matrix. According to the results of the experimental studies, the positive effects of AFB on PAN were observed and it was concluded that these effects increased its thermal resistance. Besides, SEM analysis images showed that AFB particles were homogeneously dispersed in PAN.

1. Giriş (Introduction)

Son yıllarda gerçekleştirilen nanoteknoloji uygulamaları, tekstil ürünlerinde performans artırmayı ve yeni fonksiyonel özellikler kazandırmayı amaçlamaktadır. Nano ölçekli farklı malzeme gruplarının, makro ölçekte üretilmiş durumlarına göre toplam hacim bakımından çok daha yüksek yüzey alanına sahip olduğu bilgisine dayandırılarak, tekstil ve birçok uygulamada kullanılmak üzere nanofiber üretimi alanında yapılan çalışmalarda artış gözlenmektedir [1]. Nano boyutlu malzeme grupları içinde önemli bir yere sahip olan nanofiberler, genellikle çapı 1 mikron altındaki fiber yapılar olarak tanımlanmaktadırlar. Birçok malzeme ile karşılaştırıldığında, nanofiberlerin yüksek mekanik özelliklere ve geniş yüzey alanına sahip olması, bu sınıf malzemeleri daha çok tercih edilir hale getirmiştir [2]. Nanofiber üretme yöntemlerinden biri olan elektro-eğirme yöntemi, diğer üretim yöntemleri arasında en avantajlı olanıdır. Bu yöntem, polimer çözeltisi veya eriyiğine yüksek elektrik alan uygulanarak nanoboyutlu fiberlerin oluşumu ile sonuçlanan çok yönlü bir polimer prosesidir. Polimer solüsyonunun elektrik yüklü jet oluşturabilmesi için proses boyunca yüksek voltaj kaynağı kullanılmaktadır [3]. Toplayıcı plakaya ve enjektör ucuna elektrot bağlanarak polimerik sıvının yüzeyinde yük oluşması esasına dayanarak, prosesin gerçekleştiği söylenebilir [4]. Ancak bu yöntemde, nanofiber

*Corresponding author: hkahraman@ktun.edu.tr

özelliklerini etkileyen birçok unsur vardır ve üretim esnasında bunlar muhakkak göz önünde bulundurulmalıdır. Bunlar, çözelti parametreleri (iletkenlik, yüzey gerilimi, viskozite, derişim); proses parametreleri (uygulanan voltaj, iğne ucu ve toplayıcı arasındaki mesafe, akış hızı, elektrik alan); çevresel etmenler (sıcaklık, nem) olarak sınıflandırılmaktadır. Bu unsurların dikkate alınmasıyla yerine getirilen proses optimizasyonu, istenen düzeyde ve boyutlarda nanofiber üretimine imkân sağlamaktadır.

Günümüzde organik/inorganik esaslı maddelerin, polimerler içine karıştırılarak polimerik malzemelerin uygulanabilirliğinin genişletilmesi önem kazanmaktadır. Bu amaçla, farklı nitelikler kazandırılmış nanofiber kompozitlerin üretimi, çoğunlukla elektro-eğirme işleminden önce polimer çözeltisine farklı katkı maddelerinin eklenmesiyle gerçekleştirilmektedir. Uygun alev geciktirici katkı maddeleri ile oluşturulmuş polimer sistemlerin termal özelliklerinde büyük değişimler gözlenmektedir. Bu tür maddeler, yanmanın başlamasını ve/veya ilerlemesini engelleyerek, müdahale etme süresini artırmaktadırlar. Alev geciktirici özellikteki katkılar, içerdikleri kimyasallara göre ve hedefledikleri polimer tiplerine göre, halojen esaslı, fosfor esaslı, azot esaslı, silikon esaslı, bor esaslı ve inorganik alev geciktiriciler olmak üzere farklı sınıflara ayrılmaktadır [5]. Nihai ürünlere termal dayanım kazandırmak amacıyla borat bileşikleri yaygın olarak kullanılmaktadır. Borat bileşikleri, yüksek dehidrasyon sıcaklığına sahip olmaları, ucuz olmaları ve etkili duman bastırıcı özellik taşımaları nedeniyle polimer esaslı ürünlerin imalatında tercih edilmektedir [6,7]. Bor içerikli floroboratlar grubu da alev geciktirici olarak kullanılan katkı maddelerindendir ve en yaygın kullanılanı amonyum floroborattır (AFB) [8,9]. Bu çalışmada kullanılan AFB, beyaz kristal yapıdadır ve katı haldeki kristal yapısı NH_4BF_4 şeklindedir. AFB, yüksek sıcaklıklarda kübik yapıya sahipken, düşük sıcaklıklarda ortorombik yapıda kristallenmektedir [10]. AFB, alev geciktirici malzeme üretiminde kullanılmasının yanı sıra organik reaksiyonlarda katalizör olarak görev almaktadır. Metal ve lehim işlemlerinde, etanolden su ve metanolün ayrılması prosesinde, mantar ve böcek ile mücadele uygulamalarında olmak üzere endüstrinin birçok farklı alanında kullanılmaktadır [11,12].

Bu çalışmada, termal direnci arttırılmış nanofiber üretimi hedeflenmiştir. Bu amaçla, polimer matris olarak PAN seçilmiş ve AFB katkılanarak elektro-eğirme yöntemiyle PAN nanofiber kompozit üretimi gerçekleştirilmiştir. PAN; kimyasal ve termal kararlılığı, düşük alevlenebilirliği ve yüksek mekanik dayanım göstermesinden dolayı yaygın olarak tercih edilen bir polimerdir [13,14]. Çalışmada kullanılan floroborat bileşiği ile termal direncinin artırılması amaçlanmıştır. Deneysel çalışma sonucu hazırlanan nanofiberlerin termal dayanım dirençleri TGA analizi ile yapısal ve morfolojik özelikleri ise FT-IR ve SEM analizleri ile incelenmiştir.

2. Malzemeler ve Yöntemler (Materials and Methods)

2.1. Malzemeler (Materials)

Çalışma kapsamında kullanılan, PAN, Dimetil Formamid (DMF), Sigma-Aldrich firmasından temin edilmiştir. AFB (NH_4BF_4) ise tarafımızdan Eş. 1'de verilen reaksiyon dikkate alınarak laboratuvar koşullarında üretilmiştir [12].

$$2NH_4HF_2 + H_3BO_3 \leftrightarrow NH_4BF_4 + 3H_2O + NH_3 \quad (1)$$

2.2. Nanofiberlerin Üretimi (Production of Nanofibers)

Deneysel çalışmaların başlangıcında, belirli çalışma şartlarında saf PAN çözeltisinden elektro-eğirme yöntemi (Şekil 1) ile nanofiberler elde edilmiş ve belirlenen bu koşullar, sonrasındaki çalışmalar için standart olarak kabul edilmiştir. 20 kV voltaj uygulanarak, enjektör ucu ve kollektör arasındaki uzaklık 15 mm'de sabit tutularak, 0,1 mL/sa besleme debisi ile AFB katkılı nanofiber üretimine geçilmiştir. Bu aşamada, PAN-AFB nanofiber üretimi amacıyla; ilk olarak DMF ortamında AFB çözülerek, uygun miktarda PAN polimeri ortama eklenmiştir. Farklı miktarlardaki (w/w; %0,2, %0,4 ve %0,6) AFB'nin ayrı ayrı 10 mL DMF ortamında çözünmesi, ultrasonikasyon tekniği ile sağlanmış ve 1 g PAN polimeri eklenerek elektro-eğirme çözeltisi hazırlanmıştır. Homojen çözelti elde etmek amacıyla mekanik karıştırıcıda (50°C) bir gece boyunca karışması sağlanmıştır. En son aşamada, besleme hızının, nanofiber özellikleri üzerine etkisini saptamak amacıyla 0,05 mL/sa, 0,1 mL/sa ve 0,3 mL/sa debileri dikkate alınarak nanofiber örnekleri üretilmiş ve SEM analizi ile fiber çaplarındaki değişimler incelenmiştir.

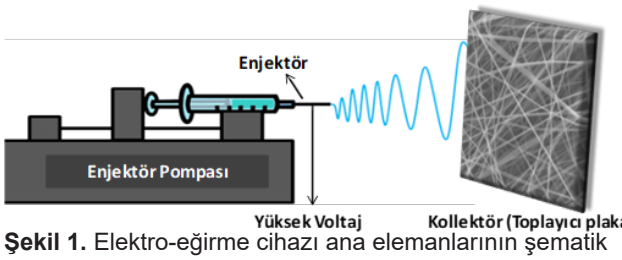

Şekil 1. Elektro-eğirme cihazı ana elemanlarının şematik gösterimi (Schematic representation of the main elements of electro-spinning device).

2.3. Karakterizasyon (Characterization)

2.3.1. Termogravimetrik analiz (Thermogravimetric analysis)

Elektro-eğirme yöntemi ile elde edilen nanofiberlerin termal dayanımlarını tespit etmek amacıyla Mettler Toledo TGA/DSC II Star cihazı kullanılmıştır. Azot atmosferi altında 10°C/dk. ısıtma hızı ile 25-700°C sıcaklık aralığında analiz yapılmıştır.

2.3.2. Fourier dönüşümlü kızıötesi analizi (Fourier transform infrared analysis)

PAN-AFB nanofiberlerin fonksiyonel grup analizleri,

FT-IR spektroskopisi kullanılarak gerçekleştirilmiştir. Infrared çalışmaları, Bruker Bruker-Platinum ATR-vertex 70 spektrometresiyle gerçekleştirilmiştir. Spektrumlar, 400-4000 cm^{-1} aralığında kaydedilmiştir.

2.3.3. Taramalı elektron mikroskobu analizi (Scanning electron microscobe analysis)

Hazırlanan PAN ve PAN-AFB nanofiberlerinin morfolojisi, EVO 1510 ZEISS marka cihaz ile incelenmiştir. Bu teknik aynı zamanda, farklı besleme debilerinin nanofiber boyutlarına olan etkisini incelemek amacıyla kullanılmıştır.

3. Sonuçlar ve Tartışma (Results and Discussion)

3.1. Termogravimetrik Analiz (Thermogravimetric Analysis)

Termal dayanımı incelenecek malzeme ısıtılırken meydana gelen kütle kayıpları gözlenerek, sıcaklık-kütle kaybı eğrisinde kırılmanın oluştuğu sıcaklık değeri bozunma sıcaklığı olarak değerlendirilmektedir. PAN ve PAN-AFB nanofiber örneklerinin 25-700°C aralığında elde edilen termogramları Şekil 2'de verildiği gibidir. Katkısız PAN nanofiber örneğinin TGA termogramı incelendiğinde, görülen bozunma eğrisinde, yapıda yer alan nemin uzaklaşmasından dolayı birinci kütle kaybının yaklaşık 100°C'de gerçekleştiği görülmektedir. İlk dramatik kütle kaybı, %6 oranı ile 285°C'de gerçekleşmiştir. PAN nanofiberinin tüm bozunma eğrisi incelendiğinde, geriye kalan kül oranı, %34,24 olarak hesaplanmıştır.

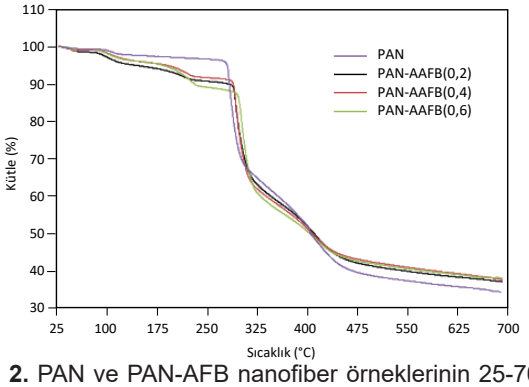

Şekil 2. PAN ve PAN-AFB nanofiber örneklerinin 25-700ºC aralığında elde edilen termogramları (Thermograms of PAN and PAN-AFB nanofibers obtained in the range of 25-700ºC).

Üretilen PAN-AFB nanofiber örnekleri için alınan termogramlar incelendiğinde ise kütle kaybının daha düşük sıcaklıklarda başladığı görülmektedir. Yine aynı şekilde 100°C civarında nanofiber yapısında yer alan nemin uzaklaştığı söylenebilir. Bozunma eğrisinde görülen ilk büyük kütle kaybı, %10-14 oranıyla 282-295°C'de izlenmektedir. İkinci ve üçüncü büyük kütle kaybı, 315°C ile 420°C sıcaklık aralığında gerçekleşmektedir. PAN-AFB (%0,2, %0,4 ve %0,6) nanofiber örneklerinin tüm bozunma sonuçlarına bakıldığında ölçülen kül oranları sırasıyla %37,01, %37,64 ve %38,08 olarak tespit edilmiştir. Bu sonuçlar ışığında nanofiber içeriğinde kullanılan AFB'nin çok düşük miktarlarda kullanılmasına rağmen polimerin termal dayanım özelliklerini artırdığı belirlenmiştir.

Ayrıca polimerik malzemelerin aleve dayanım davranışını belirlemek için dikkate alınan bir diğer değer limit oksijen indeksi (LOI)'dir. Oksijen indeksi, malzemenin yanmaya devam edebilmesi için ortamdan alması gereken oksijen miktarını ifade eder. Bu değerin pratik olarak hesaplanabilmesi için van Krevelen bir eşitlik türetmiş ve TGA termogramından faydalanarak LOI değerini hesaplamıştır [15]. Bu yöntem, ekonomik ve pratik olması açısından malzemelerin alev dayanım direncini belirlemede sıklıkla kullanılır. Bu çalışmada üretilen nanofiberlerin LOI değerleri, Eş. 2 yardımıyla hesaplanmış ve Tablo 1'de verilmiştir. Eş. 2'de yer alan CY (Char Yield) ifadesi, TGA analizi sonucunda her bir örnek için hesaplanan kalıntı miktarını (kül oranını, %) temsil etmektedir.

$$LOI = 17{,}5 + 0{,}4(CY) \quad (2)$$

Tablo 1'de yer alan LOI değerlerine bakıldığında, artan AFB miktarlarıyla birlikte yükselen LOI değerleri tespit edilmiştir. Katkısız PAN nanofiber örneği için hesaplanan değer 31,19 iken, PAN-AFB(0,6) örneğinde yer alan çok düşük miktardaki AFB katkısı (%0,6), LOI değerini yükseltmeyi başarabilmiştir. Bu sonuç, yüksek dehidrasyon sıcaklığına sahip olan AFB partiküllerinin aleve dayanıklı polimerik malzemelerin üretiminde yaygın olarak kullanılabileceği bilgisini desteklemektedir [6]. Ceyhan ve arkadaşları tarafından yapılan çalışmada, AFB'ye özgü üretim şartları belirle¬nerek, yanmaya dayanıklı farklı malze¬melerin üretiminde kullanılabilir yapıda olduğu ifade edilmiştir [12].

3.2. Fourier Transform Infrared Analizi (Fourier Transform Infrared Analysis)

Şekil 3'de PAN ve PAN-AFB(0,4) nanofiberlerine ait FT-IR spektrum analizi verilmiştir. Grafikte yer alan PAN nanofibere ait spektrum incelendiğinde; 3260 cm^{-1}'de C=N-H gerilim bandı tespit edilmiştir. 2940 cm^{-1} ve

Table 1. PAN ve PAN-AFB nanofiberlerinin termogravimetrik analiz sonuçları ve LOI değerleri (Thermogravimetric analysis results and LOI values of PAN and PAN-AFB nanofibers).

	200	250	300	450	700	LOI
PAN	%97,13	%96,64	%70,13	%41,29	%34,46	31,19
PAN-AFB(0,2)	%92,94	%90,71	%74,37	%43,50	%37,01	32,30
PAN-AFB(0,4)	%94,43	%91,69	%74,29	%44,25	%37,64	32,56
PAN-AFB(0,6)	%94,50	%89,12	%79,90	%44,77	%38,08	32,73

2243 cm^{-1} pikleri sırası ile [(C-H) gerilim] ve (-C≡N)'e aittir. 2160 cm^{-1} β-amino-C≡N gerilim bandına işaret etmektedir. 1450 cm^{-1}, 1382 cm^{-1} ve 1251 cm^{-1} pikleri (C-H) eğilme bandına ait piklerdir. 1677 cm^{-1}'deki band, amid gruplarının C=O geriliminden dolayı oluşurken, 1070 cm^{-1} piki C-C gerilim bandını göstermektedir.

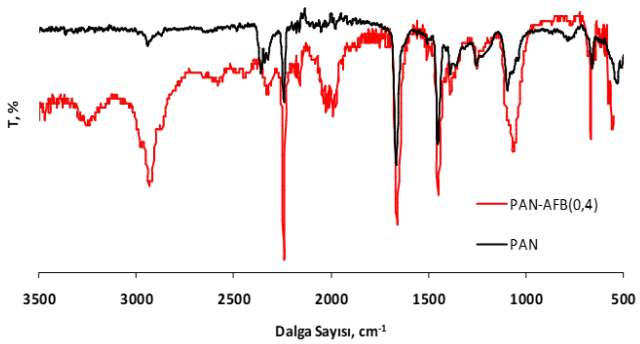

Şekil 3. PAN ve PAN-AFB(0,4) nanofiberlerine ait FT-IR spektrumu (FT-IR Spectra of PAN and PAN-AFB(0.4) nanofibers).

PAN-AFB(0,4) nanofiberlerinin FT-IR sonuçlarına bakıldığında ise NH_4^+ katyonunun, 3240-3290 cm^{-1} ve 1436-1390 cm^{-1} dalga sayısı aralıklarında sırasıyla deformasyon ve gerilme şeklinde iki adet dejenere titreşimine sahip olduğu görülmektedir. Ayrıca, 559 cm^{-1} dalga sayısında B-F geriliminden kaynaklanan bir titreşim mevcuttur [12]. PAN'da bulunan -CN grubundan kaynaklanan pik, 2244 cm^{-1}'de daha keskin olarak gözlenmiştir. Analizde, AFB partiküllerinin katkılandırılmasıyla pik şiddetlerinde değişimler, dalga sayılarında az da olsa değişikliklerin olduğu görülmektedir. Özellikle, 2940 cm^{-1}'de alifatik C-H gerilmelerine işaret eden pik, PAN-AFB nanofiberinde şiddetini artırmıştır. Yapıdaki değişime neden olan yeni bir pik değildir. PAN'ın karakteristik piklerini korumuş olduğu gözlenmektedir. Bu sonuç, PAN nanofiberinin sahip olduğu işlevsel grupların yüzeylerde muhafaza edildiğini göstermektedir.

3.2.1. Taramalı elektron mikroskobu analizi (Scanning electron microscobe analysis)

AFB'nin PAN nanofiber çapları üzerine etkisini incelemek amacıyla SEM analizi yapılmıştır. Şekil 4'te görüldüğü gibi, nanofiberler %0,4 AFB varlığında başarılı bir şekilde elde edilmiştir. Boncuksuz yapıya sahip homojen PAN-AFB nanofiberleri 250-300 nm aralığında düzgün bir yapıya sahiptir. İşlem parametrelerinin hassas kontrolü ile farklı çaplara ve yapıya sahip nanofiberlerin elde edilebileceği sonucuna varılabilir.

Nanofiber çapını ve yapısını etkileyen parametrelerden biri olan polimer çözeltisi besleme hızının etkisini gözlemlemek için farklı besleme debileriyle nanofiber örnekleri üretilmiştir. SEM mikrografları ve çap dağılım grafikleri 0,05; 0,1; 0,3 mL/sa besleme debisi değerleri kullanılarak üretilen nanofiberler için Şekil 5'te verilmiştir.

Her üç besleme debisinde de elde edilen nanofiberlerin homojen ve hemen hemen boncuksuz bir yapıya sahip olduğu gözlenmiştir. Ancak nanofiber çaplarına bakıldığında farklılık hemen göze çarpmaktadır. En düşük besleme debisinde fiber çapı 380-400 nm; 0,1 mL/sa. debi ile üretilen fiber çapları 300-310 nm iken, 0,3 mL/sa debi ile elde edilen fiberlerin çapları ise 220-240 nm aralığında değiştiği görülmektedir.

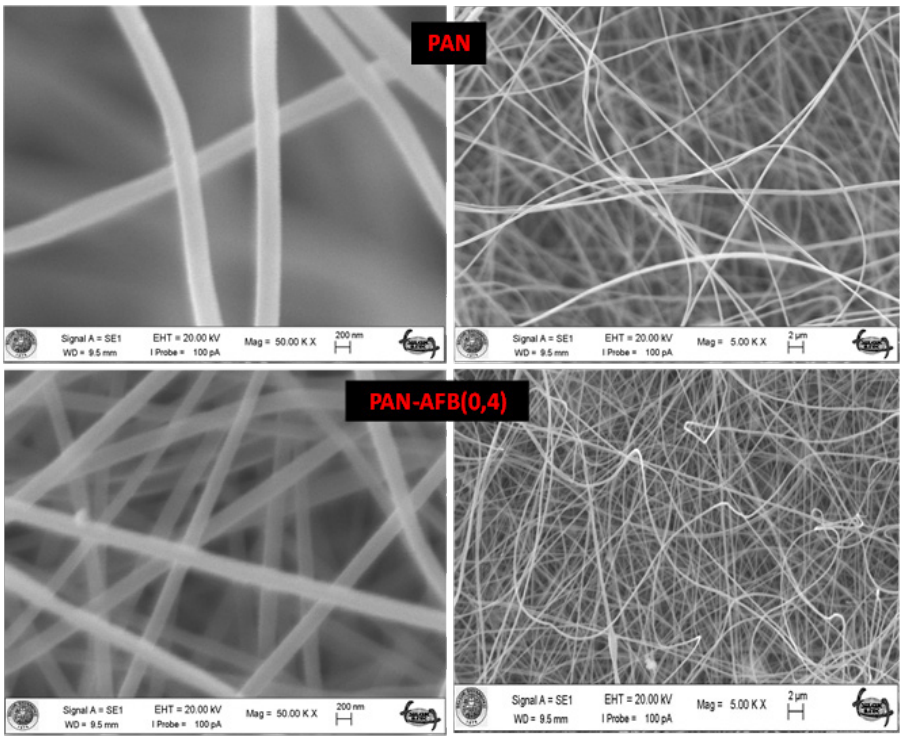

Şekil 4. PAN ve PAN-AFB(0,4) nanofiberlerine ait SEM görüntüleri (SEM images of PAN and PAN-AFB(0.4) nanofibers).

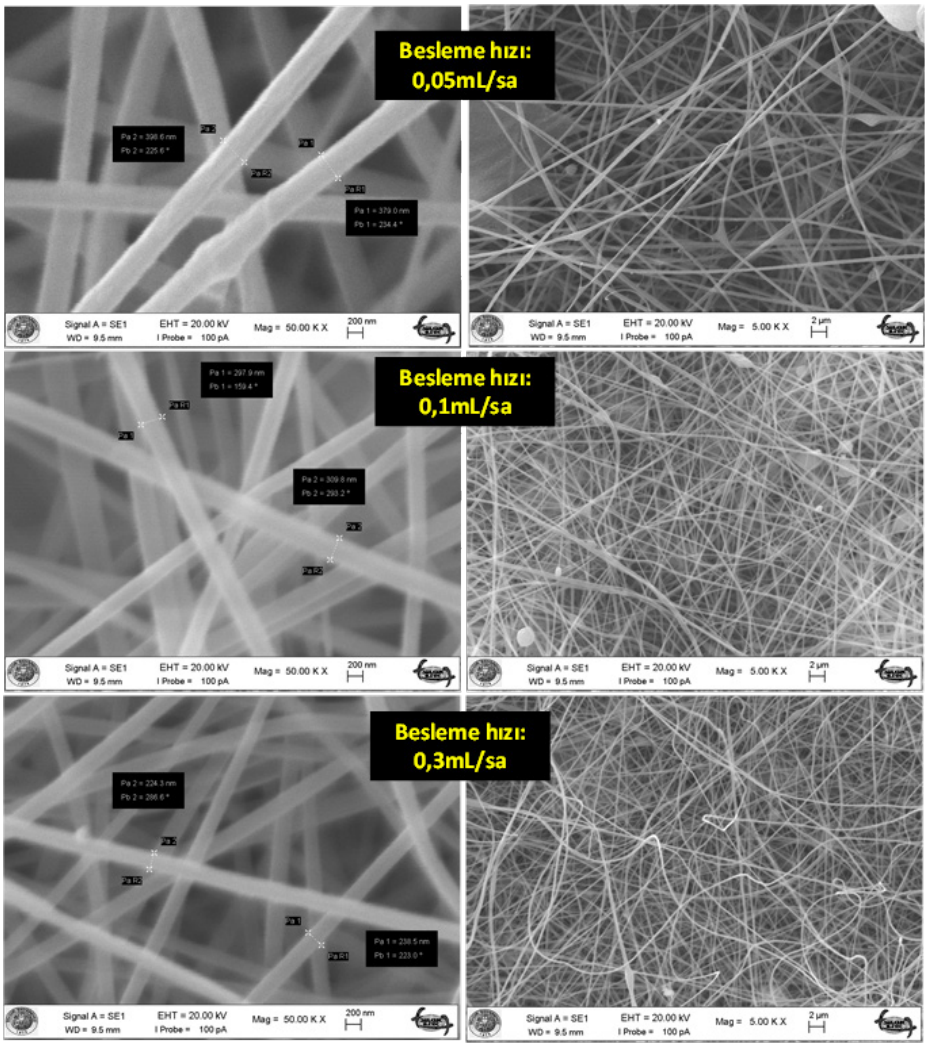

Şekil 5. Farklı besleme debileriyle üretilmiş PAN-AFB nanofiberlerinin SEM görüntüleri (SEM images of PAN-AFB nanofibers produced at different flow rates).

Nasir ve arkadaşları tarafından yapılan bir çalışmada benzer bir sonuç elde edilmiştir [16]. Bu çalışmada, artan besleme debisiyle fiber çapının giderek düştüğü ve yine artan besleme debisinde yüzey yük yoğunluğunun da düştüğü sonucuna varılmıştır. Farklı morfolojilerin, çözelti besleme debisini kontrol ederek elde edilebileceği belirtilmiştir. Aynı zamanda, belirli bir elektrik alanda denge şartlarında ancak oluşabilen Taylor Konisi teorisinin göz önünde bulundurulmasının önemli olduğu vurgulanmıştır. Benzer şekilde, Theron ve ark. tarafından yapılan bir çalışmada PVDF nanofiberleri elde edilmiş ve besleme debisinin artmasıyla fiber çaplarının düştüğü ve daha homojen bir dağılım sergilediği belirlenmiştir [17].

4. Sonuçlar (Conclusions)

Polimer ve tekstil endüstrisinde malzemelerin alev dayanım özelliklerini iyileştirmek için farklı inorganik katkı maddeleri kullanılmaktadır. Borat bileşikleri, diğer alev geciktirici kimyasallara nazaran, yandığında zehirli gaz açığa çıkarmadığı için çevre dostu bir kimyasal olarak karşımıza çıkmaktadır. Bu çalışmada, bir borat bileşiği olan AFB'nin, PAN'ın termal dayanım özelliği üzerine etkisi incelenmiştir. Elektro-eğirme tekniği ile PAN ve AFB içerikli PAN-AFB nanofiberleri başarılı bir şekilde üretilmiştir. Yapılan çalışmada ana hedef, PAN'ın termal direnci üzerine AFB etkisini ortaya koymaktır. Bu amaçla, artan miktarlarda AFB katkılanarak polimer çözeltileri hazırlanmış ve nanofiber formunda üretilmiştir. Uygulanan TGA analizi ve bu analiz yardımıyla hesaplanan LOI değerlerine göre PAN'ın termal dayanımının yükseldiği ve sıcaklığa karşı bir direnç kazandığı gözlemlenmiştir. Bunun yanı sıra, yapılan SEM analizi ile AFB'nin nanofiber formunu deforme etmediği, boncuksuz homojen dağılım gösteren kesiksiz lifsi yapıların üretimine olanak tanıdığı sonucuna varılmıştır. Polimerin LOI değerlerinde belirgin etkisi olduğu saptanan AFB'nin, farklı uygulamalarda alev geciktirici olarak kullanılabileceği düşünülmektedir. Bu amaçla gerçekleştirilen bu çalışma, bir ön çalışma niteliğindedir.

Kaynaklar (References)

[1]. Park, M., Kuk, Y. S., Kwon, O. H., Acharya, J., Ojha, G. P., Ko, J. K., Kong, H. S. & Pant, B. (2022). Fly ash-incorporated polystyrene nanofiber membrane as a fire-retardant material: Valorization of discarded materials.

Nanomaterials, *12*(21), 3811. https://doi.org/10.3390/nano12213811.

[2]. Ko, F. K., & Wan, Y. (2014). *Introduction to Nanofiber Materials*. Cambridge University Press. ISBN: 978-0-521-87983-5.

[3]. Li, D., & Xia, Y. (2004). Electrospinning of nanofibers: Reinventing the wheel?. *Advanced Materials*, *16*(14), 1151-1170. https://doi.org/10.1002/adma.200400719.

[4]. Li, W.J., & Tuan, R.S. (2009). Fabrication and application of nanofibrous scaffolds in tissue engineering. *Current Protocols in Cell Biology*, *42*(1), 25.2.1-25.2.12. https://doi.org/10.1002/0471143030.cb2502s42.

[5]. Horrocks, A.R., & Price, D. (Eds.). (2001). *Fire Retardant Materials*. Woodhead Publishing. ISBN: 9781855734197.

[6]. Yılmaz Aydın, D., Gürü, M., Ayar, B., & Çakanyıldırım, Ç. (2016). Applicability of boron compounds as flame retardant and high temperature resistant pigments. *Journal of Boron*, *1*(1), 33-39. https://dergipark.org.tr/tr/pub/boron/issue/18612/196469.

[7]. Gürü, M., Güngör, G., Yılmaz Aydın, D., & Çakanyıldırım, Ç. (2022). The investigation of synthesis parameters, kinetic and flame retardant properties of magnesium fluoroborate. *Chemical Papers*, *76*, 1313-1320. https://doi.org/10.1007/s11696-021-01941-z.

[8]. Gürü, M., Güngör, G., Yılmaz Aydın, D., & Çakanyıldırım, Ç. (2021). Calcium fluoroborate synthesis, determination of kinetics and flame retardant properties. *Journal of Boron*, *6*(3), 326-331. https://doi.org/10.30728/boron.880116.

[9]. Kusakli, S., Kocaman, S., Ceyhan, A. A., & Ahmetli, G. (2020). Improving the flame retardancy and mechanical properties of epoxy composites using flame retardants with red mud waste. *Journal of Applied Polymer Science*, *138*(13), 50106. https://doi.org/10.1002/app.50106.

[10]. Clark, M. J. R., & Lynton, H. (1969). Crystal structures of potassium, ammonium, rubidium, and cesium tetrafluoroborates. *Canadian Journal of Chemistry*, *47*(14), 2579-2586. https://doi.org/10.1139/v69-426.

[11]. Kartal, S. N., Brischke, C., Rapp, A. O., & Imamura, Y. (2006). Biological effectiveness of didecyl dimethyl ammonium tetrafluoroborate (DBF) against basidiomycetes following preconditioning in soil bed tests. *Wood Science and Technology*, *40*, 63-71. https://doi.org/10.1007/s00226-005-0048-3.

[12]. Ceyhan, A. A., Bağcı, S., Baytar, O., & Şahin, Ö. (2020). Ammonium fluoroborate production and determination of production parameters. *Journal of Boron*, *5*(2), 63-72. https://doi.org/10.30728/boron.687130.

[13]. Makaremi, M., De Silva, R. T., & Pasbakhsh, P. (2015). Electrospun nanofibrous membranes of polyacrylonitrile/halloysite with superior water filtration ability. *The Journal of Physical Chemistry C*, *119*(14), 7949-7958. https://doi.org/10.1021/acs.jpcc.5b00662.

[14]. Kahraman, H. T., Avcı, A., & Pehlivan, E. (2019). Novel sandwiched composite electro-spun mats based on polyacrylonitrile and polyvinyl butyral for fast oil-water separation. *Iranian Polymer Journal*, *28*, 445-453. https://doi.org/10.1007/s13726-019-00713-7

[15]. Van Krevelen, D. W., (1975). Some basic aspects of flame resistance of polymeric materials. *Polymer,16*(8), 615-620. https://doi.org/10.1016/0032-3861(75)90157-3.

[16]. Nasir, M., Matsumoto, H., Danno, T., Minagawa, M., Irisawa, T., Shioya, M., & Tanioka, A. (2006). Control of diameter, morphology, and structure of PVDF nanofiber fabricated by electrospray deposition. J*ournal of Polymer Science Part B: Polymer Physics, 44*(5), 779-786. https://doi.org/10.1002/polb.20737.

[17]. Theron, S. A., Zussman, E., & Yarin, A. L. (2004). Experimental investigation of the governing parameters in the electrospinning of polymer solutions. *Polymer, 45*(6), 2017-2030. https://doi.org/10.1016/j.polymer.2004.01.024.

BOR DERGİSİ
JOURNAL OF BORON
https://dergipark.org.tr/boron

Boron and beyond: Where do we stand in cancer diagnosis and treatment?

Öykü Irmak Dikkatli [1,2], Özlem Darcansoy İşeri [3,*]

[1]*Turkish Energy Nuclear Mineral Research Agency (TENMAK), Boron Research Institute (BOREN), Ankara, 06510, Türkiye*
[2]*Department of Molecular Biology and Genetics, Institute of Science, Başkent University, Ankara, 06790, Türkiye*
[3]*Department of Molecular Biology and Genetics, Faculty of Science and Letters, Başkent University, Ankara, 06790, Türkiye*

ARTICLE INFO

Article History:
Received May 17, 2023
Accepted October 1, 2023
Available online December 29, 2023

Review Article

DOI: 10.30728/boron. 1292418

Keywords:
Anti-cancer effects
BNCT
Boron
Boron delivery agents
Cancer

ABSTRACT

The element boron (B) is in the IIIA group of the periodic table, with atom number 5 and molecular weight of 10.81 mol/g. B is a rare element involving many biological processes such as embryonic development, bone structure, and function, oxidative stress, etc. Over the last decades, studies have shown that B-containing compounds regulate reactive oxygen species (ROS) levels, involve DNA damage mechanisms, and inhibit different enzymes. Improvements in medicine led researchers to think about B's potential usage in cancer diagnosis, treatment, and prevention. Nowadays, different research groups have studied B-based compounds on several types of cancer including prostate, lung, breast, colon, skin, brain, melanoma, etc. Studies revealed that B compounds can affect different types of cancers with different pathways/mechanisms. Based on the potential therapeutic effects of B, the first B-containing anti-cancer drug and a first-in-class proteasome inhibitor Bortezomib (Velcade®), was approved by the Food and Drug Administration (FDA) in 2003. On the other hand, boron neutron capture therapy (BNCT) is a very important clinical cancer treatment based on B and B-containing delivery agents. During the past 20 years, researchers developed several new B delivery agents both for BNCT and B itself. In summary, this review article offers an overview of B compounds used for cancer diagnosis and treatment, delivery agents for BNCT, new therapeutic approaches containing B carriers, and novel B-based cancer detection approaches.

1. Introduction

Boron (B) is a rare element on Earth, and it generates just 0.001% of all the elements in the world [1]. 73.4% of all known B reserves are in Türkiye [2]. Two major producers, approximately 62% of Türkiye and 23% of America supply most of the world's B consumption [3]. B belongs to the periodic table's IIIA group, which is a metalloid (half-metal) with an atom number 5 with molecular weight of 10.81 mol/g. There are 230 known B derivatives, however, there is no B in its free form in nature. The most important B types are borax or tincal ($Na_2B_4O_7.10H_2O$), boric acid (H_3BO_3, BA), colemanite ($CaB_3O_4(OH)_3.H_2O$), kernite or rasorite ($Na_2B_4O_7.4H_2O$), and ulexite ($NaCaB_5O_9.8H_2O$). B is found in sedimentary rocks, water, soil, and air in nature. Organisms absorb a trace quantity of the B into their bodies through the water and food they consume. Almost all the B entering living systems is absorbed by the gastrointestinal system. Green vegetables and fruits, nuts, fish, milk, and meat have a high content of B [4]. A wide range of application areas may benefit from B's advantages, and it can be used in more than 400 different industries, including the nuclear, pharmaceutical, fertilizer, automotive, glass and ceramics, chemistry, cleaning, aerospace, cosmetics, weapon, agri-food industries, energy and construction industries, metallurgy, superconductors, electronics, and medicine [5]. Studies on the biological and toxicological effects of B on a variety of organisms have led to an increase in the usage of B in medicine. Studies have shown that it participates in calcium metabolism and hormone activity. However, the role of B in biological processes is not fully known yet. Though it is not classified as an "absolutely essential element" for humans, the World Health Organization (WHO) defined B as a "possibly essential element" in 1996 [6]. Daily consumption of B shows different rates in every country and human. However, the average amount of B taken was determined as 1.5-3.0 mg B/ day. WHO defined the maximum daily consumption amount of B as 1-13 mg B/ day for adults [4]. B has effects on many mechanisms, including carbohydrate metabolism, mineral uptake, enzyme function, and the regulation of hematological processes along with the undefined effects. In addition, studies have shown that B and its derivatives may have important roles in the treatment and prevention of some cancer types [7,8].

1.1. Effects of Boron on Human Health

Human intestinal epithelia are capable of absorbing B, and most of the B that has been ingested into the body is excreted in the urine, whereas 2% is excreted

*Corresponding author: odiseri@baskent.edu.tr

in feces and a negligible amount by sweat, breath, and bile. Over the decades, studies have shown that B has a good influence and important roles in embryonic development, energy metabolism, hormone metabolism, bone structure and function, inflammatory response, wound healing, oxidative stress, etc. (Figure 1).

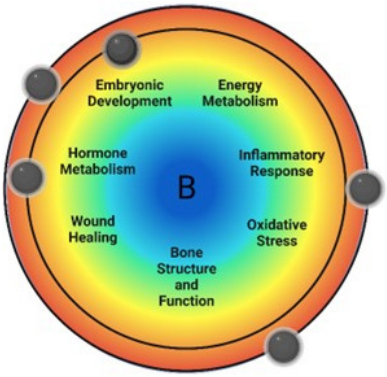

Figure 1. Important processes and pathways that B is involved and has regulatory role (Created with BioRender.com).

B can interact with riboflavin, adenosine monophosphate, pyridoxine, pyrimidine nucleotides, ribose, and polysaccharides [9]. Furthermore, B functions as an inhibitor for proteasome, arginase, nitric oxide synthase, and transpeptidase. Therefore, B-containing drugs could be beneficial for the treatment of various diseases like; arthritis, metabolic abnormalities, neurological issues, and numerous chronic and infectious diseases. For decades, several B compounds have been investigated as antibacterial and antifungal agents such as natural biomolecules, diazaborine, oxazaborolidines, diphenyl borinic esters, and benzoxaborole [10-12]. Studies showed that B-containing compounds regulate reactive oxygen species (ROS) levels and are involved in DNA damage response mechanisms. Based on these properties, researchers defined B and B-containing compounds as important chemopreventive agents [13-16].

1.2. Boron-containing Drugs in Use

To develop new pharmaceutical drugs, the utilization of substances that aren't typically found in organisms has a high chance of yielding unexpected biological action. If a B atom is logically placed into a biologically active molecule (at a site that is close to a donor area in the target protein), interactions with the target protein may be anticipated that involve both covalent and hydrogen bonds, and these interactions would result in a powerful biological activity [17]. Based on this knowledge, various B-containing small molecules have been reported to inhibit different enzymes (Figure 2).

The proteasome inhibitor and anti-cancer drug Bortezomib (Velcade®) was approved by the Food and Drug Administration (FDA) in 2003. In solid tumors and hematological malignancies, it facilitates

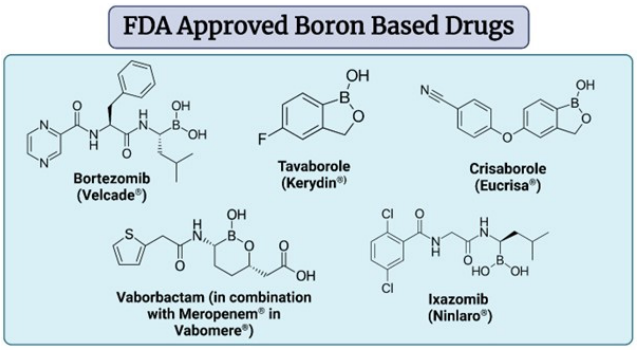

Figure 2. B-containing drugs approved by FDA (Created with BioRender.com).

apoptosis and disrupts the cell cycle [18]. It was the first B-containing drug on the market and a first-in-class proteasome inhibitor. A significant association has been observed with the bortezomib doses and positive regulation of prostate-specific antigen (PSA). When combined with other treatments like radiation or other chemotherapeutics, bortezomib is effective to treat androgen-independent prostate cancer [19]. In addition, the anti-cancer activity of bortezomib has been demonstrated alone and with other cytotoxic agents such as 5-fluorouracil (5-FU), paclitaxel (PTX), gemcitabine (GMT), or doxorubicin (DOX) in other tumor types [18]. Late, two more B compounds, Tavaborole (Kerydin®) and Crisaborole (Eucrisa®), were approved by the FDA in 2014 for treating onychomycosis and atopic dermatitis, respectively [20]. The second-generation B-containing proteasome inhibitor Ixazomib (Ninlaro®) was approved by the FDA in 2015, for multiple myeloma patients who have already undergone at least one prior therapy [21]. Vaborbactam® was the first boronic acid β-lactamase inhibitor to receive FDA approval in 2017 [22]. The FDA also approved the use of Vaborbactam® in combination with Meropenem® (namely Vabomere®) to treat urinary tract infections.

2. Boron as a Chemopreventive and Chemotherapeutic Agent

As the number of people suffering from the disease is increasing around the world, development of novel treatment strategies is gaining more importance. Investigations aim to identify new compounds with novel and effective anti-cancer characteristics. Amongst, B-containing compounds have been demonstrated to have promising effects so far for prostate, breast, cervical, lung, and melanomas [23-25]. Several studies have shown that low B intake is associated with the progression of different types of cancer. An epidemiological study by Cui and coworkers (2014) suggested an inverse relationship between daily B uptake and prostate cancer [23]. Furthermore, some studies revealed that B intake was adversely related to the ratio of cervical cancer [24] and lung cancer [25]. Based on these studies, natural and synthetic B compounds such as borates, sugar-borate esters (SBEs), B polyketides, boranes, boronic acids/esters, borinic acids/esters, and dipyrromethene

boron difluoride (BODIPY) for cancer therapy have been further investigated (Figure 3).

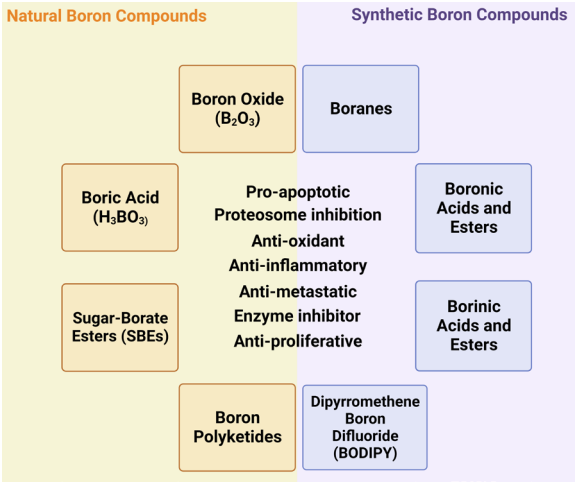

Figure 3. B-containing natural and synthetic compounds and their potential therapeutic effects on cancer (Created with BioRender.com).

Natural B compounds contain BA, boron oxide (BO), sodium pentaborate pentahydrate (NaB), disodium pentaborate decahydrate (DPD), sodium perborate tetrahydrate (SPT), sodium pentaborate decahydrate (SPD), borax pentaborate decahydrate (BP) and numerous different molecules. These natural chemicals contain B-oxygen bonds, and they belong to the borate family. Since they are natural compounds and showed effective therapeutic effects on different diseases, various studies have been investigating their effects on cancer. SBEs are one of the most important members of B-containing natural compounds, and may be found in many different structures like trigonal or tetragonal and mono- or di-esters [26] (Figure 4).

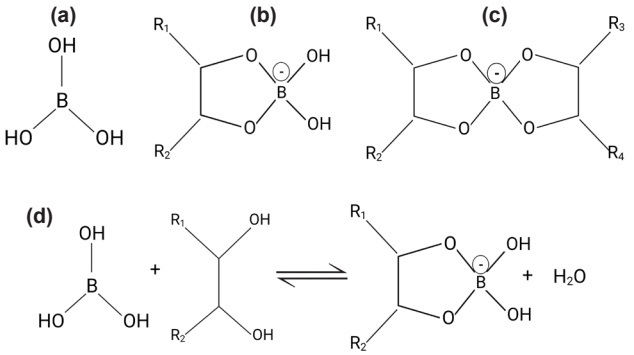

Figure 4. BA a). anionic monoesters b). and anionic diesters with sugars containing cis-hydroxy groups c). d). Esterification reaction of BA with sugars containing cis-hydroxy groups (R=H, alkyl, aryl, acyl, created with BioRender.com).

Amongst, calcium fructoborate (CaFB) is naturally absorbed by animals, and it is less toxic than almost all B compounds. CaFB has shown to be effective in preventing and treating several diseases, including osteoporosis and osteoarthritis. Besides, it also exerted anti-cancer effects through different mechanisms [27]. Another important group is B-containing antibiotics, which include boromycin, tartolons, borophycin, etc. which have been studied for their antibacterial, antifungal, and anti-cancer properties [28].

Boromycin may also cause selective cell cycle arrest of different cancer cell types during the G2 phase and increase the susceptibility of cells to a variety of anti-cancer drugs [29]. In addition, boranes showed important therapeutic effects on many diseases. The most important borane compounds are amine-carboxyboranes, amine-cyanoboranes, carboranes, trimethyl cyanoborane (TACB), and amine-boranes. Studies revealed that amine-carboxyboranes were cytotoxic and exhibited antineoplastic properties against leukemias, lymphomas, sarcomas, and carcinomas [30]. Amine-boranes also showed cytotoxic activities on a variety of cancer cells, and they are potential boron neutron capture therapy (BNCT) agents. TACB was also suggested as a therapeutic agent for its inhibitory function on DNA and protein synthesis [31]. Due to their distinctive characteristics and anti-cancer effects, boronic acids and esters have been researched for decades as potential cancer treatments. Boronic acids are more selective for cancer cells and more stable than BA, which make them attractive compounds for clinical use. Recent developments in BNCT and targeted drug delivery strategies based on boronic acids showed important results for the treatment of cancer. Phenylboronic acid (PBA) and diphenylboronic esters (DPBE), which function as serine protease inhibitors, are the most effective boronic acids and derivatives [30,31]. Another synthetic group, borinic acids contain borinates and oxoboranes which function as enzyme inhibitors and regulators of membrane ion channels. Amongst, BODIPYs are one of the most promising agents for development of therapeutic and diagnostic strategies. BODIPYs are B-based fluorophores probes that can be used to identify specific molecules. BODIPY derivatives can also be used as diagnostic or prognostic tools to identify biomarkers of infections, diabetes, chronic nervous diseases, cancer, and metabolic disorders [31]. Over the decades, important developments in cancer treatment based on B-containing compounds showed very promising results for future clinical applications. Recent studies showed that B-containing compounds can be used for chemotherapy, radiation therapy, targeted drug delivery, bio-imaging tools, and other therapeutic and diagnostic strategies. In this review article, we are mainly interested in the anti-cancer effects of BA, BO, CaFB, PBA, boron nitride (BN), and BODIPYs which are the most investigated and promising B compounds. Furthermore, we will also discuss their potential use in novel drug delivery systems as well as combinational cancer treatment and diagnostic strategies.

2.1. Borates and Their Anti-cancer Effects

As discussed in the previous section, borates are very important B-containing therapeutics. Among these compounds, BO, and BA (Figure 5) tests for cancer treatment are a very common strategy.

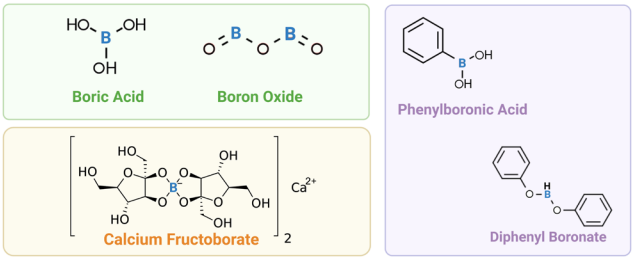

Figure 5. Structures of the most studied B compounds for their chemopreventive and chemotherapeutic potencies (Created with BioRender.com).

Due to its structural characteristics, like carbon, BA can serve as a competitive inhibitor for a variety of carbon-containing molecules. Due to this quality, BA is an excellent candidate to work as a pharmaceutical agent [16,29]. Therefore, chemopreventive and chemotherapeutic effects of BA have been investigated on different types of cancer cells. The proliferation of prostate cancer cells was inhibited in a concentration-dependent manner [32,33], as well as the non-tumorigenic prostate cell lines, though the required concentrations to kill DU-145 and LNCaP prostate cancer cells were lower respectively [32]. BA induced apoptosis, upregulated the pro-apoptotic genes, and downregulated the anti-apoptotic ones in ovarian cancer cells [34]. Cell cycle arrest-related genes were unaffected by BA application. Additionally, the expression of miR-21, miR-200a, miR-130a, and miR-224 was downregulated in the BA-treated groups. Findings suggested that the anti-tumor activity of BA may be related to altered miRNA levels as these miRNAs are indicators of poor prognosis of ovarian cancer. Interestingly, the oxidative stress index was higher in the BA-treated groups, which also claims partition of oxidative stress in cell death [34]. Hepatocellular carcinoma cells had also showed decreased cell viability, survival, colony formation capacity, migration, and spheroid growth due to BA treatment. Furthermore, reduction of the AKT phosphorylation was observed suggesting BA-induced downregulation of the AKT survival pathway [35]. Cebeci and colleagues (2022) demonstrated the anti-cancer properties of borates against a small-cell lung cancer model, DMS-114, for the first time. The findings demonstrated that BA, NaB, and SPT caused apoptosis by upregulating pro-apoptotic genes and downregulating anti-apoptotic ones. Additionally, cell cycle arrest in the G2/M and sub-G1 stages was brought on by BA and NaB. Conclusively, three B-containing compounds studied showed promising results for their effects on small-cell lung cancer cells in comparison to their effects on healthy cells [36]. In another study, 24 mM BA caused a senescence-like profile and DNA breaks on hepatocellular carcinoma HepG2 cells [37]. BA also inhibited growth, caused cell cycle arrest, and promoted apoptosis in medullary thyroid carcinoma cells, and therefore, may be employed as a potential treatment agent for medullary thyroid carcinoma [38].

Tütüncü and associates (2022) examined the impact of BA and DPD on cell survival and apoptosis induction using metastatic prostate cancer cells; DU-145 and PC-3. In both cell lines, DPD and BA therapy lowered cell invasion and decreased cell proliferation. Additionally, BA and DPD-induced the caspase-3-dependent apoptosis. Results indicated that the anti-cancer effects of DPD on the prostate cancer cells were superior over BA [39]. To test the possible effects of BA as a PSA inhibitor and chemopreventive supplement, Gallardo-Williams and coworkers (2004) used androgen-dependent human LNCaP cells to obtain mice xenografts that produce PSA after transplantation [40,41]. Although LNCaP cells developed tumors in nude mice supplemented with BA supplementation, treatment with low and intermediate doses of BA had impacts on growth rate and size of the tumors [42]. Korkmaz and colleagues (2014) showed that DPD therapy caused DU-145 prostate cancer cells to undergo apoptosis by decreasing the activity of the human telomerase reverse transcriptase (hTERT) enzyme at a rate of 38%. In DPD-exposed cells, the regular arrangement of actin filaments was also disturbed, causing change in cell shapes. Overall, findings suggested that DPD may cause cytotoxicity by reducing telomerase and interfering with the dynamic characteristics of actin polymerization [43]. Another compound from the borate family is BO. Albuz and coworkers (2019) studied the effects of BO on colorectal cancer cells for the first time [44]. BO showed strong cytotoxicity on both healthy mouse L929 and DLD-1 colorectal adenocarcinoma cell lines, with no genotoxicity. Kirlangic and coworkers (2022) investigated the cytotoxicity and apoptotic effects of borax on the DLD-1 colorectal adenocarcinoma cell line in combination with 5-FU. The viability of DLD-1 cells significantly decreased by the combined therapy, and the anti-proliferative effects of BA or 5-FU alone or in combination were by induction of apoptosis [45]. Simsek and coworkers (2019) tested the anti-carcinogenic, anti-angiogenic, and anti-oxidant effects of BA, BP, and SPD on the breast adenocarcinoma MDA-MB-231 cells. Results showed that BP and SPD inhibit the angiogenic potential of cells via the vascular endothelial growth factor (VEGF) pathway. This study was also the first one to report the relationship of BP and SPD application with VEGF and inducible nitric oxide synthase (iNOS) expression in a breast cancer cell line [46].

Overall, borates are amongst the most investigated B-containing compounds for their cancer treatment potencies. Single borates and borates in combination with chemotherapeutics have been mostly studied on colon, breast, lung, prostate, and hepatocellular carcinomas. Different types of borates have anti-cancer effects on various cancer types through complex cellular pathways and mechanisms which involve VEGF release, PI3K/Akt pathway, hTERT activity, DNA damage, induction of apoptosis, etc.

2.2. SBEs and Their Anti-cancer Effects

CaFB (Figure 5) is one of the most intriguing SBE compounds due to its properties (Section 2). Tepedelen and coworkers (2017) first investigated the link between CaFB and VEGF expression on MDA-MB-231 cells. According to cytotoxicity tests, CaFB reduced cell viability. Additionally, there was a rise in the levels of phosphorylated ATM and p53 levels, and, but there is no noticeable alteration in ATM or p53 expression. Results also indicated a decrease in VEGF and an increase in caspase-3 and 9 levels [47]. Another study described the time-course biodistribution of liposome-encapsulated CaFB in the BALB/c mice breast cancer model for the first time [48]. Accordingly, a concentration of 35 mg 10B/g enhanced the accumulation of the drug within a 24-hour incubation period following the drug introduction. The findings can be used as a reference point for biologic distribution, and accumulation of the designed drug-containing B for the better understanding of B targeting linked to the drugs. Kisacam and associates (2020) sought to shed light on the preventive effects of CaFB by studying effect of CaFB on the PI3K/Akt pathway in a DMBA (7,12-Dimethylbenz(a)anthracene)-TPA (12-O-tetradecanoylphorbol13-acetate) induced *in vivo* skin cancer model. 92 female ALB/c mice were separated into 6 experimental groups. HRAS, HIF1, Akt, and PTEN protein and mRNA levels increased significantly after topical DMBA and TPA treatments with more TUNEL-positive cells in the DMBA-TPA group. CaFB decreased the mRNA and protein levels of HRAS and HIF1[49]. In addition, the anti-inflammatory and anti-oxidant effects of CaFB were also studied in this model. In contrast to control groups, the DMBA-TPA group had higher levels of GAPDH activity, PGD, GSH, IL-6, IL-1, and TNF-α, but malondialdehyde levels were lower. Depending on the distribution time, the CaFB application reduced the DMBA-TPA-induced effects. Conclusively, CaFB was suggested as a potential chemopreventive against skin cancer [50]. In another study, they have also shown that CaFB affects Akt and PTEN levels and apoptosis in the same skin cancer model [51]. IC_{50} of CaFB for colon cancer cells was reported to be 10 mM, at which apoptosis and autophagy were induced. CaFB modulated the P13K/Akt/p70S6k pathway, elevated Bax, and decreased Bcl-2 levels at 10 and 20 mM. CaFB has the potential to inhibit carcinogenesis, particularly for the skin.

2.3. Boronic Acids/Esters and Their Anti-cancer Effects

As we previously discussed in section 2 PBA and DPBE (Figure 5) are the most effective derivatives of boronic acids, which show selective inhibitory effects on the migration and viability of various types of cancer cells. Therefore, they are considered one of the most important B compounds for the treatment of various cancer types. The inhibitory effects of PBA and BA on the migration of breast and prostate cancer cells were investigated [13]. One mM BA and PBA was administered to DU-145 prostate cancer cells for 8 days. Cell migration decreased after 24-hour treatment with BA or PBA. PBA, on the other hand, had a long-term effect that reduced cell viability whereas exerted short-term anti-migratory effect. In a different experiment, the use of BA or PBA altered the actin distribution of DU-145 cells that were grown on fibronectin, reduced the activity of spreading proteins including the Rho family GTPases and their targets, and caused growth arrest [14]. Another study examined the anti-cancer effects of PBA against mouse dermal fibroblasts L929, hamster lung fibroblast V79, mouse mammary adenocarcinoma 4T1, and mouse squamous cell carcinoma SCC VII cell lines [52]. All cancer and non-cancer cell lines were affected in a concentration-dependent manner. After tumor transplantation into mice, PBA was found to suppress the proliferation of tumor cell lines in comparison to the control. In conclusion, PBA is a better candidate as a novel anti-cancer agent since it is a more effective and specific inhibitor than BA. The use of PBA in diagnostic biosensors and as a drug carrier will be covered in section 3.3.

3. Boron Carriers and Their Applications for Cancer Treatment

Non-specificity, quick clearance, development of drug resistance, toxicity, and damage to healthy cells, side effects, and immune system failures are the major drawbacks of conventional chemotherapy [53]. Innovative targeted drug delivery systems can increase therapeutic and diagnostic efficacy and minimize negative side effects for cancer treatment. Targeted and controlled drug delivery methods are one of the most significant and appealing subjects of nanotechnology to fight against cancer. Main goal in a controlled delivery system is to maintain the medicine at optimum therapeutic levels that are below toxic thresholds while increasing the effectiveness through continuous drug release. The goal of controlled drug delivery systems is to give the drug or chemotherapy at a specific location at a set pace for a longer period of time [54]. For the delivery of chemotherapeutics, many polymeric delivery systems have been developed, such as hydrogels, liposomes (LP), dendrimers, micelles, and nanoparticles (NPs) (both inorganic and polymeric) (Figure 6) [55].

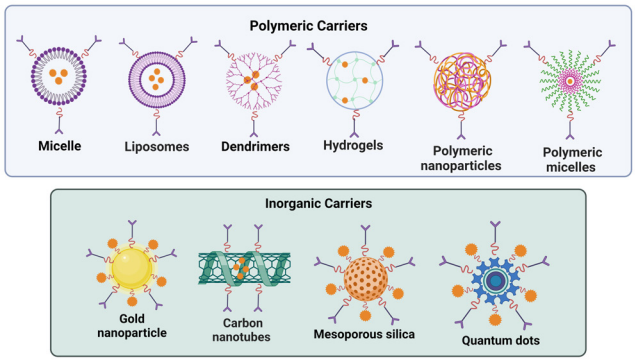

Figure 6. Nano-sized drug delivery systems for cancer treatment (Created with BioRender.com).

Furthermore, these nanocarriers have also been used in different therapeutic strategies, including both photodynamic and photothermal therapies (PDT and PTT), chemotherapy, radiation, hormone, gene, and immunotherapy therapy (Figure 7). When treating cancer, combined chemotherapy is clearly superior to single-agent therapy due to its increased efficacy and fewer restrictions brought on by the emergence of multidrug resistance (MDR) [54]. Combining diverse therapeutic mechanisms in one carrier improves anti-cancer benefits, and using two or more anti-cancer drugs at once maximizes their therapeutic effects [56]. BNCT and advanced B-compounds for drug delivery strategies have taken attention and B-containing compounds and treatment strategies were combined with traditional cancer therapy and chemotherapeutic drugs [57].

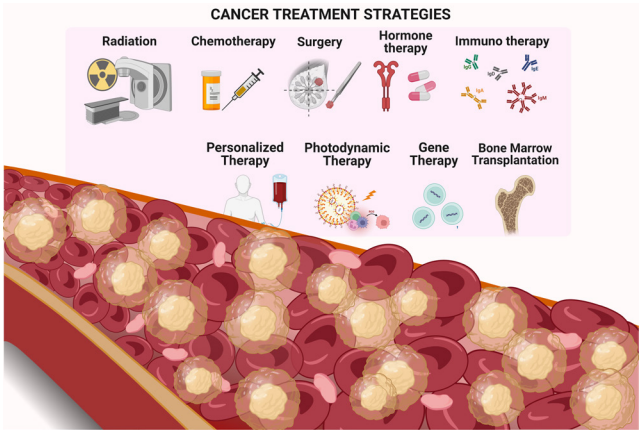

Figure 7. Different strategies for cancer treatment (Created with BioRender.com).

The cutting-edge advancements in pharmaceutical nanotechnology, particularly in BNCT, have found crucial uses for B-based nanomaterials. Both boron nitride nanotubes (BNNT) and hexagonal boron nitrides (h-BN) are desirable nanostructures because they have an enormous surface area, outstanding mechanical properties, and necessary biocompatibility [58]. In addition, PBA has been frequently introduced to drug nanocarriers [59]. So, in this part of the review, the focus is BNCT with emphasis on the different B-containing compounds as drug carriers, and PBA, h-BN, and BODIPY application areas in terms of treatment and diagnosis of cancer.

3.1. BNCT for Cancer Treatment

Since the last decades, BNCT has been used to treat cancer when chemotherapy and radiation therapy have been ineffective. A two-part radiotherapeutic method BNCT employs B neutrons to cure cancer. When the stable isotope B-10 (^{10}B) is exposed to low-energy thermal neutrons (0.025 eV), which turn out thermalized as they diffuse the tissue, nuclear capture, and fission processes happen. This results in the production of recoiling lithium-7 (^{7}Li) nuclei and high-linear energy transfer (LET) alpha (α) particles (^{4}He) [60] (Figure 8).

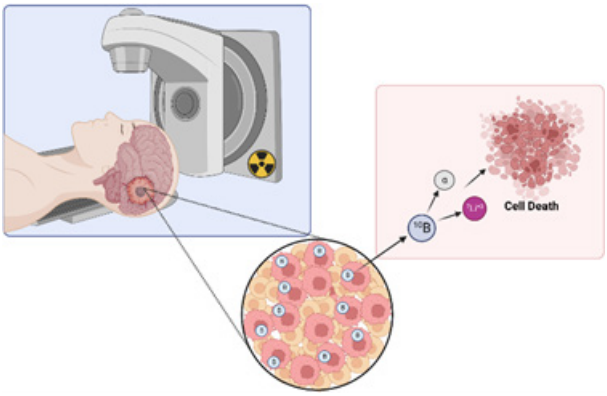

Figure 8. Illustration of the BNCT principle in graphical form (Created with BioRender.com).

A deadly ^{10}B (n, α) ^{7}Li capture reaction must be able to occur for the tumor cells to receive approximately ~20 μg/g of ^{10}B per weight of the tumor and be able to absorb enough neutrons. Particles can only injure cells that contain B because of their incredibly short travel distances (5-9 m), while they save nearby healthy cells. The majority of clinical attention in BNCT has been interested in patients with high-grade gliomas, individuals with repetitive head and neck malignancies who have not responded to traditional therapies, and a far smaller population of individuals suffering from cutaneous or extracutaneous melanomas. The most crucial criteria for BNCT delivery agents are low intrinsic toxicity, high tumor absorption (~20-50 μm ^{10}B), swift removal from the bloodstream and healthy tissue, and constant in tumor for at least a few hours during neutron radiation exposure. For this, new formulations with significant B contents are generated.

3.1.1. Boron delivery agents for BNCT

The proper number of ^{10}B atoms needs to be added to neoplastic cells that can survive an enough amount of neutron radiation to successfully complete the BNCT reaction. More than 1000 individuals have received BNCT treatment using two different types of B-containing compounds i.e. boronophenylalanine (BPA) and sodium borocaptate (BSH) [61]. New B delivery agents have emerged over the past 20 years, along with new methods of chemical synthesis and enhanced biological and biochemical understanding of B delivery. These agents are divided into three generations [62-65] (Figure 9). In this part of the review, we will be focusing on the 3-generation B delivery agents for BNCT with *in vitro* and *in vivo* applications.

3.1.1.1. First and second-generation BNCT compounds

The first-generation B-containing compounds used for BNCT were not developed for this use but were chosen since they were readily available, had well-known pharmacology, and had non-toxic properties. BA and its derivatives were the earliest B agents used in BNCT in the 1950s and early 1960s. However, they lacked tumor retention and had a low tumor/tissue

therapeutic index since they were non-selective drugs [62]. Second-generation agents BSH and BPA were used in the 1960s, and they are less toxic, stay inside the tumor longer, and show supra-unitary therapeutic indices for the brain, blood, and tumor. BSH is the most promising one among the B clusters due to its superior and stable B amounts in tumors with low systemic toxicity. There is a lot of interest in the use of BPA for the treatment of malignant melanoma. BPA can preferentially be absorbed by malignant melanoma cells due to its chemical structural similarity with tyrosine, which is necessary for melanogenesis. However, neither BSH nor BPA meets the requirements of effective B delivery agents [64-67]. The difficulty in accurately determining the optimum B concentration in a patient's tumor due to patient-to-patient variability is one of the most important drawbacks of BNCT. This issue might be solved by double-modality agents used in positron emission tomography (PET) guiding BNCT, which provide real-time tracking of B accumulation in patients' tumors. The radiolabeled derivative of BPA called 4-borono-2-^{18}F-flurophenylalanine (^{18}F-BPA) is a dual-modality BNCT agent. Numerous other tumor forms, including malignant melanomas, malignant gliomas, and various head and neck cancers, have also been treated with ^{18}F-BPA [66].

3.1.1.2. Third-generation BNCT compounds

To eliminate the drawbacks of first and second-generation BNCT compounds, a wide spectrum of low- to high-molecular-weight B delivery agents targeting tumor cells have been developed in recent years. Third-generation compounds that contain one or multiple polyhedral anions of borane or carboranes have been investigated. This group includes stable B delivery molecules with low and high molecular weights covalently bound to tumor-targeting moieties [68]. The three subgroups of low and high-molecular-weight substances include B-containing molecules with small sizes, B-compound conjugates, and B-delivery NPs.

3.1.1.2.1. Low molecular weight agents

This section will concentrate on low molecular weight substances that comprise boronated amino acids, peptides, nucleosides, derivatives of boronated porphyrins, and DNA-binding compounds.

3.1.1.2.1.1. Boronated natural and unnatural amino acids for BNCT

During the past 60 years, different amino acid-based B carriers have been synthesized. However, only a few of them have been investigated based on their biological properties. Among these boronated amino acids, the most-studied compound is BPA [69,70]. There are boronated amino acids both non-natural and natural. Naturally amino acids that have been examined include cysteine, tyrosine, aspartic acid, alanine, methionine, and glycine (Figure 10) [71]. The advantage is that, based on their weight, they contain more B than BPA, which enables them to deliver more intratumoral B without increased toxicity. The boronated derivatives of 1-aminocyclobutane-1-carboxylic acid (ABCHC) (Figure 10 a,b) and 1-amino-3-boron cyclopentane carboxylic acid (ABCPC) (Figure 10 c,d) are two examples of these substances [72]. Most amino acids used in BNCT have been documented for the precise treatment of malignant brain tumors [73]. As a theragnostic agent for both B administration and cancer diagnostics, Li and coworkers (2019) [74] reported the metabolically sustainable B-derived tyrosine (fluoroboronotyrosine, FBY) (Figure 10 e),

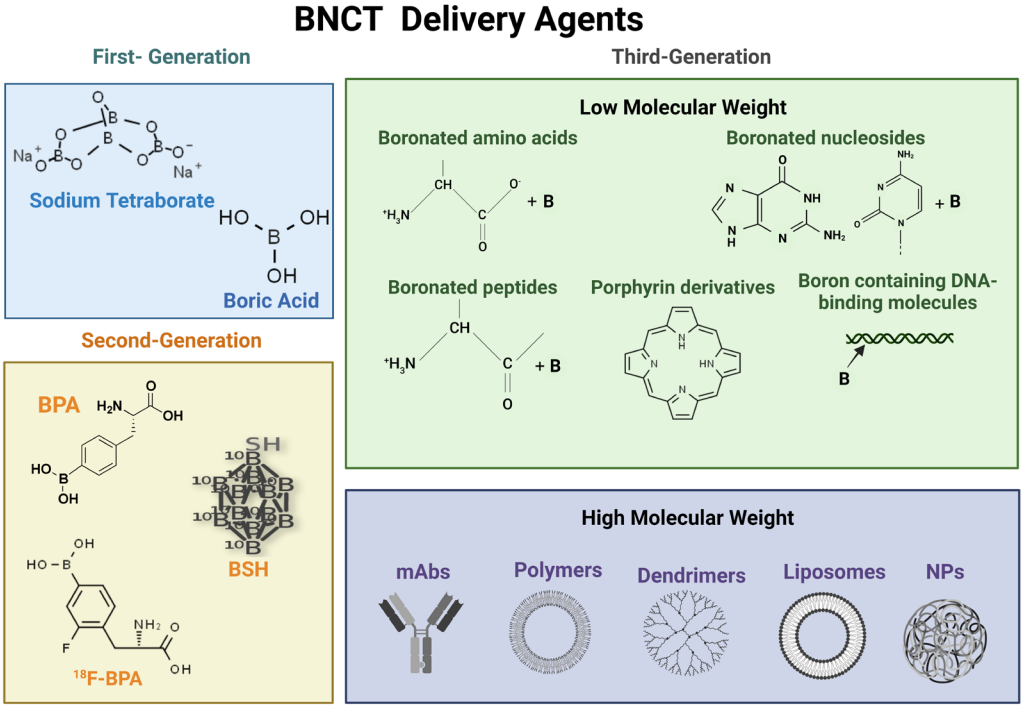

Figure 9. 3 generations of BNCT delivery agents (Created with BioRender.com).

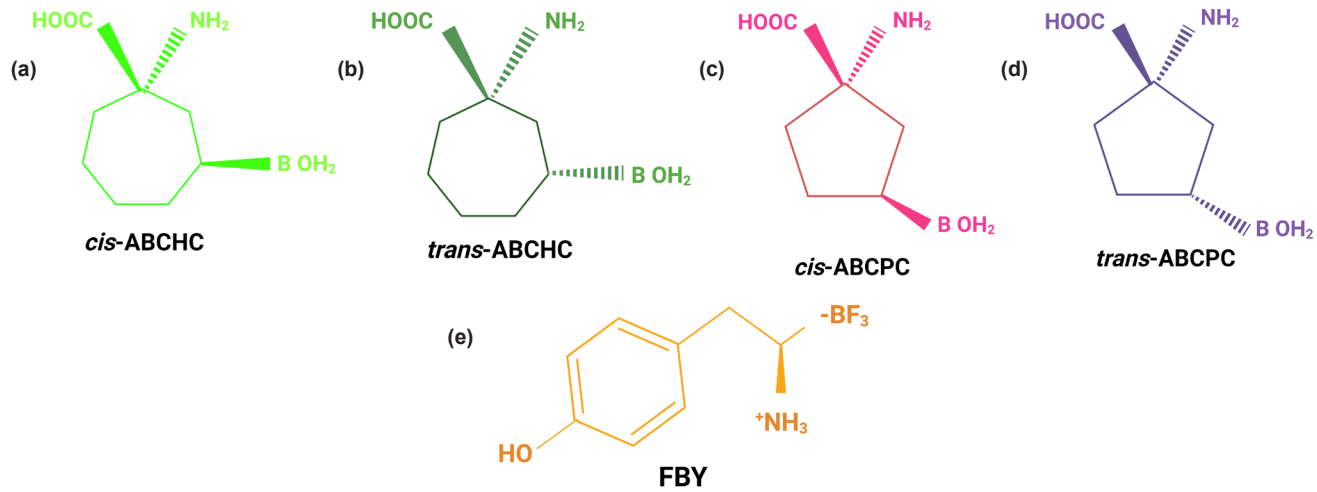

Figure 10. Examples of boronated amino acids. a). *cis*-ABCHC, b). *trans*-ABCHC, c). *cis*-ABCPC, d). *trans*-ABCPC, and e). FBY (Created with BioRender.com).

which paved the way for PET imaging-guided BNCT. The produced FBY was shown to have a high degree of resemblance to natural tyrosine. Additionally, the administration of an effective dose of FBY combined with an (^{18}F) FBY tracer revealed significant accumulation in the tumor of B16-F10 melanoma cells derived mouse model and minimal uptake in healthy tissue. The prospect of detecting B concentration by a noninvasive technology is suggested by the link between the PET images and B biodistribution. Thermal neutron irradiation was performed on B16-F10 tumor-bearing mice that received FBY injections, and the mice had longer median lives without experiencing any systemic damage. The use of FBY in clinical trials and as an effective diagnostic agent for imaging-guided BNCT offers a practical means of determining the local B concentration using PET imaging. 4-Borono-L-phenylalanine (4-BPA) was launched as Borofalan (Steboronine®) in Japan in May 2020 for people suffering from severe or localized chronic unreported head and neck cancer [75] following the publication of encouraging findings from two clinical trials. Even though 4-BPA is the only BNCT agent that is commercially available, there are several problems with it because of how poorly it dissolves in water. This research produced 3-borono-L-phenylalanine (3-BPA), an isomer of 4-BPA that is considerably more soluble in water. In an experiment, Kondo and coworkers (2022) administered 3-BPA without the solubilizer fructose, which is contained in 4-BPA formulations and has adverse consequences due to its great water solubility. Studies utilizing 3-BPA-Fru and 4-BPA-Fru demonstrated identical levels of B accumulation both *in vitro* and *in vivo*. Additionally, 3-BPA had a similar distribution within cells to 3-BPA-Fru, which made it possible to get rid of the solubilizer. 3-BPA becomes a promising agent for BCNT because it targets tumor tissue as effectively as 4-BPA and has a higher level of water solubility [76].

3.1.1.2.1.2. Boronated peptides for BNCT

Due to their significant capacity to bind receptors or transporters that are overproduced in tumor cells with excellent sensitivity and selectivity, peptides have garnered a lot of interest as targeted B delivery agents [61]. Peptides both linear and cyclic containing B administered to BSH have been investigated since they exhibit low toxicity, simple to synthesize, non-immunogenic, and strong tissue penetration properties [86]. Peptide ligands targeting overexpressed receptors on tumor cells, such as the somatostatin receptors, the VEGRF [78], and the endothelial growth factor (EGFR) [79-81] are of special interest. Isocyanato-closo-dodecaborate was used to functionalize poly ($_{DL}$-lysine) and bind it to monoclonal antibodies (mAbs) [80]. Polymeric linker minimized the reduction of immunoreactivity of mAb when the B clusters were present. Because they maintain 40 to 90% of immunogenicity and contain over 1000 B atoms per macromolecule, the bioconjugates are able to distribute BNCT. To attack the excessively expressed human Y1 (hY1) receptor seen in cancerous cells, a peptide molecule was created. The deoxygalactopyranosylated carborane building blocks used to create this peptide were functionalized by two lysines. The saccharide moieties made the peptides appropriately soluble in water and permitted the inclusion of up to 80 B atoms. Low *in vitro* toxicity on MCF-7 cells and high receptor responsiveness with hY receptor subgroups, in (d) rticular with hY1, were two characteristics of the bioconjugate systems [82]. A prospective diagnostic and therapeutic target, peptide transporter 1 (PepT1) is an oligopeptide transporter that is overexpressed in a variety of malignancies [83,84]. Miyabe and coworkers (2019) discovered that a PepT1-mediated mechanism was responsible for the uptake of dipeptides of BPA and tyrosine to AsPC-1 human pancreatic cancer cells [85] which paved the way to administer B to tumor cells via PepT1.

3.1.1.2.1.3. Boronated nucleosides for BNCT

Other substances that have been proposed as BNCT compounds include pyrimidine compounds thymidines, purines, nucleosides, and nucleotides.

As an illustration, the thymidine kinase-1 (TK1)-expressing cancer cells are preferentially targeted by 3-carboranyl thymidine analogs (3CTAs) (Figure 11 a,b) [86-88]. These substances may increase the caption and intratumoral retention of B through nucleotide synthesis. Since the incorporation of these agents into DNA takes place in the S phase and the mechanism of action is cell cycle-dependent, the effects may be enhanced by combining with a cell cycle-independent agent [86]. For instance, *in vivo*, biodistribution, and BNCT tests were performed on rats with brain tumors after *in vitro* experiments of the thymidine analog N5-2OH showed specific tumor absorption, a good rate of phosphorylation, and minimal toxicity (Figure 11 c) [89]. Convection-enhanced delivery (CED) with N5-2OH showed success in delivering efficacious dosages of B to tumors with incredibly high tumor: blood and tumor: brain percentages in rats bearing intracerebral RG2 gliomas without producing any concomitant toxicity. The median survival time (MST) in the tumor-bearing rats significantly increased following BNCT. Studies utilizing the nearly same F98 rat glioma, which also showed elevated TK1, suggest that N5-2OH may not be as a successful B delivery agent as originally believed. In these tests, there was just a very slight rise in MS [87].

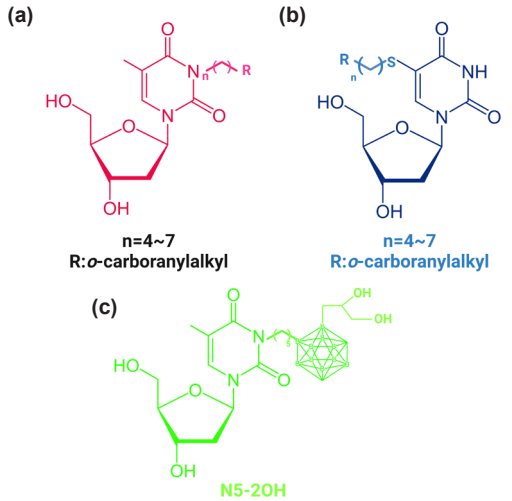

Figure 11. BExamples of boronated nucleosides as BNCT agents. a) and b). 3-carboranyl thymidine analogs, c). N5-2OH (Created with BioRender.com)

3.1.1.2.1.4. Boron-containing porphyrin derivatives for BNCT

B-containing porphyrin derivatives have been extensively studied because of their minimal toxicity and natural affinity for tumors. Several B clusters might be joined to a single porphyrin skeleton to give a lot of B. Due to the development of porphyrin-DNA conjugates that cause significant tumor uptake and protracted retention of the chemical substrates, porphyrin derivatives as B carriers have come under increased scrutiny. Research on selective B delivery of porphyrin derivatives *in vitro* and *in vivo* will be covered in this section. Since 1992, Miura and colleagues have concentrated on lipophilic porphyrins that include the B atom and created a small number of metal-complexed porphyrins (Figure 12a) [90-93].

The most extensively *in vitro* and *in vivo* studied porphyrin derivatives have been Cu (II) and Zn (II) complexed porphyrins, which are CuTCPH and ZnTCPH. After receiving injections of ZnTCPH or CuTCPH, the macro distributions of B in various organs were comparable with EMT-6-bearing animals, with the liver absorbing a greater quantity of B than the cancerous tissue. The ZnTCPH-injected tumor-bearing animals also displayed fluorescence in the spleen, liver, and tumors. Additionally, CuTCPH or ZnTCPBr probes are applied to ^{67}Cu-based single-photon emission

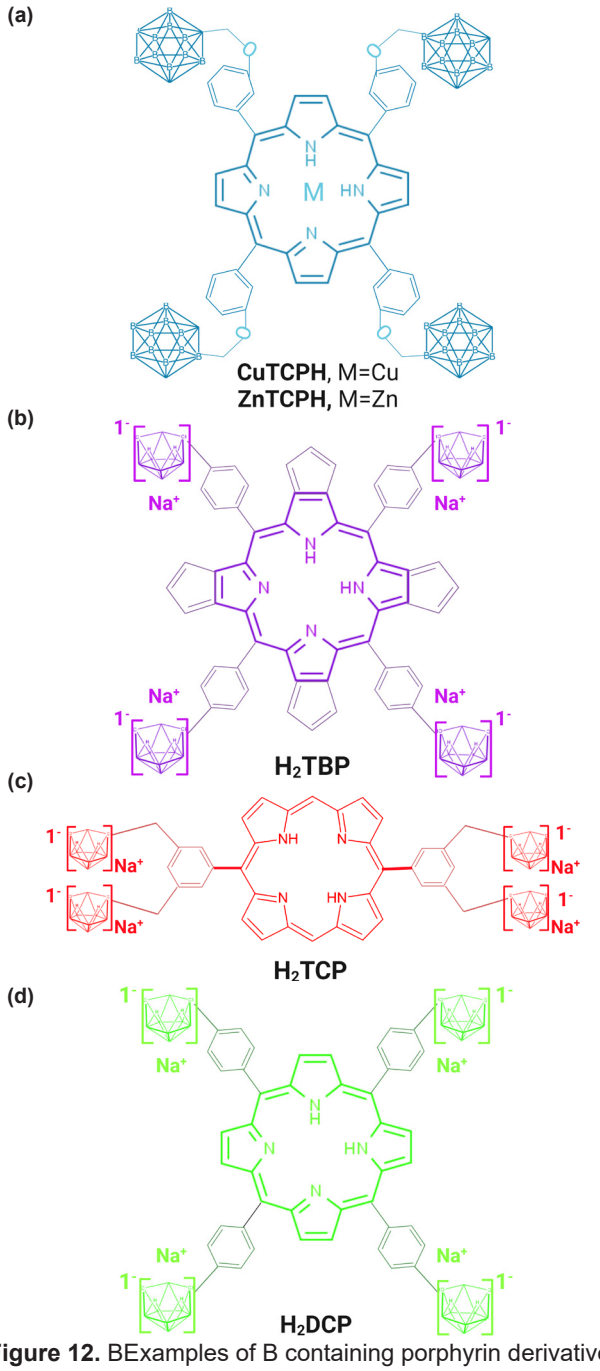

Figure 12. BExamples of B containing porphyrin derivatives as BNCT agent. a). metal-complexed porphyrins, b). H2TBP, c). H2TCP, d). H2DCP (Created with BioRender.com)

computed tomography (SPECT) or ^{64}Cu-based PET for imaging tumors [94]. Vicente and coworkers (2018) focused on the evaluation, characterization, synthesis, and biological assessment of porphyrin analogs for BNCT, such as anionic carbonylated porphyrins, porphyrin-labeled carbonyl phosphate diesters, cobaltacarborane-porphyrin-HIV1-Tat 48-60 conjugate, etc. [95]. The derivatives and conjugates were successful in penetrating T98G cells and were visible under fluorescence microscopy, but they had limited blood-brain barrier (BBB) solubility *in vitro*, which may be related to their elevated hydrophilic properties, high molecular weight, and propensity to aggregate [96]. Carborane was included in BODIPY to further increase permeability. The BBB permeability was increased throughout human hCMEC/D3 brain endothelial cell monolayers, with higher cellular uptake and B content, less cytotoxicity, and minimum cell damage [97,98].

The effectiveness of carboranyl porphyrins as B delivery agents for BNCT was first demonstrated by Kawabata and coworkers (2011) [99] in brain tumor-bearing rats. After assessing the photosensitizing potential and positioning of water-soluble H2TBP (Figure 12b), H2TCP (Figure 12c), and H2DCP (Figure 12d), the researchers determined the biodistribution and effectiveness of H2TBP and H2TCP as B delivery systems for BNCT in F98 glioma-bearing rats. Rats given an intracerebral injection with either CED or ALZET osmotic pump infusion experienced increased tumor B concentrations that persisted for 24 hours. Low B amounts were found in the healthy brain. Histopathologic analysis of the brains of BNCT-treated rats revealed enormous amounts of extracellular aggregation and porphyrin-containing macrophages, suggesting limited tumor cellular absorption and intracellular localization.

Viaggi and colleagues (2004) have investigated the effects of the B-containing tetrakis-carborane carboxylate ester of 2,4-bis-(a b-hydroxyethyl)-deutero-porphyrin IX (BOPP) (Figure 13a) on animal models of different malignancies [100,101]. In the Phase I clinical trial of PDT for high-grade early-stage gliomas, they assessed the appropriate dosage, toxic effects, and pharmacokinetics of BOPP and discovered moderate effects [102]. These are used as a point of reference for the BOPP application in BNCT. When BOPP and BPA were administered together, thyroid tumors exhibited higher B uptake. In their study of BOPP's toxicity, biodistribution, and CED. Ozawa and coworkers (2005) found that switching from intravenous injection to CED, BOPP delivery dramatically increased the B content in 9L tumor-bearing rats [103]. Additionally, Ozawa and the research group (2004) synthesized a series of tetraphenyl porphyrins (TABP, TEBP, and TOBP) (Figure 13b) with polyhedral borane anions, and they assessed the biological characteristics of the compounds *in vivo* [104]. Studies on the production of porphyrin analogs containing B and their application in BNCT have been carried out over the years. Patients with various malignancies may benefit from using porphyrin derivatives as BNCT agents.

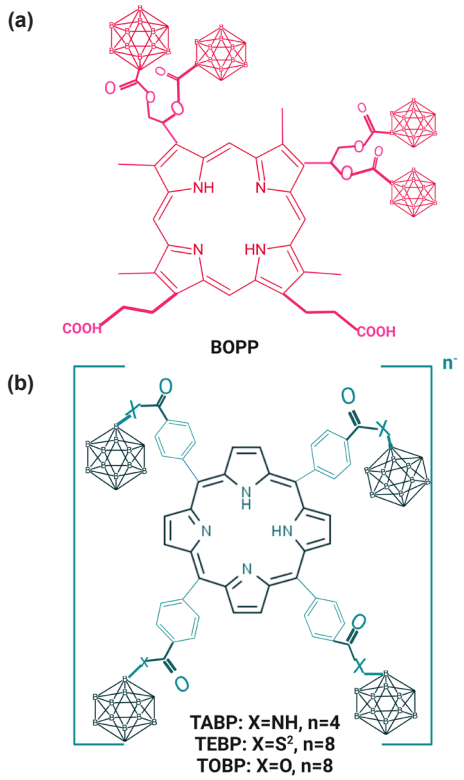

Figure 13. BExamples of B containing porphyrin derivatives as BNCT agent. a). BOPP, b). Tetraphenyl porphyrin derivatives (Created with BioRender.com)

3.1.1.2.1.5. Boron-containing DNA binding compounds for BNCT

Alkylating compounds, minor groove binding agents, platinum complexes, DNA intercalators, polyamines, and derivatives of aziridines, acridines, phenanthridines, and carbonyl polyamines are examples of B-containing-DNA binding substances. Because of their affinity for binding to the DNA of healthy cells and/or numerous cationic charges, some of these chemicals exhibit minimal tumor selectivity and substantial toxicity. Peptides, polyamines, and antisense oligonucleotides have also been studied as alternative agents to B delivery. Nicotinamides, which also have radio-sensitizing properties, have been studied either in combination with a B delivery agent or administered prior to the agent. B-complexed sugars, including analogs of glucose, maltose, ribose, mannose, and galactose have been studied, and the results showed increased water solubility. This group of compounds often has low tumor uptake but low tumor toxic effects, in part because of their hydrophilic properties and quick tissue elimination. They can be connected to other compounds, such as steroid hormone antagonists, that have an affinity for certain [105,106].

3.1.1.2.2. High molecular weight agents

Due to their exceptional characteristics, advanced

nanomaterials have drawn a lot of interest as potential new B delivery systems. The most studied high molecular weight boronated agents include mAbs, polymeric systems, NPs, dendrimers, and LPs. This class of agents has the most significant outcomes due to their targeting and selective binding properties. High molecular weight agents are studied *in vivo* and *in vitro* for various cancer types.

3.1.1.2.2.1. mAbs for BNCT

High molecular weight B delivery methods based on mAbs have been intensively studied based on mAb's ability to detect tumor-associated epitopes. Barth and coworkers have used EGFR mAbs for BNCT [79-81,107]. As B delivery agents, tEGF bioconjugates that exhibit sensitivity for tumors overexpressing EGFR can be employed. Highly boronated dendrimers with five dendritic generations to bind EGFR targeting mAbs cetuximab (Erbitux™) [81], EGFRv targeting mAbs L8A4 [80] or EGF [107] itself have been employed as heterobifunctional reagents. These bioconjugates led to a two- to three-fold enhancement of MST in comparison to controls when combined with intravenous BPA injection. Rats carrying receptor-positive F98 glioma-bearing animals [99] received these bioconjugates intracerebrally through CED. Additionally, according to Sun and colleagues (2016), a highly boronated poly (amido amine) (PAMAM) dendrimer might be delivered to specifically target stem cells both *in vitro* and *in vivo* using a mAb against the widely expressed stem cell marker CD133 on glioma cells. BSH was used to fill the gaps in the PAMAM dendrimer structure (Figure 14).

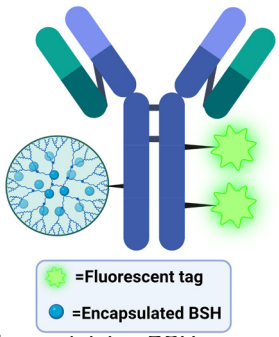

Figure 14. BmAbs containing BSH encapsulated within the PAMAM dendrimer (Created with BioRender.com)

Glioma stem cells are resilient cells that avoid cell death induced by traditional radiation and chemotherapy and promote tumor development. Studies showed that the CD133 negative SU2 cells received more than 10^9 B atoms which are above the B concentration threshold defined for BNCT. Survival was significantly prolonged when BNCT was given to BALB/c mice with intracerebral CD133(+) SU2 cells as opposed to CD133(-) SU2 cells. When the B-containing bioconjugate and free BSH were given before neutron irradiation, the MST was prolonged. Compared to animals with intracerebral CD133(-) SU2 glioma cells, BALB/c mice with these cells had a considerably longer lifespan [108]. These results suggest that more investigation on bioconjugates is required to evaluate their potential. Overall, mAbs have been used extensively for BNCT treatment. Researchers used combination therapy strategies with chemotherapeutic agents and radiation and combined the agents that are already used for BNCT such as BSH. When B-containing drugs were combined with mAbs, they showed effective results for cancer treatment as they are targeting the factors that are overexpressed in tumors.

3.1.1.2.2.2. Polymeric systems for BNCT

Due to their high B content, most polymeric systems use carborane derivatives as B compounds. Polymers are an alternative delivery system for B compounds, and they may improve their solubility and pharmaceutical kinetics by increasing their half-lives in the bloodstream and tumor accumulation. Over the past 20 years, different strategies to generate B-based polymeric systems such as B-conjugation, B-encapsulation, or conjugation with specific targeting or labeling moieties (Figure 15) have been studied.

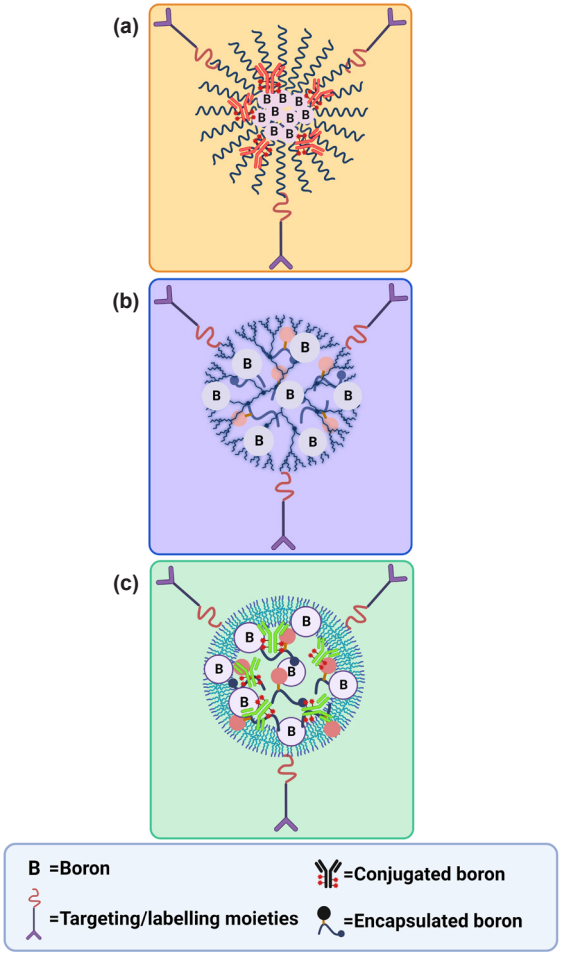

Figure 15. BA list of the various B-based polymeric systems, including those that are conjugated or encapsulated, along with any potential conjugations to targeting or marking moieties. a). Micelles derived from polymers or polymers that have been dendronized; b). Dendrimers; and c). LPs (Created with BioRender.com)

Amphiphilic carborane-conjugated polycarbonate micelles were synthesized using a carborane cyclic carbonate monomer and a poly (ethylene glycol) (PEG) macroinitiator. Polymeric micelles with varied sizes were produced. Even though the larger ones showed more liver uptake, tumor cells were more probable to be absorbed by the smaller ones. The NPs were not cytotoxic to L929 and HeLa cells, but the monomer containing carborane had a higher 50% inhibitory concentration on L929 cells (1.8 mM) compared to other small molecules [109]. In order to produce polymeric NPs via the thiol-ene reaction in a slightly different manner, researchers emulated the organization of a tiny surfactant with the carborane unit as the hydrophobic head and the PEG2000 unit as the hydrophilic tail [110]. The hydrophilic rhodamine B dye was applied to the second accessible site of the carborane unit to further mark the polymeric chains. When compared to BSH, either alone or in combination with other carborane-containing PEG compounds, the molecules did not cause toxicity in HepG2 cells and had a greater *in vivo* circulation time. *In vitro* fluorescence analyses of U87 cells revealed that the fluorescent substance had accumulated in the cytoplasm. The fluorescent molecules were administered intravenously to mice, and it was found that they concentrated in the spleen but not in other organs, indicating their potential as drug delivery systems. As boronic acid delivery methods, different acrylamide and N-acryloyl-diaminoethane pipes were produced to form boronated cationic copolymers [111]. After boronic polymers were administered intravenously, the resulting tri-block polymer produced 14 to 21 g/g of B/g of tumor and had a higher cationic monomer ratio in the cancerous tissue compared to healthy peri-colonic tissue. PEGylated-polyglutamic acid is one such polymer that was created by coupling BSH with sulfur via a disulfide bond. After 24 hours, there was a 5-fold increase in tumor B content when BSH was combined with PEGylated-Polyglutamic Acid (PEG-b-P(Glu-BSH), which boosted tumor cell absorption within an hour [112,113]. BALB/c mice that had received dermal implantation of the C26 malignant colon cancer cell line was given the PEG-b-P(Glu-BSH) intravenous injection.

24 hours after providing mice with tumors through intravenous injection of PEG-b-P(Glu-BSH), *in vivo* BNCT was carried out to show that enough ^{10}B had been given to eradicate the tumor. Accordingly, larger tumor: normal tissue ratios and better tumor: blood ratios suggested that Glu-BSH was more effective than BSH [114]. For the active and targeted administration of B and DOX in BNCT, Chen and colleagues (2019) suggested iRGD-modified polymeric NPs. They synthesized ^{10}B-polymers by covalently grafting the 10B-enriched BSH onto PEG-PCCL, altering their surface with iRGD, and then physically incorporating DOX into the polymers. After 24 hours of injection, the resultant polymers exhibit improved ^{10}B accumulation in tumors and longer blood circulation when compared to BSH as well as optimal B concentration ratios for human normal tissue in A549 tumor-bearing mice. However, additional research is required to use these polymers in clinical trials [125]. Another important type of polymeric materials for drug delivery systems and cancer therapy strategies is NPs. Polymeric NPs have been investigated as promising delivery systems for gadolinium neutron capture therapy (Gd-NCT) and delivery of drugs to metastatic malignancies [116].

It has been demonstrated that micelles containing B have better blood circulation, tumor accumulation, and stability [117]. Redox NPs made of B clusters have recently been obtained, and they exhibited great therapeutic efficacy, little side effect, and scavenged ROS [118]. They were created by combining positively charged polymers with BSH conjugates and positively loaded polymers with redox-responsive sections in a static process. After 48 hours, these NPs increased C26 tumor absorption by more than 5% of the injected amount per gram tumor and demonstrated an extended blood circulation length.

3.1.1.2.2.3. Nanoparticles for BNCT

Directing the drug to the tumor with minimal harm to healthy tissue is one of the key challenges of cancer chemotherapy. Since all chemotherapeutic agents are naturally cytotoxic, targeting or localizing these drugs close to the tumor enables the administration of decreased drug concentrations. This can be achieved by coupling the therapeutic agent to a biomolecule that is highly expressed in cancer cells or a receptor molecule. Using some external means to physically drive a cancer drug to the tumor also increases its effectiveness. Fundamentals of magnetically targeted therapy are based on this strategy [119]. The benefit of this approach is that fewer cytotoxic medications would be needed, lowering the risk of unfavorable side effects. This method can be considered a suitable vector for BNCT treatment. Pure B NPs are effective B carriers because of their substantial B content. The production of magnetic dopamine-functionalized B NPs with a size range of 100-700 nm was reported [120]. The production of magnetic compositions including PEG, Fe_3O_4, and mono- or bis-(ascorbatoborate) was also studied by this group [121]. The final nanocomposites were typically 10-15 nm in size and exhibit good paramagnetic properties. Since the composites are effective anti-cancer agents and radical scavengers when paired with ascorbic acid, these materials are considered possible magnetic biomedicine components. One study showed that it is possible to create encapsulated magnetic materials with an efficient amount of loaded carborane cages and analyze their biodistribution properties in cancer cell lines [122].

There have also been reports of other B-containing NPs made from B carbides, block copolymers, B powder, borosilicates, and gold NPs (AuNPs) with mercaptocarborane caps [123-131]. B carbide

functionalized with the transacting transcriptional activator peptide and the synthetic dye lissamine; the final nanomaterials can be relocated into B16-F10 malignant melanoma cells. Following neutron irradiation, the particles considerably suppressed the proliferation of both loaded and unloaded neighboring cells [123]. By using neutron capture, the functionalized B carbide NPs exhibited promising results for suppression of the growth of aggressive solid tumor B16-OVA melanoma *in vivo* [124]. By radical copolymerization of acetal-PEG-block-poly(lactide)-methacrylate with 4-vinyl benzyl substituted closocarboranes, polymer-based B-containing NPs were synthesized. The particles from the copolymerization of 1,2bis(4vinylbenzyl) closocarboranes demonstrated prolonged circulation time and increased tumor cell accumulation [118]. The same group has reported similar outcomes for particles made from mono-4-vinyl benzyl substituted closocarborane self-assembly and copolymerization [125]. By milling a $2SiO_2$-BO xerogel, borosilicate NPs with a size range of 100 to 200 nm were obtained [126]. The resultant particles showed enhanced incorporation to the tumor cells and hemocompatibility after being functionalized with FA [127]. Two nm AuNPs with mercaptocarborane ligands on the surface were obtained, and these monolayer-protected clusters (MPCs) displayed substantial toxicity, the ability to access the majority of cell sections, and an increased tendency to accumulate inside membranes [128]. The material should be appealing as a B-rich BNCT agent. Ciani and associates (2013) obtained unique B carriers utilizing ortho-carborane functionalized AuNPs (GNPs). The hydrophilic nature of GNPs was further increased to facilitate cell absorption by covering them with a properly suited diblock copolymer (PEObPCL). To anchor the pre-functionalized GNPs, this polymer additionally included pendant carboranes. Testing on osteosarcoma cells revealed outstanding biocompatibility in addition to the ability to concentrate B atoms in the target, which is encouraging for further *in vivo* applications. *In vitro* tests on rats with osteosarcoma cells revealed that these modified AuNPs had no discernible toxicity and were capable of accumulating B atoms which is extremely encouraging for their use in BNCT [129]. Using the water-in-oil emulsion approach, the production of pure B NPs made of an LP of azolectin-based phospholipid has been recently suggested [130]. This unique substance is composed of poly (maleic anhydride-alt-1-octadecene) and PEG on the surface, along with B NPs and Cy5 near-infrared (NIR) dye that is fluorescent in its center (3PCB). A folate-functionalized LP was made by combining folic acid (FA), a tumor-specific targeting ligand, with PEG. This increased B accumulation and allowed for more precise delivery to cancer cells. The aggregation of FA-conjugated LP in C6-brain cancer cells was discovered to be significantly greater than that of non-FA-conjugated LPs under the same conditions. Under physiological circumstances, these LPs exhibit exceptional stability, BBB crossing capability, and low cytotoxicity. Therefore, these LPs are thought to be novel B carriers for BNCT. Wu and colleagues (2019) [131] have employed theranostic AuNPs with B cage assembly (B-AuNPs) to assess its practicality for BNCT use. The commercially available citrate-coated AuNPs experienced PEGylation, azide addition, and surface carborane change. They also created 61-BAuNPs by coupling anti-HER2 antibodies with B-containing AuNPs with increased absorption. Based on the findings of this study, noninvasive imaging may prove to be a practical technique for monitoring the concentration of B in the tumor and assessing the mechanism of action of AuNPs.

3.1.1.2.2.4. Dendrimers for BNCT

Dendrimers are interesting materials for drug delivery and imaging applications because of their negligible toxicity, accessibility to reactive terminating groups, and potential inclusion into active targeting moieties [132]. Numerous researchers have investigated the selectivity of dendrimers and tumor-targeting agents in BNCT. The targeting of dendrimers with EGF, FA, and VEGF may enhance the targeted transport of B [78,107,133]. mAbs and other biomolecules attached to boronated PAMAM dendrimers have been thoroughly explored by Barth and colleagues (2003). Wu and colleagues (2004) linked Cetuximab, an anti-EGFR mAbs, to B-rich PAMAM dendrimers to function as a B delivery agent for BNCT. In rats with F_{98}EGFR gliomas, the combination was effective in specific targeting of EGFR by intratumoral injection [134]. The thiol-maleimide "click" chemical reaction is one among the several techniques developed to obtain boronated EGF. Starburst dendrimers of repeated PAMAM groups have their terminal amine groups functionalized by an isocyanate polyhedral borane to engage with the maleimide groups of EGF derivatives. It was found that 960 B atoms were included in each stable bioconjugate with a fourth-generation dendrimer. Each antibody molecule needs to travel 1000 B atoms to achieve a critical local B concentration [107] (Figure 16).

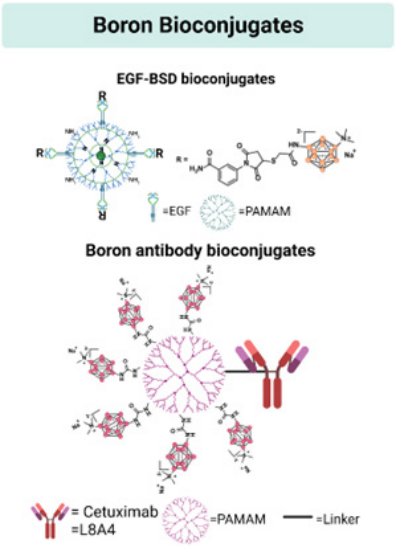

Figure 16. B bioconjugates used for BNCT (Created with BioRender.com).

The initial focus of BNCT was glioblastomas, which could not be treated using current therapeutic methods. To improve tumor absorption, CED (Figure 17) was studied by Yang and colleagues (2002) utilizing a highly boronated dendrimer EGF bioconjugate. CED is a method that can transport drugs directly into the extravascular area of the central nervous system skipping the BBB [135].

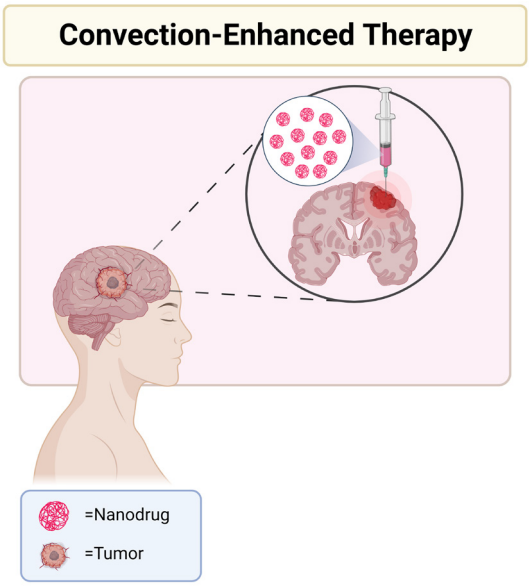

Figure 17. Schematic representation of convection-enhanced delivery (CED) (Created with BioRender.com).

Additionally, the IB16-6 antibody was linked to PAMAM dendrimers that were functionalized using a decaborane cluster. The presence of the antibody on the outer shell of the dendrimer enabled localization in *in vitro* studies. However, *in vivo* studies on rats with B16 melanomas showed that there was no tumor-specificity, and the tumors tended to be concentrated in the liver and spleen [136]. Parrott and colleagues (2005) developed polyester dendrimers rich in B with interiors filled with as many as 16 p-carboranes to improve the efficacy of boronated dendrimer delivery to tumor sites. They demonstrated the possibility of using these structures as BNCT agents in the future [137]. In additional trials, carborane cages were also incorporated into the dendritic structure to improve the distribution of boronated dendrimers to tumor cells [138]. These findings suggest that dendrimers are good platforms for B delivery in BNCT because they naturally have low cytotoxicity and may be generated with a range of reactive terminal functionalities [139]. According to Shukla and coworkers (2003), boronated PEG containing PAMAM dendrimers modified with FA that lowers their absorption by using reticuloendothelial system (RES) via mononuclear phagocyte system (MPS) might attain the B concentrations required for BNCT [133]. Hosmane and colleagues (2012), obtained tiny dendrimers with phenylene cores and three, six, or nine o-carborane clusters on the periphery [138]. The dendrimer containing nine carborane units was evaluated *in vitro*, and the results revealed that after 20 hours of incubation, it either accumulated in or was bound to the surface of human hepatocellular carcinoma cells. However, no additional research has been done on these systems. Additionally, the use of an exclusive core composed of AuNPs that is customized by dendrons with thiol moieties on the top and carborane and PEG units at the outside was investigated [140], though the BNCT properties of these water-soluble AuNPs have not been investigated.

3.1.1.2.2.5. Liposomes for BNCT

LPs have drawn attention for therapeutic and diagnostic applications due to the entrapment capacity of hydrophilic agents and the prevention of their release in circulation. LPs were the first nanomedicines in clinical trials after Doxil®, a PEGylated LP formulation encapsulating DOX, was approved by the FDA in 1995 [141]. B LPs stand as another possible agent for B delivery. Similar to the dendrimers, LPs may be coupled with mAbs, peptides, or polymeric materials. The first LP-encapsulated ^{10}BSH which coupled with mAbs was reported in 1989. It has been demonstrated that the immunoliposomes specifically target tumor cells *in vitro* and inhibit their proliferation after thermal neutron irradiation [142]. Though numerous B-encapsulated LPs have been obtained over the past few decades, most of these formulations lacked the necessary amount of B in their core, preventing them from achieving the therapeutic range required for BNCT [143]. The production of encapsulated BSH with 10% distearoyl B lipid (DSBL) LPs with a high B concentration to be used as a BNCT carrier has been reported demonstrating high performance for B delivery to the tumor [144]. The functionalized LPs combined with thermal neutron irradiation had better anti-cancer activity. Three weeks after receiving thermal neutron irradiation at a dose of 15 mg B/kg through injection, the tumors in mice carrying C26 had entirely vanished. The conjugation of LP with a v3 ligand and a cyclic arginine-glycine-aspartic acid-tyrosine-cysteine peptide (c(RGDyC)-LP) was demonstrated by thiol maleimide coupling. These functionalized LPs demonstrated promising results for delivering precise amounts of B to glioblastoma multiforme (GBM) when connected to a B cage. As a result, 70-80% cell death was attained in 3 hours [145].

3.2. PBA-based Diagnostic and Therapeutic Strategies for Cancer

As previously discussed in section 2.3. boronic acid derivative PBA has significant roles in cancer treatment and has been investigated extensively. PBA has advantages like being inexpensive, highly stable, compact, immune-suppressive, and simplicity of chemical modification. Based on these properties' materials functionalized with PBA have a wide range of application areas. PBA can quickly and irreversibly bind with 1,2 or 1,3-diols to obtain cyclic boronated esters [13,14,146]. The use of PBA compounds as an affinity chromatography ligand for the separation of

RNA has received substantial attention. The following developments involved applications for optical and electrical chemosensing, some of which focused on glucose detection. PBA can also interact with a range of biological membranes.

PBA-based functional compounds have been used in drug administration, cellular imaging, and glycoprotein detection (Figure 18). Since PBA-based chemicals can detect glycoproteins, whether these materials might bind to sialic acid (SA) on the surface of cancer cells was investigated.

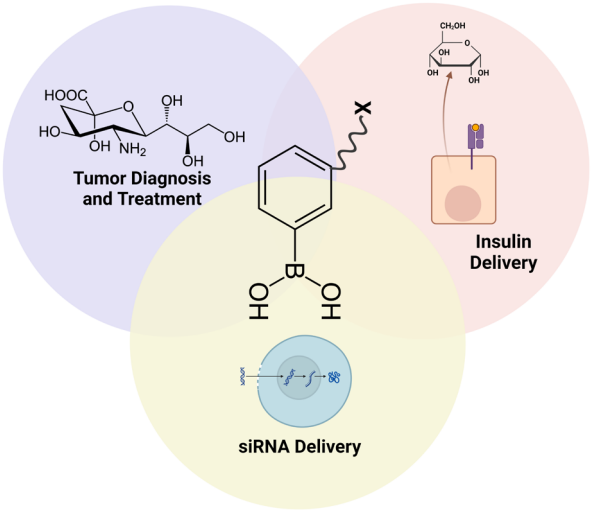

Figure 18. PBA-based therapeutic strategies (Created with BioRender.com).

The diol structure of PBA and SA can combine to produce reversible borate (Figure 19), which aids malignant cells to accept PBA-based functional chemical compounds. In concordance, it is possible to visualize cancer cells that overexpress SA using PBA and fluorophores. PBA and nanocarriers make it possible for therapeutic medications to be transported effectively, improving their accumulation at tumor locations, and boosting their anti-cancer potential. PBA contains a chemical functional group that can be used to target therapeutic medicines and nano drugs to tumors and malignant cells. This section of the article will provide a summary of the most current uses of PBA-based effective nanomaterials in cancer therapy, imaging, and diagnosis.

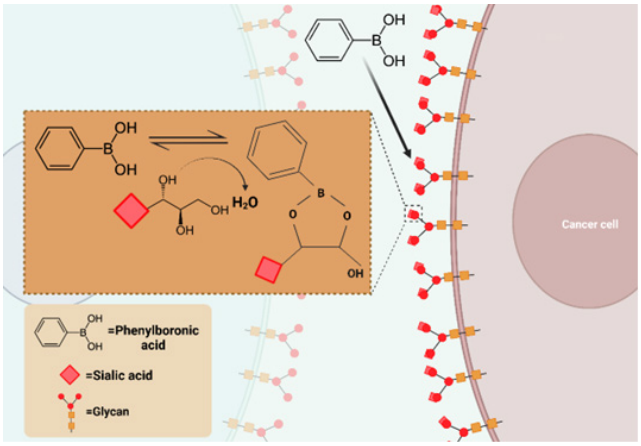

Figure 19. Phenyl boronic acid and sialic acid interaction and cyclic boronated esters formation via binding to 1,2-diols or 1,3-diols (Created with BioRender.com).

3.2.1. SA targeting strategies

PBA and its derivatives are most frequently employed in insulin delivery for diabetes mellitus treatment using glucose-responsive polymers that can detect blood glucose [147]. The capacity of PBA-based polymeric NPs to bind SA in acidic environments, such as the tumor microenvironment, makes them useful in anti-cancer drug delivery systems. The strong specificity and selectivity of PBA to SA can improve carriers' capacity to target cancer cells, increase duration in tumors, and slow down the quick clearance from tumors, which places PBA in an important place in nanomedicine. SA overexpression on cell membrane is related to the malignant and metastatic phenotypes of numerous cancer types, including lung, breast, prostate, colon, bladder, and stomach [148]. Therefore, methods for tracking SA expression would have particular importance for both diagnosis and treatment of cancer [149]. Based on this, PBA and SA detection methods such as biosensors have been investigated for both synthetic and natural polymeric materials.

Chen and colleagues (2013) generated a density-tunable dendrimeric array for in situ monitoring of glycan density based on overexpressed SA on the BGC-823 cell surface. They first modified the slide with PAMAM before electrostatically coating it with functionalized gold nanoclusters (AuNCs) made of 3-aminophenyl boronic acid (APBA). The plot of change compared to dendrimer density was used to determine the SA density on the cell surface [150]. Based on the PBA's capacity for the selective recognition of SA from other saccharides, Matsumoto and coworkers (2009) developed a technique to directly assess the expression of SA on the surface of cancerous cells by a PBA-modified electrode. Potentiometric detection can measure SA on cell surfaces under physiological circumstances without the use of enzymes or labeling techniques. The experiments with the electrode showed that the amount of SA presented on metastatic murine melanoma cells B16-F10 was about four times as high as the number of healthy pneumocytes. It was discovered that the amount of SA on the outside of the H22 murine hepatic cancer cell was roughly 1.9-fold greater than that on the surface of normal murine hepatocytes, showing that the enhanced expression of SA on the cell surface is related to malignancy and cancer spread. Thus, it has been demonstrated that SA is overexpressed on the surfaces of numerous different types of cancer cells utilizing borate ester chemistry [151].

Using surface-enhanced Raman scattering spectroscopy (SERS), Deng and colleagues (2018) designed a glucose-bridged and 4-mercapto

phenylboronic acid-decorated silver NPs (Glucose-MPBA@AgNPs) as a nanoprobe for hypersensitive identification of SA expression profiles on the surface of both normal and cancer cells. This unique complex demonstrated extraordinarily strong SERS enhancement activity, which is comparable to the SERS hot spot effect. Accumulation was significantly different from HepG2 cells and BNL CL.2 cells expressing differing quantities of SA on their surfaces. Nanoprobe may be advantageous in delivering highly efficient recognition of the edges of tumor tissues in clinical settings [152]. In recent years, numerous studies have used polymeric NPs with diverse designs and combinations as drug delivery agents based on PBA-SA recognition for cancer therapy. For instance, Zhang and colleagues (2016) used AuNP-labeled biotinylated PBA (biotin-APBA) to design an SA-recognition system. The average amounts of SA expressed on MCF-7 and HepG2 cell surfaces were reported to be $7.0x10^9$ and $5.4x10^9$, respectively [153]. This approach may be applied to diverse biological research and clinical diagnostics. Because SA overexpression is correlated with tumor aggressiveness and a bad prognosis, PBA-mediated targeting presents a highly translational approach to the clinical diagnosis and therapy of solid malignancies. It also offers safety and non-immunogenicity. Deshayes and coworkers (2013) developed PBA-functionalized polymeric micelles by incorporating PBA moieties into block copolymers to target SA overproduced on cancer cells. Additionally, they synthesized a PBA-PEG-b-poly (L-glutamic acid) copolymer (PBA-PEG-b-PLGA) [154]. To show the selectivity of the PBA-modified copolymer for SA, they investigated the steady-state fluorescence quenching affinities of PBA-PEG-b-PLGA and a number of sugars, including glucose, mannose, galactose, and N-acetylneuraminic acid (Neu5Ac). It was discovered that PBA had a higher SA binding affinity in the intratumoral environment, suggesting that SA would be the main target of the PBA-containing micelles in the highly acidic environment of tumors. Based on these tests, dichloro (1,2-diamino-cyclohexane) platinum (II) (DACHPt), an anti-cancer drug, was added to the PBA-PEG-b-PLGA micelles. DACHPt-loaded PBA-installed micelles exhibit better anti-cancer efficacy than DACHPt-loaded micelles without PBA providing another practical strategy for the treatment of solid malignancies. Another drug delivery system was generated by Zhao and colleagues (2016) which is the PBA-terminated PEG monostearate (PBA-PEG-C_{18}) and pluronic P_{123} (PEG_{20}-PPG_{70}-PEG_{20}) targeted system. They created fructose-coated PBA-targeted mixed micelles that could precisely attach and be absorbed by tumor cells via pH-triggered competitive binding to overcome the nonspecific interaction of PBA with normal cells or other components in the circulation. In a physiological environment, the shielding of fructose on the outside of the combined micelles successfully lowered the targeting affinity of PBA for normal cells; however, in a highly acidic tumor environment, it would reactivate due to the competitive binding of fructose and SA overexpressed on tumor cells. Therefore, this simple decorating method may make it simpler to create PBA-targeted NPs for the delivery of chemotherapeutics to tumors [155].

In addition to synthetic polymers, natural polymers could also be coated with PBA to target SA specifically. In order to enhance targeting and delivery to tumors, NPs containing 3-aminomethyl phenylboronic acid (AMPB)-functionalized chondroitin sulfate A (CSA)-deoxycholic acid (DOCA) have been synthesized. CSA-DOCA-AMPB NPs could target and penetrate tumors through reactions of boronic acid with SA and CSA with CD44 receptor, which could be tracked by NIR fluorescence imaging. In xenograft animal models, multiple intravenous injections of CSA-DOCA-AMPB NPs packed with DOX successfully inhibited the growth of A549 tumors. These NPs with high boronic acid content demonstrated promise as imaging and cancer therapy tools [156,157].

3.2.2. Drug delivery strategies

Chemotherapeutic medications have severe adverse effects and systemic toxicities. For chemotherapy to be effective, patients must give and utilize the drugs often over an extended period of time. Multidrug resistance (MDR) may also develop against chemotherapeutic drugs. PBA, combined with various materials, is frequently used to transport and administer anti-cancer drugs. Exosomes have recently received attention as potential anti-cancer drug delivery systems as they are nanosized particles made by cells. To achieve anti-cancer effects, significant concentrations of drugs must be loaded into exosomes. The surface is decorated with APBA and 4-carboxyphenylboronic acid (CPBA) to load DOX into exosomes. The DOX-loaded PBA-conjugated exosomes showed enhanced cytotoxicity in comparison to free DOX and DOX-loaded non-conjugated exosomes on the MDA-MB-231 cells. Results indicated that PBA might increase the uptake of DOX by exosomes, leading to increased cytotoxicity of PBA-conjugated exosomes in tumor cells [158]. Consequently, PBA conjugation to exosomes for the delivery of anti-cancer agents is a potential method to enhance the efficacy of chemotherapy. In another study, DOX-loaded low molecular weight gels (LMWGs) based on oligopeptides modified with PBA were administered by intratumoral injection to reduce systemic toxicity and increase treatment effectiveness. According to *ex vivo* imaging, DOX was continuously released from gels while maintaining an efficient chemotherapeutic concentration. The addition of gel caused a decrement in the systemic toxicity of DOX, and its adverse effects were significantly diminished, which makes the gel a promising local chemotherapeutic drug delivery mechanism [159].

In order to obtain a water-soluble nano construct, Kim and colleagues (2017) first synthesized a boronic ester of the cis-1,3-diol of andrographolide (AND) and hydrophilically polymerized PBA (pPBA). This construct

displayed improved tumor targeting both *in vitro* and *in vivo* [160]. DOX-loaded fluorescent NPs based on PLA-PEI copolymer with boronic acid modifications were developed by Li and colleagues (2014) for cellular imaging and pH-responsive drug administration. DOX-loaded NPs showed pH-responsive drug release and effectively slowed the growth of MCF-7 breast cancer cells. The fluorescent NPs also allowed for real-time imaging to track the endosomal escape procedure [161]. Zhang and coworkers (2017) [162] presented enzyme and redox dual-reaction polymeric micelles with active targeting capacity. Polymerized micelle prodrugs were also created by conjugating camptothecin (CPT) to monomethyl PEG by a redox-responsive linker. Through receptor-mediated endocytosis, micelles were able to specifically infiltrate tumor cells, and by simultaneously energizing redox and enzyme processes in the cytoplasm, therapeutic medicines could be released quickly. With only minor negative effects on healthy tissues, this had strong inhibitory effects on tumor cells. CPT and GMT were successfully self-delivered in a synergistic manner via a rod-shaped nanomicelle coated with CPBA [163]. Assembled nanomicelles modified with 4 CPBA also improved cellular internalization. Based on the PBA's active targeting capability, assembled nanomicelles appeared to congregate preferentially near the site of the tumor, decreased adverse effects, and enhanced the therapeutic potential.

3.2.3. siRNA delivery systems

Another application area of PBA is siRNA delivery. Amphiphilic PBA-decorated PEI (PEI-PBA) NPs were obtained as a quick and adaptable siRNA delivery strategy to study anti-cancer RNA interference efficiency. Findings demonstrated that PEI-PBA NPs encapsulated siRNA to generate a stable form of PEI-PBA/siRNA nano complexes. These nano complexes not only significantly increased the cellular uptake of siRNA via the chemical interactions between PBA and SA on cancerous cell surfaces, but also influenced siRNA to escape from the lysosome effectively inhibiting the target gene expression. Gene silencing and anti-tumor effects of PEI-PBA/siRNA were also tested in nude mice which revealed considerably increased effectiveness. PEI-PBA was identified as a straightforward and highly effective nanocarrier that could bind with increased SA residues on cancer cell membranes to transport siRNA specifically to cancer cells [164].

In order to obtain composites based on polyion complex (PIC) micelles, electrostatic relations among anionic siRNA and cationic polymers are used. Using simple PBA functionality, Naito and colleagues (2012) published a method that includes all the siRNA stabilizing techniques mentioned previously [165]. A platform cationic polymer known as 3-fluoro-4-carboxyphenylboronic acid (FPBA)-modified PEG-block-poly(L-lysine) (PEG-b-PLys) has been assembled. The ratio of siRNA to polymer and the level of PBA modification were both tuned. The stability of the complex under quasi-extracellular circumstances was demonstrated to be maintained by the hydrophobic interactions of PBA and the binding of the PBA moieties to the 3'-ends of ribose at both ends of the double-stranded siRNA. They also found that ATP interfered with the ideal complex at a range near its intracellular concentration. A well-known proto-oncogene called polo-like kinase 1 (PLK-1) was dose-dependently silenced by the PIC micelle. PIC micelles with PBA may be able to deliver siRNA to intracellular settings.

3.2.4. Imaging-guided phototherapy

Phototherapy (PT) is a noninvasive method that targets the treatment spot and minimizes the adverse effects of therapy. It holds great promise for cancer treatment. Examples of PT include photothermal therapy (PTT) and photodynamic therapy (PDT). With the development of cellular imaging technologies, a novel cancer treatment approach called image-guided tumor therapy has also evolved. The PTT generates heat while damaging the cells at the light-irradiated site. The most frequently used photothermal agents are magnetic NPs, polydopamine (PDA), and AuNPs [166]. LAPONITE (LAP)-Fe_3O_4 NPs were coated with PBA as a novel photothermal agent for the improvement of surface modification capacity and the PTT effect [167]. PBA photothermal NPs presented multimode imaging and selective targeting properties. Magnetic resonance image of the tumor deteriorated after intravenous delivery, although the photoacoustic (PA) signal increased. The NPs were collected in the tumor through the bloodstream. The tumor responded positively to the PBA targeting in terms of suppression within two weeks. Indocyanine green (ICG) and the anti-cancer agent SN38 loaded PBA-functionalized multivalent peptide nanotubes (I/S-PPNT) for the controlled release were assembled [168]. Confocal imaging was carried out utilizing PNNTs with different PBA graft densities in order to demonstrate the roles of PBA and SA in targeting. The intracellular fluorescence intensity grew gradually as graft density increased, but it reduced abruptly in cells treated with PBA, suggesting that PBA can target cells with high SA expression selectively. To demonstrate the effectiveness of tumor therapy, intravenous injections of PBS, PPNT, I-PPNT, and I/S-PPNT solutions were administered at the same ICG and SN38 dosages. Combining PDT and chemotherapy resulted in an approximate 90% I/S PPNT-mediated tumor inhibition. In addition to significant inhibition of pulmonary metastasis and tumor growth, the combination of precisely targeted and locally activated therapy also led to significant PPNT material accumulation in tumors. Another study is interested in an optical substance known as an up-conversion nanomaterial (UCNP), which is triggered by NIR light to produce ROS. When activated by NIR light, UCNPs-lanthanide-doped optical nanomaterials-can emit UV and visible light. Hyaluronated fullerene (HAC60) and amino APBA-functionalized UCNPs

(APBAUCNPs) were employed to build the nano platform by a specific binary borate condensation. It resulted in a dual-target nano platform with dual-color fluorescence imaging [169]. Fluorescence resonance energy transfer (FRET) between APBA-UCNPs and HAC60 helped to produce $^1O_2$. The nanomaterial might concurrently target polysialic acid (polSA) and CD44 for precise targeting of cancer cells. Experiments on cells have demonstrated that PBA can target overexpressed SA on PC12 cells. Dual targeting improved tumor cell uptake as evidenced by the simultaneous presentation of higher fluorescence intensities in tumor cells by UCNPs with dual targeting. Functional compounds based on PBA that are used as photosensitizers and photothermal agents are currently being investigated as potential pharmaceuticals to carry out proper PT.

3.2.5. Fluorescence imaging

The technique of biological imaging is crucial for understanding the composition and biological processes. Fluorescence imaging (FLI) has a variety of uses for biological imaging due to its high sensitivity, selectivity, variation, and noninvasive nature. When FLI is utilized for *in vivo* cell imaging, fluorescent probes are typically stimulated with light in order to generate fluorescence signals for imaging. By effectively differentiating normal cells from cancer cells and normal tissues and tumor tissues, the functionalized fluorescent probes enable early cancer diagnosis and imaging-based tumor therapy. A glycoprotein that is overexpressed on cancer cells can be recognized by fluorescent probes with PBA groups, enabling fluorescence imaging of tumors. A modular and affordable fluorescence-based imaging system was generated in 1999 by Atlamazoglu and colleagues by using Rhodamine derivatives [170]. Rhodamine B-leucine amide and rhodamine B-phenyl boronic acid discriminate healthy tissue from malignant colon tissue sections. Both products are primarily accumulated in neoplastic crypts. Both fluorescence-based optical biopsy approach and fluorescence microscopy can be used to diagnose colon cancer using this strategy. As SA imaging agents, cyclic metal iridium (III) polypyridine complexes functionalized with APBA and transition metal complexes as fluorophores [171] were developed. While the probe without PBA (complexes2) only showed sporadic fluorescence in cells, the PBA-containing probe (complexes1) was successful in imaging HepG2 cells. Since the binding affinity of PBA to SA on the cell surface reduces in the presence of free Neu5Ac and neuraminidase, the probe was unable to image cells. Because HEK293T cells have less SA on their surface, they did not emit any light when incubated with complexes1 under identical conditions, demonstrating that complexes1 are able to recognize SA residues on the cell surface and exhibit cellular selectivity. These results suggested a novel approach to the cancer diagnostic probes. The surface glycosylation of polymers, "clicking" polymer brushes, and cell surface modification are only a few biological alterations that could be made via the thiol-ene click reaction. In this study, well-dispersed FSNPs were first produced via reverse microemulsion, and these FSNPs were afterward surface-modified with PBA tags using a 'thiol-ene' click reaction [172]. Effective silica fluorescent probes with PBA tags were created for visualizing SA on living HeLa cells. As a result, the PBA-FSNPs can be utilized to develop a rapid, precise, and non-invasive method for tagging SA on living cells. This method may one day be useful for the clinical diagnosis of cancer and its therapy. Fluorescent 3-(dansylamino) phenylboronic acid (DAPB) was used to functionalize AuNPs embedded with polSA for in situ imaging and detection of SA. The assembly of DAPB was released from the surface of polSA-embedded AuNPs in the presence of more SA or SA-abundant cells due to the competitive binding of DAPB with SA and polSA, which caused DAPB to fluoresce on the surface of SA-abundant cells. The proposed approach employed a dual functional molecule to generate FRET from DAPB to AuNPs and the precise recognition of SA by the boronic group. They hypothesized that the suggested methodology would be advantageous for investigating biological processes, cancer diagnosis, and developing SA-targeted anti-cancer therapies [173].

4. Boron Nitride Nanomaterials for Cancer Treatment

Designing efficient, soluble, biocompatible, and physiologically stable nanocarriers for anti-cancer medications remains difficult. Due to their biocompatibility, significant surface area, and superior mechanical strength, h-BN and BNNT are attractive nanomaterials that have the potential as anti-cancer drug nanocarriers. Due to their distinct physicochemical characteristics, hBN NPs have attracted a lot of attention [159]. On BNNTs or h-BN nanosheets, peptides, proteins, single-stranded DNA, and polysaccharides have been conjugated. The bio-conjugation improved biocompatibility and biorecognition while facilitating water solubility. Combining bN materials with conventional cancer treatment strategies such as radiation therapy, phototherapy, and delivery vehicles for anti-cancer drugs such as DOX is a promising strategy for cancer therapy (Figure 20) [174].

Investigations on the therapeutic effectiveness of hBN against prostate cancer were made in comparison to BA, a potential degradation product. The outcomes show that hBNs significantly restrict DU145 cell growth in a concentration-dependent manner. A detailed cell cycle analysis revealed that both hBN- and BA-exposed DU145 cells were arrested in the mitotic phase during extended incubation periods. Long-term incubation of the highest concentration of hBN enhanced ROS production in DU145 cells which resulted in a higher apoptosis rate. The gradual long-term breakdown of hBN NPs, which results in a therapeutic effect on prostate cancer cells, explains the inconsistencies between the effects of hBN and BA

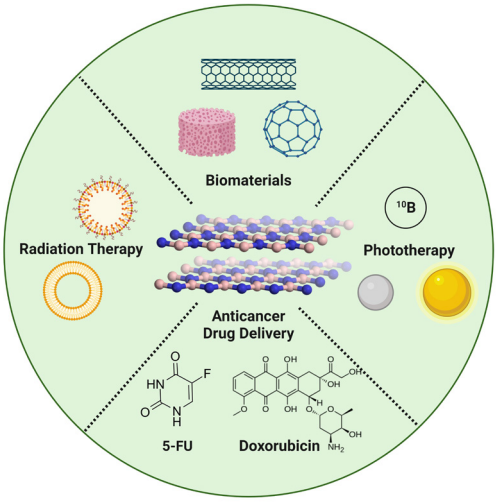

Figure 20. Different areas of boron nitride nanomaterials have been used (Created with BioRender.com).

[175]. A comparative study to explore the potential of BNNTs and hBNs as novel drug carrier was conducted by Emanet and coworkers (2017). They demonstrated that BNNTs could be loaded with a higher concentration of DOX than hBNs. The medium pH at the time of loading and release was significant. The enhanced drug release from BNNTs was sparked by the drop in pH. Since intracellular compartments like lysosomes are acidic, this can be a crucial time for optimal release following uptake into the cells. Additionally, the coupling of folate with DOX-BNNTs aids in the efficient targeting of cancer cells. The findings show that even when the DOX molecules were coupled to the carrier BNNT structures, they still accumulated in the cell nuclei. In order to increase therapeutic efficacy and lessen adverse effects [176], study reveals that BNNTs are a possible contender as an efficient carrier of chemotherapeutic medicines that include aromatic rings. AuNP-containing h-BN is regarded as a promising material for PDT and cancer medication delivery. The exfoliated h-BN was functionalized with AuNPs to produce nano-hybrid (h-BN with Au) particles. The h-BN-Au particles significantly suppressed MCF-7 cell proliferation compared to L929 cells after 72 hours of incubation. The results offer new information regarding the potential of hybrid materials for cancer treatment [177]. Li and colleagues (2017) examined the effects of hollow BN spheres on the apoptosis, necrosis, and proliferation of prostate cancer cells *in vitro*, and found that they increased caspase 3/7 activity and LDH release. Male BALB/c-nu/nu mice models implanted with LNCap cells exhibit a markedly reduced incidence and formation of tumors when hollow BN spheres are used. Hollow BN spheres and PTX work together synergistically to produce the most potent antitumor effectiveness of any combination. Rather than preventing prostate cancer in healthy people, the data suggest that hollow BN nanospheres may be used therapeutically to reduce tumor recurrence in prostate cancer patients [178]. Feng and coworkers (2018) developed a novel pH-responsive DOX delivery technique for cancer chemotherapy. pH-responsive poly (allylamine hydrochloride)-citraconic anhydride (PAH-cit) functionalized boron nitride nanospheres (BNNS) (DOX@PAH-cit-BNNS) were created for the transport and regulated release of DOX into cancer cells. Up to a high concentration of 100 g/mL, PAH-cit-BNNS complexes had no effect on MCF-7 and HeLa cells. However, DOX@PAH-cit-BNNS complexes demonstrated improved drug-release characteristics in an acidic environment. Due to their controlled drug release and pH responsiveness, PAH-cit functionalized BNNS is another promising delivery agent for cancer therapy [179].

DOX-loaded BN NPs (DOX-BNNPs) were assessed on drug-resistant cells by Zhitnyak and coworkers (2017). The DOX-BNNP nanoconjugates were internalized by both sensitive and multidrug-resistant neoplastic cells and localized in the cytoplasm between actin bundles. Results demonstrated that sensitization of the leukemia cells to doxorubicin carried by the DOX-BNNPs was the highest. DOX internalization of DOX-BNNP nanoconjugates by the endocytic mechanism was different from that of free DOX, and allowed maintenance of high and stable DOX levels in nuclei of MDR cells [180]. Sukhorukova and coworkers (2015) obtained a novel and straightforward technique for chemical vapor deposition manufacturing of BNNPs. These structures were discovered to have high cellular absorption and negligible cytotoxicity. These BNNPs, which have porous architectures, can be used as nanocontainers to transport various chemotherapeutic drugs to MDR cells. At equal concentrations, the cytotoxicity of BNNPs-DOX was comparable to that of free DOX. Endocytic pathways allowed BNNPs-DOX nanocarriers to enter IAR-6-1 cancer cells. Following the release of DOX from the nanosized drug delivery carriers, it accumulated in the cytoplasm and nucleus and caused cell death [181]. FA-conjugated BNNS complexes were created to transport DOX intracellularly. When compared to free DOX, complexes had stronger anti-cancer effects *in vitro*. These encouraging *in vitro* results and the possible application of BNNS in BNCT suggest that BNNS-FA/DOX may be further developed to improve the efficacy of cancer therapy *in vivo* [182]. The production and characterization of chitosan/OH-BNNS nanocomposites were studied by Dhanavel and coworkers (2021). Different methods were described to prepare a nanocomposite that was loaded with 5-FU and CUR in single and conjugated forms. Chitosan/OH-5-FU BNNS and CUR release profile has been studied. 5-FU-loaded, CUR-loaded, and 5-FU+CUR-loaded CS/OH–BNNS nanocomposites were prepared using the simple chemical synthesis method, and their cytotoxicity has been assessed on the HT-29 human colon cancer cell line. At dual-drug-loaded composite, the loading and encapsulation efficiencies of 5-FU were calculated to be 85.4% and 91.2%, respectively [183].

5. BODIPY Theranostics for Cancer Diagnosis and Therapy

Since John Funkhouser first presented theranostics

as a cancer treatment in 1998 [184], it has been proven to be the most successful treatment strategy. NPs or molecules with therapeutic and imaging characteristics are theranostic agents. Theranostic agents with imaging capabilities can all be used to visualize *in vivo* release and delivery of drugs, and other pharmacokinetic characteristics variables, such as FLI, photoacoustic imaging (PAI), PET, computed tomography (CT), and photothermal imaging (PTI) [185-187]. Combining theranostics with conventional cancer treatment methods provides some advantages in dose administration, therapy frequency, and recovery projections.

Theranostic medications with tumor-targeting and stimulus-responsiveness characteristics have shown tremendous promise for the treatment of cancer during the past 20 years. The 'one-for-all' theranostic system BODIPY, which typically uses multimodal imaging and treatment, is very intriguing to researchers in the medical, chemical, and life science fields. Theranostics has been applied in monotherapy via a variety of techniques. Haeberle and colleagues developed the BODIPY, a non-tetrapyrrolic photosensitizer, for the first time in 1970 [188]. BODIPYs have shown outstanding photophysical properties due to their varied electronic properties and effective transition energy. BODIPY dyes are used in a wide range of areas such as organic lasers (Figure 21a), bioimaging (Figure 21b), PDT (Figure 21c), light harvesters (Figure 21d), and photovoltaic devices (Figure 21e) [189].

BODIPY chemical dyes are simple to make and work great as a basis for various imaging modalities. High NIR absorption (kabs>650 nm), NIR-I/II emissions (650-1700 nm), and adjustable fluorescence quantum outputs are typical properties of BODIPY dyes. Modifications in the molecular structure can be used to control the PDT and PTT efficacy of BODIPY [190-192]. BODIPY agents can be modified with other chemically functionalized molecules, such as drugs, tumor-targeting ligands, etc. for novel therapies and imaging techniques. Additionally, BODIPY dyes have essentially minimal influence on biological processes with excellent photostability, minimal toxicity, strong molar extinction value, and strong phototoxicity. Therefore, a lot of BODIPY-based theranostics with applications in multimodal therapies (PDT/PTT/chemotherapy) and multimodal imaging (FLI/PAI/PTI) have been created (Figure 22) [193].

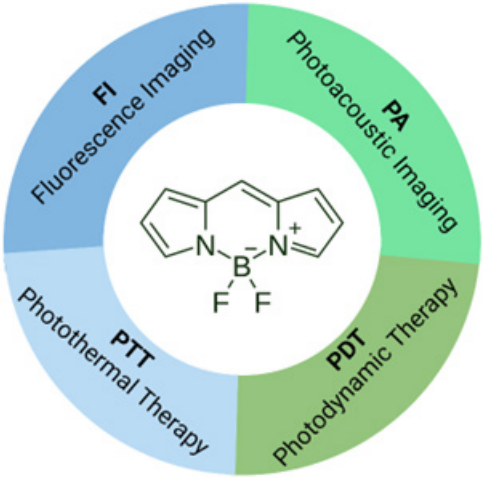

Figure 22. Different cancer diagnostic and therapeutic strategies that BODIPY can use alone or in combination with conventional strategies (Created with BioRender.com).

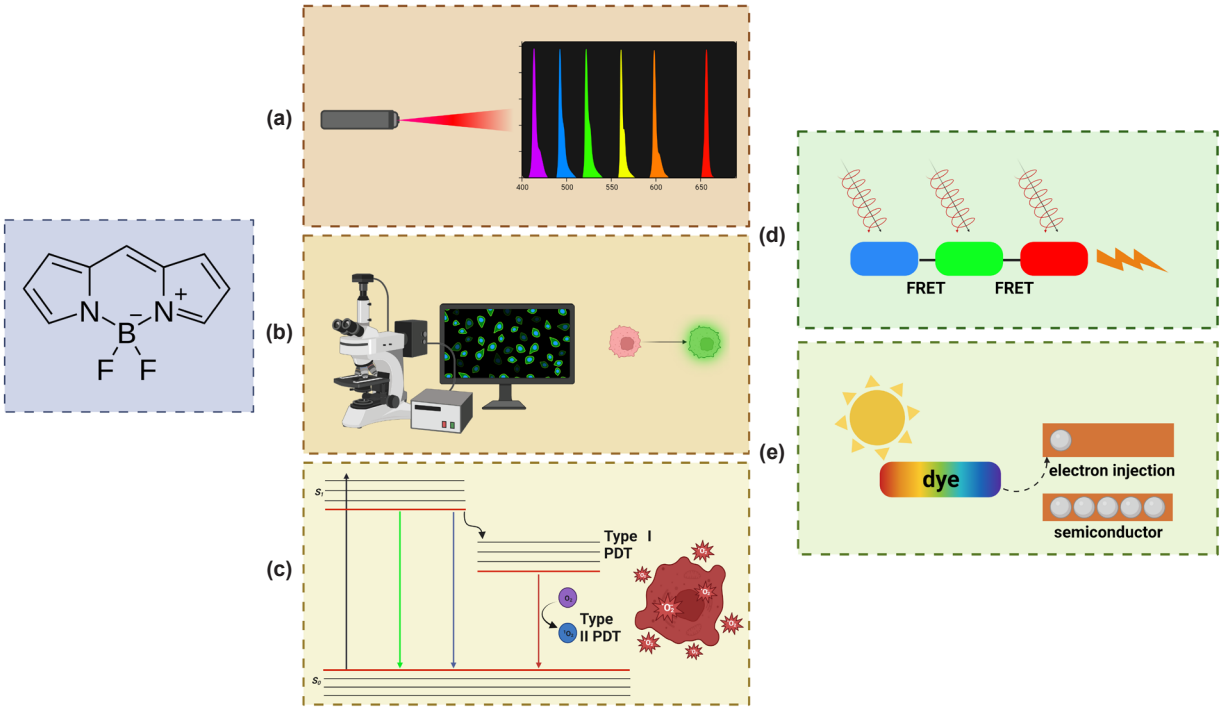

Figure 21. BODIPYs main usage areas; a). tunable organic dye lasers, b). fluorescent probes and sensors for bioimaging, c). photosensitizers for photodynamic therapy, d). light-harvesting artificial antenna, and e). dye-sensitized solar cells (Created with BioRender.com).

The chromophoric core of BODIPY, which is easily accessible for a broad variety of organic synthetic routes, is primarily responsible for the success and adaptability of the compound. The BODIPY core has been thoroughly and arbitrarily functionalized using reactions such as electrophilic and nucleophilic replacements, Pd-mediated C-C coupling, Knoevenagel, Suzuki, Sonogashira, and Liebeskind-Snögl [194].

BODIPYs cover the full visible spectrum in terms of emission and absorption. Molecular cassettes made solely of BODIPY building blocks can be modified by grafting blue-emitting and/or green-emitting derivatives to a red-emitting dye (Figure 23).

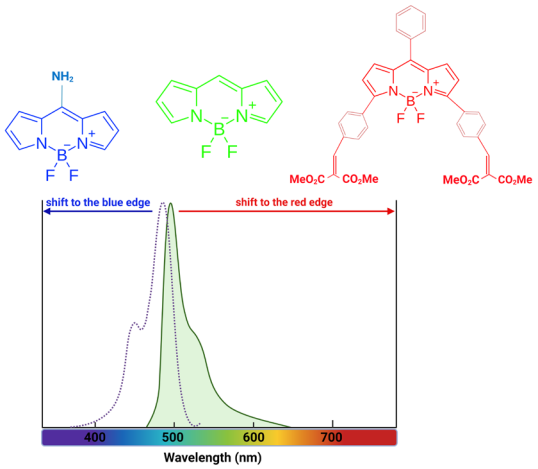

Figure 23. BODIPYs that have adjustable emission and absorption across the entire visible spectrum (Created with BioRender.com).

Other dyes, such as coumarin or rhodamine, which have complementary spectral bands at the visible orange-red and UV blue edges of the spectrum, can also be used. There are two types of BODIPY dyes: Aza-BODIPY and conventional BODIPY dyes (Figure 24 a). Aza-BODIPYs have extended NIR absorption as well as emission durations and easier chemical group modification due to the substitution of nitrogen for the meso-carbon in typical BODIPY dyes [195]. Due to the numerous modification sites, BODIPY dyes can be developed into theranostic platforms such as PAI, PDT, and PTT, in addition to NIR fluorescent fluorophores. In theory, visible to near-infrared photon absorption causes individual states of excitement (S_n, n=1,2, and 3) in BODIPY dyes. There are two probable ways for the "S_n" state BODIPY dye to reach its ground stage (S_0): fluorescence and non-radiation channels (heat or PAI signals). Intersystem transfer (ISC) crossover is used to move the "S_1" state BODIPY into the triplet state (T_1) (Figure 24 b). Through two different pathways, BODIPY dye in the "T_1" phase returns to the S_0 to create ROS. The one involved converting local oxygen into $^1O_2$, commonly referred to as "type-II PDT," via transporting energy. In contrast, "Type-I PDT" involves moving electrons to oxygen, water, or different substrates to create radicals such as the superoxide anion and hydroxyl radicals. The one entails producing $^1O_2$, also known as "type-II PDT," by transferring energy to nearby oxygen. The adjustable photochemistry characteristics of BODIPY dyes, shown in the Jablonski diagram in Figure 24 b, make them reliable theranostic platforms [196,197]. Mao and coworkers (2023) published a review article and they divided BODIPY-based theranostics into six groups fluorescence imaging-guided chemotherapy, fluorescence imaging-guided PDT and PTT, fluorescence imaging-guided multi-modal-therapies, PAI-guided phototherapy, and multi-modal imaging-guided multi-modal therapies. There have been numerous well-generated BODIPY-based theranostic platforms developed in recent years, many of which combine chemotherapy and fluorescence [190].

Overall, BODIPYs showed important improvements in cancer diagnosis and treatment. Furthermore, BODIPYs hold great promise for future clinical applications not only for cancer treatment but also for the treatment of other diseases. Since all BODIPY-based theranostics and therapy or combined therapy strategies have their unique features and important results in this article we will not discuss their specific cancer applications further.

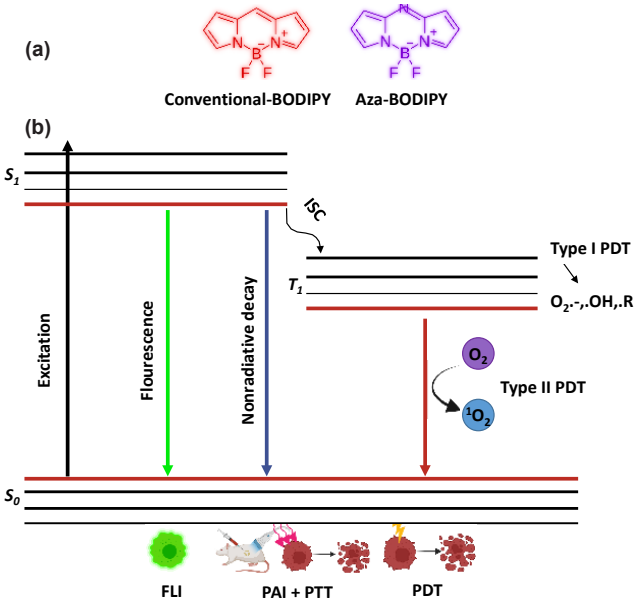

Figure 24. a). Conventional-BODIPYs and Aza-BODIPYs structures and b). therapeutic strategies for BODIPYs developed based on Jablonski Diagram (Created with BioRender.com).

6. Conclusion

Over the decades, studies showed important bioactivities of B such as regulation of cellular pathways, involvement in energy and hormone metabolisms, involvement in inflammatory and wound healing processes, and impacts on embryonic development, bone structure, and function. However, the main reason for clinical use of B is based on its enzyme inhibition properties. Studies have shown

that B-containing drugs may be beneficial for the treatment of various diseases like arthritis, metabolic abnormalities, neurological issues, and numerous chronic and infectious diseases. Over the decades, several B-based antibiotics, antimycotics, and enzyme inhibitors have been developed so far. In addition, there is growing evidence of the potential usage of B as a chemopreventive, chemotherapeutic, diagnostic agent for cancer as discussed in this review.

Some B-based drugs for clinic usage are approved by the FDA and are currently in clinical use for treatment of different diseases including cancer. Although various B derivatives have been used for cancer treatment, the underlying molecular mechanisms of B in cancer cells are still under investigation. Carbon-like features of B enable use in different drug designs, and provide the advantage of chemical modification of other bioactive agents. Cancer cells generally have very active energy metabolism due to their unlimited cell division and growth. Since B and its derivatives can interact with energy metabolism, reducing the levels of the essential molecules involved energy metabolism by B is important. In addition, cancer cells have high levels of ROS. B and B-containing molecules can be involved in ROS mechanisms and deregulate ROS levels. Interaction of B and B-containing molecules with the pyrimidine nucleotides, ribose, and other molecules seems to be another mechanism in which excess DNA damage may cause cancer cell death in transformed cells in particular with reduced DNA repair capacity. Inhibition of several crucial enzymes such as nitric oxide synthase or kinases by B compounds may disturb critical signaling pathways including cell cycle regulation, PI3K/Akt, VEGF, ATM, p53 etc.

On the other hand, the most important and most used clinical treatment approach where B is used is BNCT. A lot of strategies have been developed for the combination of B-based compounds, treatment strategies, and conventional cancer treatment methods such as chemotherapy, PDT, PTT, radiation, etc. Approaches consider B derivatives such as PBA, hBN, BODIPY, and others rather than B itself. Recently, B-based compounds gained more attention in biomedical research and applications, particularly in drug delivery systems and BNCT. Due to the unique features of the boronic acids, especially PBA is frequently introduced to drug nanocarriers. Additionally, h-BN and BNNT are promising nanomaterials due to their excellent properties. On the other hand, BODIPYs have excellent properties to be considered as diagnostic and therapeutic agents for cancer in future clinical applications. Although there are review articles based on the above-mentioned topics in the literature, almost all application areas of B and its derivatives from borates to BODIPYs with numerous studies and novel approaches in terms of cancer are covered and revisited, currently. Finally, B and B-containing compounds are of great interest for the development of new-generation bioactive diagnostic and therapeutic agents for cancer.

References

[1] Argust, P. (1998). Distribution of boron in the environment. *Biological Trace Element Research*, *66*(1), 131-143. https://doi.org/10.1007/BF02783133.

[2]. Karakaş, A. V., & Yilmaz, M. (2022). Academic perception of the strategic assessment of boron reserves in Turkey. *Ankara University Journal of Social Sciences*, *13*(2), 10-25. http://dx.doi.org/10.33537/sobild.2022.13.2.2.

[3]. Etimine S.A. (2023) 2022 *Boron Sector Report*. Strategy Development Department. https://www.etimaden.gov.tr/storage/2023/2022_Bor_Sektor_Raporu.pdf.

[4]. Białek, M., Czauderna, M., Krajewska, K. A., & Przybylski, W. (2019). Selected physiological effects of boron compounds for animals and humans. A review. *Journal of Animal and Feed Sciences*, *28*(4), 307-320. https://doi.org/10.22358/jafs/114546/2019.

[5]. Kar, Y., Şen, N., & Demirbaş, A. (2006). Boron minerals in Turkey, their application areas and importance for the country's economy. *Minerals & Energy-Raw Materials Report*, *20*(3-4), 2-10. https://doi.org/10.1080/14041040500504293.

[6]. World Health Organization (1996).Boron. *Trace Elements in Human Nutrition and Health* (pp. 175-179). ISBN 92-4-156173-4.

[7]. Nielsen, F. H. (2017). Historical and recent aspects of boron in human and animal health. *Journal of Boron*, *2*(3), 153-160. Retrieved from https://dergipark.org.tr/en/pub/boron/issue/33625/373093.

[8]. Gallardo-Williams, M. T., Maronpot, R. R., Wine, R. N., Brunssen, S. H., & Chapin, R. E. (2003). Inhibition of the enzymatic activity of prostate-specific antigen by boric acid and 3-nitrophenyl boronic acid. *The Prostate*, *54*(1), 44-49. https://doi.org/10.1002/pros.10166.

[9]. Devirian, T. A., & Volpe, S. L. (2003). The physiological effects of dietary boron. *Critical Reviews in Food Science and Nutrition*, *43*(2), 219-231. https://doi.org/10.1080/10408690390826491.

[10]. Baldwin, A. G., Tapia, V. S., Swanton, T., White, C. S., Beswick, J. A., Brough, D., & Freeman, S. (2018). Design, synthesis and evaluation of oxazaborine inhibitors of the NLRP3 inflammasome. *ChemMedChem*, *13*(4), 312-320. https://doi.org/10.1002/cmdc.201700731.

[11]. Nocentini, A., Supuran, C. T., & Winum, J. Y. (2018). Benzoxaborole compounds for therapeutic uses: A patent review (2010-2018). *Expert Opinion on Therapeutic Patents*, *28*(6), 493-504. https://doi.org/10.1080/13543776.2018.1473379.

[12]. Baker, S. J., Zhang, Y. K., Akama, T., Lau, A., Zhou, H., Hernandez, V., ... & Plattner, J. J. (2006). Discovery of a new boron-containing antifungal agent, 5-fluoro-1, 3-dihydro-1-hydroxy-2, 1-benzoxaborole (AN2690), for the potential treatment of onychomycosis. *Journal of Medicinal Chemistry*, *49*(15), 4447-4450. https://doi.org/10.1021/jm0603724.

[13]. Bradke, T. M., Hall, C., Carper, S. W., & Plopper, G. E. (2008). Phenylboronic acid selectively inhibits human prostate and breast cancer cell migration and

decreases viability. *Cell Adhesion & Migration*, *2*(3), 153-160. https://doi.org/10.4161/cam.2.3.6484.

[14]. McAuley, E. M., Bradke, T. A., & Plopper, G. E. (2011). Phenylboronic acid is a more potent inhibitor than boric acid of key signaling networks involved in cancer cell migration. *Cell Adhesion & Migration*, *5*(5), 382-386 https://doi.org/10.4161/cam.5.5.18162.

[15]. Scorei, R., & Popa, R. (2010). Boron-containing compounds as preventive and chemotherapeutic agents for cancer. *Anti-Cancer Agents in Medicinal Chemistry*, *10*(4), 346-351 https://doi.org/10.2174/187152010791162289.

[16]. Nikkhah, S., & Naghii, M. R. (2017). Using boron supplementation in cancer prevention and treatment: a review article. *The Cancer Press*, *3*, 113-119. https://doi.org/10.15562/tcp.56.

[17]. Ciani, L., & Ristori, S. (2012). Boron as a platform for new drug design. *Expert Opinion on Drug Discovery*, *7*(11), 1017-1027. https://doi.org/10.1517/17460441.2012.717530.

[18]. Palumbo, A., Gay, F., Bringhen, S., Falcone, A., Pescosta, N., Callea, V., ... & Boccadoro, M. (2008). Bortezomib, doxorubicin and dexamethasone in advanced multiple myeloma. *Annals of Oncology*, *19*(6), 1160-1165. https://doi.org/10.1093/annonc/mdn018.

[19]. Frankel, A., Man, S., Elliott, P., Adams, J., & Kerbel, R. S. (2000). Lack of multicellular drug resistance observed in human ovarian and prostate carcinoma treated with the proteasome inhibitor PS-341. *Clinical Cancer Research*, *6*(9), 3719-3728. PMID: 10999766.

[20]. Fernandes, G. F. S., Denny, W. A., & Dos Santos, J. L. (2019). Boron in drug design: Recent advances in the development of new therapeutic agents. *European Journal of Medicinal Chemistry*, *179*, 791-804. https://doi.org/10.1016/j.ejmech.2019.06.092.

[21]. Offidani, M., Corvatta, L., Caraffa, P., Gentili, S., Maracci, L., & Leoni, P. (2014). An evidence-based review of ixazomib citrate and its potential in the treatment of newly diagnosed multiple myeloma. *OncoTargets and Therapy*, 1793-1800. https://doi.org/10.2147/OTT.S49187.

[22]. Food and Drug Administration. (2018). 2017 *New Drug Therapy Approvals*. Center for Drug Evaluation And Research. Retrieved from https://www.fda.gov/drugs/new-drugs-fda-cders-new-molecular-entities-and-new-therapeutic-biological-products/novel-drug-approvals-2017.

[23]. Cui, Y., Winton, M. I., Zhang, Z. F., Rainey, C., Marshall, J., De Kernion, J. B., & Eckhert, C. D. (2004). Dietary boron intake and prostate cancer risk. *Oncology Reports*, *11*(4), 887-892. https://doi.org/10.3892/or.11.4.887.

[24]. Korkmaz, M., Uzgören, E., Bakırdere, S., Aydın, F., & Ataman, O. Y. (2007). Effects of dietary boron on cervical cytopathology and on micronucleus frequency in exfoliated buccal cells. *Environmental Toxicology: An International Journal*, *22*(1), 17-25. https://doi.org/10.1002/tox.20229.

[25]. Mahabir, S., Spitz, M. R., Barrera, S. L., Dong, Y. Q., Eastham, C., & Forman, M. R. (2008). Dietary boron and hormone replacement therapy as risk factors for lung cancer in women. *American Journal of Epidemiology*, *167*(9), 1070-1080. https://doi.org/10.1093/aje/kwn021.

[26]. Scorei, R. I., & Popa, R. (2013). Sugar-borate esters-potential chemical agents in prostate cancer chemoprevention. *Anti-Cancer Agents in Medicinal Chemistry*, *13*(6), 901-909. https://doi.org/10.2174/18715206113139990124.

[27]. Hunter, J. M., Nemzer, B. V., Rangavajla, N., Biţă, A., Rogoveanu, O. C., Neamţu, J., ... & Mogoşanu, G. D. (2019). The fructoborates: Part of a family of naturally occurring sugar-borate complexes-biochemistry, physiology, and impact on human health: A review. *Biological Trace Element Research*, *188*(1), 11-25. https://doi.org/10.1007/s12011-018-1550-4.

[28]. Petasis, N. A. (2007). Expanding roles for organoboron compounds-Versatile and valuable molecules for synthetic, biological and medicinal chemistry. *Australian Journal of Chemistry*, *60*(11), 795-798.

[29]. Arai, M., Koizumi, Y., Sato, H., Kawabe, T., Suganuma, M., Kobayashi, H., ... & Omura, S. (2004). Boromycin abrogates bleomycin-induced G2 checkpoint. *The Journal of Antibiotics*, *57*(10), 662-668. https://doi.org/10.7164/antibiotics.57.662.

[30]. Soriano-Ursúa, M. A., Das, B. C., & Trujillo-Ferrara, J. G. (2014). Boron-containing compounds: Chemico-biological properties and expanding medicinal potential in prevention, diagnosis and therapy. *Expert Opinion on Therapeutic Patents*, *24*(5), 485-500. https://doi.org/10.1517/13543776.2014.881472.

[31]. Das, B. C., Thapa, P., Karki, R., Schinke, C., Das, S., Kambhampati, S., ... & Evans, T. (2013). Boron chemicals in diagnosis and therapeutics. *Future Medicinal Chemistry*, *5*(6), 653-676. https://doi.org/10.4155/fmc.13.38.

[32]. Barranco, W. T., & Eckhert, C. D. (2004). Boric acid inhibits human prostate cancer cell proliferation. *Cancer Letters*, *216*(1), 21-29. https://doi.org/10.1016/j.canlet.2004.06.001.

[33]. Barranco, W. T., & Eckhert, C. D. (2006). Cellular changes in boric acid-treated DU-145 prostate cancer cells. *British Journal of Cancer*, *94*(6), 884-890. https://doi.org/10.1038/sj.bjc.6603009.

[34]. Cabus, U., Secme, M., Kabukcu, C., Cil, N., Dodurga, Y., Mete, G., & Fenkci, I. V. (2021). Boric acid as a promising agent in the treatment of ovarian cancer: Molecular mechanisms. *Gene*, *796*, 145799. https://doi.org/10.1016/j.gene.2021.145799.

[35]. Kahraman, E., & Göker, E. (2022). Boric acid exert anti-cancer effect in poorly differentiated hepatocellular carcinoma cells via inhibition of AKT signaling pathway. *Journal of Trace Elements in Medicine and Biology*, *73*, 127043. https://doi.org/10.1016/j.jtemb.2022.127043.

[36]. Cebeci, E., Yüksel, B., & Şahin, F. (2022). Anti-cancer effect of boron derivatives on small-cell lung cancer. *Journal of Trace Elements in Medicine and Biology*, *70*, 126923. https://doi.org/10.1016/j.jtemb.2022.126923.

[37]. Tombuloglu, A., Copoglu, H., Aydin-Son, Y., & Guray, N. T. (2020). In vitro effects of boric acid on human liver hepatoma cell line (HepG2) at the half-maximal inhibitory concentration. *Journal of Trace Elements in Medicine and Biology*, *62*, 126573. https://doi.org/10.1016/j.jtemb.2020.126573.

[38]. Yıldırım, O., Seçme, M., Dodurga, Y., Mete, G. A., & Fenkci, S. M. (2021). *Effects of boric acid on invasion, migration, proliferation, apoptosis, cell cycle and miRNAs in medullary thyroid cancer cells*. Research Square. https://doi.org/10.21203/rs.3.rs-553226/v1.

[39]. Tütüncü, M., Özşengezer, S. K., Karakayali, T., & Altun, Z. S. (2022). The effects of boric acid and disodium pentaborate dechydrate in metastatic prostate cancer cells. *Journal of Radiology and Oncology*, *6*(2), 012-017. https://doi.org/10.29328/journal.jro.1001041.

[40]. Blutt, S. E., Polek, T. C., Stewart, L. V., Kattan, M. W., & Weigel N. L. (2000).A Calcitriol Analogue, EB1089, Inhibits the Growth of LNCaP Tumors in Nude Mice. *Cancer Research*, *60*(4), 779-82. PMID: 10706079.

[41]. Bylund, A., Zhang, J. X., Bergh, A., Damber, J. E., Widmark, A., Johansson, A., ... & Hallmans, G. (2000). Rye Bran and Soy Protein Delay Growth and Increase Apoptosis of Human LNCaP Prostate Adenocarcinoma in Nude Mice. *Prostate*, *42*(4), 304-14. https://doi.org/10.1002/(SICI)1097-0045(20000301)42:4<304::AID-PROS8>3.0.CO;2-Z.

[42]. Gallardo-Williams, M. T., Chapin, R. E., King, P. E., Moser, G. J., Goldsworthy, T. L., Morrison, J. P., & Maronpot, R. R. (2004). Boron supplementation inhibits the growth and local expression of IGF-1 in human prostate adenocarcinoma (LNCaP) tumors in nude mice. *Toxicologic Pathology*, *32*(1), 73-78. https://doi.org/10.1080/01926230490260899.

[43]. Korkmaz, M., Avcı, C. B., Gunduz, C., Aygunes, D., & Erbaykent-Tepedelen, B. (2014). Disodium pentaborate decahydrate (DPD) induced apoptosis by decreasing hTERT enzyme activity and disrupting F-actin organization of prostate cancer cells. *Tumor Biology*, *35*(2), 1531-1538. https://doi.org/10.1007/s13277-013-1212-2.

[44]. Albuz, Ö., Dülger, D., Tunali, B. Ç., Aydin, F., Yalcin, S., & Türk, M. (2019). Effects of B2O3 (boron trioxide) on colon cancer cells: Our first-step experience and in vitro results. *Turkish Journal of Biology*, *43*(3), 209-223. https://doi.org/10.3906/biy-1901-34.

[45]. Kirlangic, O. F., Kaya Sezginer, E., Oren, S., Gür, S., Yavuz, O., & Ozgurtas, T. (2022). Cytotoxic and Apoptotic Effects of the Combination of Borax (Sodium Tetraborate) and 5-Fluorouracil on DLD-1 Human Colorectal Adenocarcinoma Cell Line. *Turkish Journal of Pharmaceutical Sciences*, *19*(4), 371-376. https://doi.org/10.4274/tjps.galenos.2021.29726.

[46]. Simsek, F., Inan, S., & Korkmaz, M. (2019). An in vitro study in which new boron derivatives maybe an option for breast cancer treatment. *Breast Cancer*, *13*(1), 22-27. https://doi.org/10.14744/ejmo.2018.0020.

[47]. Tepedelen, B. E., Korkmaz, M., Tatlisumak, E., Uluer, E. T., Ölmez, E., Değerli, İ., ... & İnan, S. (2017). A study on the anticarcinogenic effects of calcium fructoborate. *Biological Trace Element Research*, *178*(2), 210-217. https://doi.org/10.1007/s12011-016-0918-6.

[48]. Pirouz, F., Najafpour, G., Jahanshahi, M., & Baei, M. S. (2019). Biodistribution of calcium fructoborate as a targeting agent for boron neutron capture therapy in an experimental model of MDA-MB-231 breast cancer cells. *Biocatalysis and Agricultural Biotechnology*, *22*, 101389. https://doi.org/10.1016/j.bcab.2019.101389.

[49]. Kisacam, M. A., Kocamuftuoglu, G. O., Ozan, I. E., Yaman, M., & Ozan, S. T. (2020). Calcium fructoborate prevents skin cancer development in balb-c mice. *Biological Trace Element Research*, *196*(1), 131-144. https://doi.org/10.1007/s12011-019-01897-y.

[50]. Kisacam, M. A., Kocamuftuoglu, G. O., Ozan, I. E., Yaman, M., & Ozan, S. (2021). Calcium Fructoborate Prevents Skin Cancer Development in Balb-c Mice: Next Part, Reverse Inflammation, and Metabolic Alteration. *Biological Trace Element Research*, *199*(7), 2627-2634. https://doi.org/10.1007/s12011-020-02363-w.

[51]. Kisacam, M. A., Ambarcioglu, P., & Yakan, A. (2022). Calcium fructoborate regulate colon cancer (Caco-2) cytotoxicity through modulation of apoptosis. *Journal of Biochemical and Molecular Toxicology*, *36*(5), e23021. https://doi.org/10.1002/jbt.23021.

[52]. Marasovic, M., Ivankovic, S., Stojkovic, R., Djermic, D., Galic, B., & Milos, M. (2017). In vitro and in vivo antitumour effects of phenylboronic acid against mouse mammary adenocarcinoma 4T1 and squamous carcinoma SCCVII cells. *Journal of Enzyme Inhibition and Medicinal Chemistry*, *32*(1), 1299-1304. https://doi.org/10.1080/14756366.2017.1384823.

[53]. Ulldemolins, A., Seras-Franzoso, J., Andrade, F., Rafael, D., Abasolo, I., Gener, P., & Schwartz Jr. S. (2021). Perspectives of nano-carrier drug delivery systems to overcome cancer drug resistance in the clinics. *Cancer Drug Resistance*, *4*, 44-68. https://doi.org/10.20517/cdr.2020.59.

[54]. Fenton O. S., Olafson K. N., Pillai P. S., Mitchell M. J., & Langer R. (2018). Advances in biomaterials for drug delivery. *Advanced Materials*, *30*(29), 1705328. https://doi.org/10.1002/adma.201705328.

[55]. Chen, C. K., Law, W. C., Aalinkeel, R., Yu, Y., Nair, B., Wu, J., ... & Cheng, C. (2014). Biodegradable cationic polymeric nanocapsules for overcoming multidrug resistance and enabling drug-gene co-delivery to cancer cells. *Nanoscale*, *6*(3), 1567-1572. https://doi.org/10.1039/C3NR04804G.

[56]. Vivek, R., Thangam, R., NipunBabu, V., Rejeeth, C., Sivasubramanian, S., Gunasekaran, P., ... & Kannan, S. (2014). Multifunctional HER2-antibody conjugated polymeric nanocarrier-based drug delivery system for multi-drug-resistant breast cancer therapy. *ACS Applied Materials & Interfaces*, *6*(9), 6469-6480. https://doi.org/10.1021/am406012g.

[57]. Laurenția, G. N., & Rodica, A. M. (2016). Boron neutron capture therapy: Delivery agents used in boron administration. *Therapeutics, Pharmacology & Clinical Toxicology*, *20*(1), 25-32.

[58]. Ma, R., & Shi, L. (2014). Phenylboronic acid-based glucose-responsive polymeric nanoparticles: Synthesis and applications in drug delivery. *Polymer Chemistry*,

5(5), 1503-1518. https://doi.org/10.1039/C3PY01202F.

[59]. Sharker, S. M. (2019). Hexagonal boron nitrides (white graphene): A promising method for cancer drug delivery. *International Journal of Nanomedicine*, *14*, 9983. https://doi.org/10.2147/IJN.S205095.

[60]. Hu, K., Yang, Z., Zhang, L., Xie, L., Wang, L., Xu, H., ... & Zhang, M. R. (2020). Boron agents for neutron capture therapy. *Coordination Chemistry Reviews*, *405*, 213139. https://doi.org/10.1016/j.ccr.2019.213139.

[61]. Issa, F., Kassiou, M., & Rendina, L. M. (2011). Boron in drug discovery: Carboranes as unique pharmacophores in biologically active compounds. *Chemical Reviews*, *111*(9), 5701-5722. https://doi.org/10.1021/cr2000866.

[62]. Pitto-Barry, A. (2021). Polymers and boron neutron capture therapy (BNCT): A potent combination. *Polymer Chemistry*, *12*(14), 2035-2044.https://doi.org/10.1039/D0PY01392G.

[63]. Yuan, T. Z., Xie, S. Q., & Qian, C. N. (2019). Boron neutron capture therapy of cancer: Critical issues and future prospects. *Thoracic Cancer*, *10*(12), 2195. https://doi.org/10.1111/1759-7714.13232.

[64]. Axtell, J. C., Saleh, L. M., Qian, E. A., Wixtrom, A. I., & Spokoyny, A. M. (2018). Synthesis and applications of perfunctionalized boron clusters. *Inorganic Chemistry*, *57*(5), 2333-2350. https://doi.org/10.1021/acs.inorgchem.7b02912.

[65]. Luderer, M. J. (2019). *Development of novel tumor-targeted compounds for boron neutron capture therapy* (Publication No. 1782) [Doctoral dissertation, Washington University]. https://doi.org/10.7936/en1m-vp71.

[66]. Tani, H., Kurihara, H., Hiroi, K., Honda, N., Yoshimoto, M., Kono, Y., ... & Itami, J. (2014). Correlation of 18F-BPA and 18F-FDG uptake in head and neck cancers. *Radiotherapy and Oncology*, *113*(2), 193-197. https://doi.org/10.1016/j.radonc.2014.11.001.

[67]. Ishiwata, K. (2019). 4-Borono-2-18F-fluoro-L-phenylalanine PET for boron neutron capture therapy-oriented diagnosis: Overview of a quarter century of research. *Annals of Nuclear Medicine*, *33*(4), 223-236. https://doi.org/10.1007/s12149-019-01347-8.

[68]. Wu, G., Barth, R. F., Yang, W., Lee, R. J., Tjarks, W., Backer, M. V., & Backer, J. M. (2006). Boron containing macromolecules and nanovehicles as delivery agents for neutron capture therapy. *Anti-Cancer Agents in Medicinal Chemistry*, *6*(2), 167-184. https://doi.org/10.2174/187152006776119153.

[69]. Detta, A., & Cruickshank, G. S. (2009). L-amino acid transporter-1 and boronophenylalanine-based boron neutron capture therapy of human brain tumors. *Cancer Research*, *69*(5), 2126-2132. https://doi.org/10.1158/0008-5472.CAN-08-2345.

[70]. Wongthai, P., Hagiwara, K., Miyoshi, Y., Wiriyasermkul, P., Wei, L., Ohgaki, R., ... & Kanai, Y. (2015). Boronophenylalanine, a boron delivery agent for boron neutron capture therapy, is transported by ATB 0,+, LAT 1 and LAT 2. *Cancer Science*, *106*(3), 279-286. https://doi.org/10.1111/cas.12602.

[71]. Kabalka, G. W., Yao, M. L., Marepally, S. R., & Chandra, S. (2009). Biological evaluation of boronated unnatural amino acids as new boron carriers. *Applied Radiation and Isotopes*, *67*(7-8), S374-S379. https://doi.org/10.1016/j.apradiso.2009.03.104.

[72]. Kabalka, G. W., Shaikh, A. L., Barth, R. F., Huo, T., Yang, W., Gordnier, P. M., & Chandra, S. (2011). Boronated unnatural cyclic amino acids as potential delivery agents for neutron capture therapy. *Applied Radiation and Isotopes*, *69*(12), 1778-1781. https://doi.org/10.1016/j.apradiso.2011.03.035.

[73]. Timonen, J. M. (2020). Amino acids in boron neutron capture therapy-Prospects for precise treatment of malignant brain tumors. *General Chemistry*, *190024*. https://doi.org/10.21127/yaoyigc20190024.

[74]. Li, J., Shi, Y., Zhang, Z., Liu, H., Lang, L., Liu, T., ... & Liu, Z. (2019). A metabolically stable boron-derived tyrosine serves as a theranostic agent for positron emission tomography guided boron neutron capture therapy. *Bioconjugate Chemistry*, *30*(11), 2870-2878. https://doi.org/10.1021/acs.bioconjchem.9b00578.

[75]. Kanno, H., Nagata, H., Ishiguro, A., Tsuzuranuki, S., Nakano, S., Nonaka, T., … & Suzuki, H. (2021). Designation products: Boron neutron capture therapy for head and neck carcinoma. *The Oncologist*, *26*(7), e1250-e1255. https://doi.org/10.1002/onco.13805.

[76]. Kondo, N., Hirano, F., & Temma, T. (2022). Evaluation of 3-borono-l-phenylalanine as a water-soluble boron neutron capture therapy agent. *Pharmaceutics*, *14*(5), 1106. https://doi.org/10.3390/pharmaceutics14051106.

[77]. Mier, W., Gabel, D., Haberkorn, U., & Eisenhut, M. (2004). Conjugation of the closo-borane mercaptoundecahydrododecaborate (BSH) to a tumour selective peptide. *Journal of Inorganic and General Chemistry*, *630*(8-9), 1258-1262. https://doi.org/10.1002/zaac.200400064.

[78]. Backer, M. V., Gaynutdinov, T. I., Patel, V., Bandyopadhyaya, A. K., Thirumamagal, B. T. S., Tjarks, W., ... & Backer, J. M. (2005). Vascular endothelial growth factor selectively targets boronated dendrimers to tumor vasculature. *Molecular Cancer Therapeutics*, *4*(9), 1423-1429. https://doi.org/10.1158/1535-7163.MCT-05-0161.

[79]. Yang, W., Barth, R. F., Wu, G., Kawabata, S., Sferra, T. J., Bandyopadhyaya, A. K., ... & Wikstrand, C. J. (2006). Molecular targeting and treatment of EGFRvIII-positive gliomas using boronated monoclonal antibody L8A4. *Clinical Cancer Research*, *12*(12), 3792-3802.

[80]. Wu, G., Yang, W., Barth, R. F., Kawabata, S., Swindall, M., Bandyopadhyaya, A. K., ... & Fenstermaker, R. A. (2007). Molecular targeting and treatment of an epidermal growth factor receptor–positive glioma using boronated cetuximab. *Clinical Cancer Research*, *13*(4), 1260-1268. https://doi.org/10.1158/1078-0432.CCR-06-2399.

[81]. Yang, W., Wu, G., Barth, R. F., Swindall, M. R., Bandyopadhyaya, A. K., Tjarks, W., ... & Wikstrand, C. J. (2008). Molecular targeting and treatment of composite EGFR and EGFRvIII-positive gliomas using boronated monoclonal antibodies. *Clinical Cancer Research*, *14*(3), 883-891. https://doi.org/10.1158/1078-0432.

CCR-07-1968.

[82]. Worm, D. J., Hoppenz, P., Els-Heindl, S., Kellert, M., Kuhnert, R., Saretz, S., ... & Beck-Sickinger, A. G. (2019). Selective neuropeptide Y conjugates with maximized carborane loading as promising boron delivery agents for boron neutron capture therapy. *Journal of Medicinal Chemistry*, *63*(5), 2358-2371. https://doi.org/10.1021/acs.jmedchem.9b01136.

[83]. Gong, Y., Zhang, J., Wu, X., Wang, T., Zhao, J., Yao, Z., ... & Jian, X. (2017). Specific expression of proton-coupled oligopeptide transporter 1 in primary hepatocarcinoma a novel strategy for tumor-targeted therapy. *Oncology Letters*, *14*(4), 4158-4166. https://doi.org/10.3892/ol.2017.6724.

[84]. Inoue, M., Terada, T., Okuda, M., & Inui, K. I. (2005). Regulation of human peptide transporter 1 (PEPT1) in gastric cancer cells by anti-cancer drugs. *Cancer Letters*, *230*(1), 72-80. https://doi.org/10.1016/j.canlet.2004.12.023.

[85]. Miyabe, J., Ohgaki, R., Saito, K., Wei, L., Quan, L., Jin, C., ... & Kanai, Y. (2019). Boron delivery for boron neutron capture therapy targeting a cancer-upregulated oligopeptide transporter. *Journal of Pharmacological Sciences*, *139*(3), 215-222. https://doi.org/10.1016/j.jphs.2019.01.012.

[86]. Al-Madhoun, A. S., Johnsamuel, J., Barth, R. F., Tjarks, W., & Eriksson, S. (2004). Evaluation of human thymidine kinase 1 substrates as new candidates for boron neutron capture therapy. *Cancer Research*, *64*(17), 6280-6286. https://doi.org/10.1158/0008-5472.CAN-04-0197.

[87]. Barth, R. F., Yang, W., Wu, G., Swindall, M., Byun, Y., Narayanasamy, S., ... & Riley, K. J. (2008). Thymidine kinase 1 as a molecular target for boron neutron capture therapy of brain tumors. *Proceedings of the National Academy of Sciences*, *105*(45), 17493-17497. https://doi.org/10.1073/pnas.0809569105.

[88]. Sjuvarsson, E., Damaraju, V. L., Mowles, D., Sawyer, M. B., Tiwari, R., Agarwal, H. K., ... & Tjarks, W. (2013). Cellular influx, efflux, and anabolism of 3-carboranyl thymidine analogs: Potential boron delivery agents for neutron capture therapy. *Journal of Pharmacology and Experimental Therapeutics*, *347*(2), 388-397. https://doi.org/10.1124/jpet.113.207464.

[89]. Lewis, O., Woolley, M., Johnson, D., Rosser, A., Barua, N. U., Bienemann, A. S., ... & Evans, S. (2016). Chronic, intermittent convection-enhanced delivery devices. *Journal of Neuroscience Methods*, *259*, 47-56. https://doi.org/10.1016/j.jneumeth.2015.11.008.

[90]. Miura, M., Micca, P. L., Fisher, C. D., Heinrichs, J. C., Donaldson, J. A., Finkel, G. C., & Slatkin, D. N. (1996). Synthesis of a nickel tetracarboranylphenylporphyrin for boron neutron-capture therapy: Biodistribution and toxicity in tumor-bearing mice. *International Journal of Cancer*, *68*(1), 114-119. https://doi.org/10.1002/(SICI)1097-0215(19960927)68:1<114::AID-IJC20>3.0.CO;2-A.

[91]. Miura, M., Morris, G. M., Micca, P. L., Lombardo, D. T., Youngs, K. M., Kalef-Ezra, J. A., ... & Coderre, J. A. (2001). Boron neutron capture therapy of a murine mammary carcinoma using a lipophilic carboranyltetraphenylporphyrin. *Radiation Research*, *155*(4), 603-610. https://doi.org/10.1667/0033-7587(2001)155[0603:BNCTOA]2.0.CO;2.

[92]. Miura, M., Morris, G. M., Micca, P. L., Nawrocky, M. M., Makar, M. S., Cook, S. P., & Slatkin, D. N. (2004). Synthesis of copper octabromotetracarboranylphenylporphyrin for boron neutron capture therapy and its toxicity and biodistribution in tumour-bearing mice. *The British Journal of Radiology*, *77*(919), 573-580. https://doi.org/10.1259/bjr/71404908.

[93]. Miura, M., Morris, G. M., Hopewell, J. W., Micca, P. L., Makar, M. S., Nawrocky, M. M., & Renner, M. W. (2012). Enhancement of the radiation response of EMT-6 tumours by a copper octabromotetracarboranylphenylporphyrin. *The British Journal of Radiology*, *85*(1012), 443-450. https://doi.org/10.1259/bjr/87260973.

[94]. Smilowitz, H. M., Slatkin, D. N., Micca, P. L., & Miura, M. (2013). Microlocalization of lipophilic porphyrins: Non-toxic enhancers of boron neutron-capture therapy. *International Journal of Radiation Biology*, *89*(8), 611-617. https://doi.org/10.3109/09553002.2013.782446.

[95]. Xuan, S., & Vicente, M. D. G. H. (2018). Recent advances in boron delivery agents for boron neutron capture therapy (BNCT). In E. Hey-Hawkins, & C. Viñas Teixidor (Eds.). *Boron-Based Compounds: Potential and Emerging Applications in Medicine* (pp. 298-342). John Wiley & Sons Ltd. https://doi.org/10.1002/9781119275602.ch3.2.

[96]. Sibrian-Vazquez, M., Hao, E., Jensen, T. J., & Vicente, M. G. H. (2006). Enhanced cellular uptake with a cobaltacarborane-porphyrin-HIV-1 Tat 48-60 conjugate. *Bioconjugate Chemistry*, *17*(4), 928-934. https://doi.org/10.1021/bc060047v.

[97]. Gibbs, J. H., Wang, H., Bhupathiraju, N. D. K., Fronczek, F. R., Smith, K. M., & Vicente, M. G. H. (2015). Synthesis and properties of a series of carboranyl-BODIPYs. *Journal of Organometallic Chemistry*, *798*, 209-213. https://doi.org/10.1016/j.jorganchem.2015.05.009.

[98]. Xuan, S., Zhao, N., Zhou, Z., Fronczek, F. R., & Vicente, M. G. H. (2016). Synthesis and in vitro studies of a series of carborane-containing boron dipyrromethenes (bodipys). *Journal of Medicinal Chemistry*, *59*(5), 2109-2117. https://doi.org/10.1021/acs.jmedchem.5b01783.

[99]. Kawabata, S., Yang, W., Barth, R. F., Wu, G., Huo, T., Binns, P. J., ... & Vicente, M. G. H. (2011). Convection enhanced delivery of carboranylporphyrins for neutron capture therapy of brain tumors. *Journal of Neuro-oncology*, *103*(2), 175-185. https://doi.org/10.1007/s11060-010-0376-5.

[100]. Viaggi, M., Dagrosa, M. A., Longhino, J., Blaumann, H., Calzetta, O., Kahl, S. B., ... & Pisarev, M. A. (2004). Boron neutron capture therapy for undifferentiated thyroid carcinoma: preliminary results with the combined use of BPA and BOPP. *Applied Radiation and Isotopes*, *61*(5), 905-909. https://doi.org/10.1016/j.apradiso.2004.05.005.

[101]. Dagrosa, M. A., Viaggi, M., Rebagliati, R. J., Batistoni, D., Kahl, S. B., Juvenal, G. J., & Pisarev, M. A. (2005). Biodistribution of boron compounds in an animal model of human undifferentiated thyroid cancer for boron

neutron capture therapy. *Molecular Pharmaceutics*, *2*(2), 151-156. https://doi.org/10.1021/mp049894a.

[102]. Rosenthal, M. A., Kavar, B., Hill, J. S., Morgan, D. J., Nation, R. L., Stylli, S. S., ... & Kaye, A. H. (2001). Phase I and pharmacokinetic study of photodynamic therapy for high-grade gliomas using a novel boronated porphyrin. *Journal of Clinical Oncology*, *19*(2), 519-524.

[103]. Ozawa, T., Afzal, J., Lamborn, K. R., Bollen, A. W., Bauer, W. F., Koo, M. S., ... & Deen, D. F. (2005). Toxicity, biodistribution, and convection-enhanced delivery of the boronated porphyrin BOPP in the 9L intracerebral rat glioma model. International *Journal of Radiation Oncology*Biology*Physics*, *63*(1), 247-252. https://doi.org/10.1016/j.ijrobp.2005.05.030.

[104]. Ozawa, T., Santos, R. A., Lamborn, K. R., Bauer, W. F., Koo, M. S., Kahl, S. B., & Deen, D. F. (2004). In vivo evaluation of the boronated porphyrin TABP-1 in U-87 MG intracerebral human glioblastoma xenografts. *Molecular Pharmaceutics*, *1*(5), 368-374. https://doi.org/10.1021/mp049933i.

[105]. Crossley, E. L., Ziolkowski, E. J., Coderre, J. A., & Rendina, L. M. (2007). Boronated DNA-binding compounds as potential agents for boron neutron capture therapy. *Mini Reviews in Medicinal Chemistry*, *7*(3), 303-313. https://doi.org/10.2174/138955707780059808.

[106]. Nakamura, H., & Kirihata, M. (2012). Boron compounds: new candidates for boron carriers in BNCT. N*eutron Capture Therapy*, 99-116. https://doi.org/10.1007/978-3-642-31334-9_7.

[107]. Capala, J., Barth, R. F., Bendayan, M., Lauzon, M., Adams, D. M., Soloway, A. H., … & Carlsson, J. (1996). Boronated epidermal growth factor as a potential targeting agent for boron neutron capture therapy of brain tumors. *Bioconjugate Chemistry*, *7*(1), 7-15. https://doi.org/10.1021/bc950077q.

[108]. Sun, T., Li, Y., Huang, Y., Zhang, Z., Yang, W., Du, Z., & Zhou, Y. (2016). Targeting glioma stem cells enhances anti-tumor effect of boron neutron capture therapy. *Oncotarget*, *7*(28), 43095. https://doi.org/10.18632/oncotarget.9355.

[109]. Xiong, H., Wei, X., Zhou, D., Qi, Y., Xie, Z., Chen, X., ... & Huang, Y. (2016). Amphiphilic polycarbonates from carborane-installed cyclic carbonates as potential agents for boron neutron capture therapy. *Bioconjugate Chemistry*, *27*(9), 2214-2223. https://doi.org/10.1021/acs.bioconjchem.6b00454.

[110]. Chen, G., Yang, J., Lu, G., Liu, P. C., Chen, Q., Xie, Z., & Wu, C. (2014). One stone kills three birds: Novel boron-containing vesicles for potential BNCT, controlled drug release, and diagnostic imaging. *Molecular Pharmaceutics*, *11*(10), 3291-3299. https://doi.org/10.1021/mp400641u.

[111]. Azab, A. K., Srebnik, M., Doviner, V., & Rubinstein, A. (2005). Targeting normal and neoplastic tissues in the rat jejunum and colon with boronated, cationic acrylamide copolymers. *Journal of Controlled Release*, *106*(1-2), 14-25. https://doi.org/10.1016/j.jconrel.2005.03.015.

[112]. Mi, P., Yanagie, H., Dewi, N., Yen, H. C., Liu, X., Suzuki, M., ... & Nishiyama, N. (2017). Block copolymer-boron cluster conjugate for effective boron neutron capture therapy of solid tumors. *Journal of Controlled Release*, *254*, 1-9. https://doi.org/10.1016/j.jconrel.2017.03.036.

[113]. Dewi, N., Mi, P., Yanagie, H., Sakurai, Y., Morishita, Y., Yanagawa, M., ... & Takahashi, H. (2016). In vivo evaluation of neutron capture therapy effectivity using calcium phosphate-based nanoparticles as Gd-DTPA delivery agent. *Journal of Cancer Research and Clinical Oncology*, *142*(4), 767-775. https://doi.org/10.1007/s00432-015-2085-0.

[114]. Luderer, M. J., De La Puente, P., & Azab, A. K. (2015). Advancements in tumor targeting strategies for boron neutron capture therapy. *Pharmaceutical Research*, *32*(9), 2824-2836. https://doi.org/10.1007/s11095-015-1718-y.

[115]. Chen, J., Yang, Q., Liu, M., Lin, M., Wang, T., Zhang, Z., ... & Wei, Q. (2019). Remarkable boron delivery of iRGD-modified polymeric nanoparticles for boron neutron capture therapy. *International Journal of Nanomedicine*, *14*, 8161-8177. https://doi.org/10.2147/IJN.S214224.

[116]. Mi, P., Dewi, N., Yanagie, H., Kokuryo, D., Suzuki, M., Sakurai, Y., ... & Kataoka, K. (2015). Hybrid calcium phosphate-polymeric micelles incorporating gadolinium chelates for imaging-guided gadolinium neutron capture tumor therapy. *ACS Nano*, *9*(6), 5913-5921. https://doi.org/10.1021/acsnano.5b00532.

[117]. Sumitani, S., Oishi, M., & Nagasaki, Y. (2011). Carborane confined nanoparticles for boron neutron capture therapy: improved stability, blood circulation time and tumor accumulation. *Reactive and Functional Polymers*, *71*(7), 684-693. https://doi.org/10.1016/j.reactfunctpolym.2011.03.010.

[118]. Gao, Z., Horiguchi, Y., Nakai, K., Matsumura, A., Suzuki, M., Ono, K., & Nagasaki, Y. (2016). Use of boron cluster-containing redox nanoparticles with ROS scavenging ability in boron neutron capture therapy to achieve high therapeutic efficiency and low adverse effects. *Biomaterials*, *104*, 201-212. https://doi.org/10.1016/j.biomaterials.2016.06.046.

[119]. Sincai, M., Ganga, D., Ganga, M., Argherie, D., & Bica, D. (2005). Antitumor effect of magnetite nanoparticles in cat mammary adenocarcinoma. *Journal of Magnetism and Magnetic Materials*, *293*(1), 438-441. https://doi.org/10.1016/j.jmmm.2005.02.074.

[120]. Icten, O., Hosmane, N. S., Kose, D. A., & Zumreoglu-Karan, B. (2016). Production of magnetic nano-bioconjugates via ball milling of commercial boron powder with biomolecules. *Journal of Inorganic and General Chemistry*, *642*(14), 828-832. https://doi.org/10.1002/zaac.201600181.

[121]. Icten, O., Hosmane, N. S., Kose, D. A., & Zumreoglu-Karan, B. (2017). Magnetic nanocomposites of boron and vitamin C. *New Journal of Chemistry*, *41*(9), 3646-3652. https://doi.org/10.1039/C6NJ03894H.

[122]. Zhu, Y., Lin, Y., Zhu, Y. Z., Lu, J., Maguire, J. A., & Hosmane, N. S. (2010). Boron drug delivery via encapsulated magnetic nanocomposites: A new approach for BNCT in cancer treatment.

Journal of Nanomaterials, *2010*, 1-8. https://doi.org/10.1155/2010/409320.

[123].Mortensen, M. W., Björkdahl, O., Sørensen, P. G., Hansen, T., Jensen, M. R., Gundersen, H. J. G., & Bjørnholm, T. (2006). Functionalization and cellular uptake of boron carbide nanoparticles. The first step toward T cell-guided boron neutron capture therapy. *Bioconjugate Chemistry*, *17*(2), 284-290. https://doi.org/10.1021/bc050206v.

[124].Petersen, M. S., Petersen, C. C., Agger, R., Sutmuller, M., Jensen, M. R., Sørensen, P. G., ... & Hokland, M. (2008). Boron nanoparticles inhibit tumour growth by boron neutron capture therapy in the murine B16-OVA model. *Anticancer Research*, *28*(2A), 571-576. https://doi.org/10.0250-7005/2008

[125].Sumitani, S., Oishi, M., Yaguchi, T., Murotani, H., Horiguchi, Y., Suzuki, M., ... & Nagasaki, Y. (2012). Pharmacokinetics of core-polymerized, boron-conjugated micelles designed for boron neutron capture therapy for cancer. *Biomaterials*, *33*(13), 3568-3577. https://doi.org/10.1016/j.biomaterials.2012.01.039.

[126].Gao, Z., Walton, N. I., Malugin, A., Ghandehari, H., & Zharov, I. (2012). Preparation of dopamine-modified boron nanoparticles. *Journal of Materials Chemistry*, *22*(3), 877-882. https://doi.org/10.1039/C1JM12655E.

[127].Grandi, S., Spinella, A., Tomasi, C., Bruni, G., Fagnoni, M., Merli, D., ... & Balduini, C. (2012). Synthesis and characterisation of functionalized borosilicate nanoparticles for boron neutron capture therapy applications. *Journal of Sol-Gel Science and Technology*, *64*, 358-366. https://doi.org/10.1007/s10971-012-2865-9.

[128].Cioran, A. M., Musteti, A. D., Teixidor, F., Krpetic, Z., Prior, I. A., He, Q., ... & Vinas, C. (2012). Mercaptocarborane-capped gold nanoparticles: electron pools and ion traps with switchable hydrophilicity. *Journal of the American Chemical Society*, *134*(1), 212-221. https://doi.org/10.1021/ja203367h.

[129].Ciani, L., Bortolussi, S., Postuma, I., Cansolino, L., Ferrari, C., Panza, L., ... & Ristori, S. (2013). Rational design of gold nanoparticles functionalized with carboranes for application in boron neutron capture therapy. International *Journal of Pharmaceutics*, *458*(2), 340-346. https://doi.org/10.1016/j.ijpharm.2013.10.008.

[130].Singh, A., Kim, B. K., Mackeyev, Y., Rohani, P., Mahajan, S. D., Swihart, M. T., ... & Prasad, P. N. (2019). Boron-nanoparticle-loaded folic-acid-functionalized liposomes to achieve optimum boron concentration for boron neutron capture therapy of cancer. *Journal of Biomedical Nanotechnology*, *15*(8), 1714-1723. https://doi.org/10.1166/jbn.2019.2800.

[131].Wu, C. Y., Lin, J. J., Chang, W. Y., Hsieh, C. Y., Wu, C. C., Chen, H. S., ... & Kuo, W. Y. (2019). Development of theranostic active-targeting boron-containing gold nanoparticles for boron neutron capture therapy (BNCT). *Colloids and Surfaces B: Biointerfaces*, *183*, 110387. https://doi.org/10.1016/j.colsurfb.2019.110387.

[132].Liko, F., Hindre, F., & Fernandez-Megia, E. (2016). Dendrimers as innovative radiopharmaceuticals in cancer radionanotherapy. *Biomacromolecules*, *17*(10), 3103-3114. https://doi.org/10.1021/acs.biomac.6b00929.

[133].Shukla, S., Wu, G., Chatterjee, M., Yang, W., Sekido, M., Diop, L. A., ... & Tjarks, W. (2003). Synthesis and biological evaluation of folate receptor-targeted boronated PAMAM dendrimers as potential agents for neutron capture therapy. *Bioconjugate Chemistry*, *14*(1), 158-167. https://doi.org/10.1021/bc025586o.

[134].Wu, G., Barth, R. F., Yang, W., Chatterjee, M., Tjarks, W., Ciesielski, M. J., & Fenstermaker, R. A. (2004). Site-specific conjugation of boron-containing dendrimers to anti-EGF receptor monoclonal antibody cetuximab (IMC-C225) and its evaluation as a potential delivery agent for neutron capture therapy. *Bioconjugate Chemistry*, *15*(1), 185-194. ttps://doi.org/10.1021/bc0341674.

[135].Yang, W., Barth, R. F., Adams, D. M., Ciesielski, M. J., Fenstermaker, R. A., Shukla, S., ... & Caligiuri, M. A. (2002). Convection-enhanced delivery of boronated epidermal growth factor for molecular targeting of EGF receptor-positive gliomas. *Cancer Research*, *62*(22), 6552-6558.

[136].Barth, R. F., Adams, D. M., Soloway, A. H., Alam, F., & Darby, M. V. (1994). Boronated starburst dendrimer-monoclonal antibody immunoconjugates: evaluation as a potential delivery system for neutron capture therapy. *Bioconjugate Chemistry*, *5*(1), 58-66. https://doi.org/10.1021/bc00025a008.

[137].Parrott, M. C., Marchington, E. B., Valliant, J. F., & Adronov, A. (2005). Synthesis and properties of carborane-functionalized aliphatic polyester dendrimers. *Journal of the American Chemical Society*, *127*(34), 12081-12089. https://doi.org/10.1021/ja053730l.

[138].Dash, B. P., Satapathy, R., Bode, B. P., Reidl, C. T., Sawicki, J. W., Mason, A. J., ... & Hosmane, N. S. (2012). “Click” chemistry-mediated phenylene-cored carborane dendrimers. *Organometallics*, *31*(7), 2931-2935. https://doi.org/10.1021/om201255b.

[139].Cabrera-Gonzalez, J., Xochitiotzi-Flores, E., Vinas, C., Teixidor, F., Garcia-Ortega, H., Farfan, N., ... & Nunez, R. (2015). High-boron-content porphyrin-cored aryl ether dendrimers: Controlled synthesis, characterization, and photophysical properties. *Inorganic Chemistry*, *54*(10), 5021-5031. https://doi.org/10.1021/acs.inorgchem.5b00618.

[140].Li, N., Zhao, P., Salmon, L., Ruiz, J., Zabawa, M., Hosmane, N. S., & Astruc, D. (2013). “Click” star-shaped and dendritic PEGylated gold nanoparticle-carborane assemblies. *Inorganic Chemistry*, *52*(19), 11146-11155. https://doi.org/10.1021/ic4013697.

[141].Bobo, D., Robinson, K. J., Islam, J., Thurecht, K. J., & Corrie, S. R. (2016). Nanoparticle-based medicines: a review of FDA-approved materials and clinical trials to date. *Pharmaceutical Research*, *33*(10), 2373-2387. https://doi.org/10.1007/s11095-016-1958-5.

[142].Yanagie, H., Tomita, T., Kobayashi, H., Fujii, Y., Takahashi, T., Hasumi, K., ... & Sekiguchi, M. (1991). Application of boronated anti-CEA immunoliposome to tumour cell growth inhibition in in vitro boron neutron

capture therapy model. *British Journal of Cancer*, *63*(4), 522-526 https://doi.org/10.1038/bjc.1991.124.

[143].Nakamura H. (2013). Boron lipid-based liposomal boron delivery system for neutron capture therapy: Recent development and future perspective. *Future Medicinal Chemistry*, *5*(6), 715-730. https://doi.org/10.4155/fmc.13.48.

[144].Koganei, H., Ueno, M., Tachikawa, S., Tasaki, L., Ban, H. S., Suzuki, M., ... & Nakamura, H. (2013). Development of high boron content liposomes and their promising antitumor effect for neutron capture therapy of cancers. *Bioconjugate Chemistry*, *24*(1), 124-132. https://doi.org/10.1021/bc300527n.

[145].Zhu, Y., & Hosmane, N. S. (2018). Nanostructured boron compounds for cancer therapy. *Pure and Applied Chemistry*, *90*(4), 653-663. https://doi.org/10.1515/pac-2017-0903.

[146].Cambre, J. N., Roy, D., & Sumerlin, B. S. (2012). Tuning the sugar-response of boronic acid block copolymers. *Journal of Polymer Science Part A: Polymer Chemistry*, *50*(16), 3373-3382. https://doi.org/10.1002/pola.26125.

[147].Fuster, M. M., & Esko, J. D. (2005). The sweet and sour of cancer: Glycans as novel therapeutic targets. *Nature Reviews Cancer*, *5*(7), 526-542. https://doi.org/10.1038/nrc1649.

[148].Otsuka, H., Uchimura, E., Koshino, H., Okano, T., & Kataoka, K. (2003). Anomalous binding profile of phenylboronic acid with N-acetylneuraminic acid (Neu5Ac) in aqueous solution with varying pH. *Journal of the American Chemical Society*, *125*(12), 3493-3502. https://doi.org/10.1021/ja021303r.

[149].Djanashvili, K., Frullano, L., & Peters, J. A. (2005). Molecular recognition of sialic acid end groups by phenylboronates. *Chemistry-A European Journal*, *11*(13), 4010-4018. https://doi.org/10.1002/chem.200401335.

[150].Chen, Y., Ding, L., & Ju, H. (2013). In situ tracing of cell surface sialic acid by chemoselective recognition to unload gold nanocluster probe from density tunable dendrimeric array. *Chemical Communications*, *49*(9), 862-864. https://doi.org/10.1039/C2CC37761F.

[151].Matsumoto, A., Sato, N., Kataoka, K., & Miyahara, Y. (2009). Noninvasive sialic acid detection at cell membrane by using phenylboronic acid modified self-assembled monolayer gold electrode. *Journal of the American Chemical Society*, *131*(34), 12022-12023. https://doi.org/10.1021/ja902964m.

[152].Deng, R., Yue, J., Qu, H., Liang, L., Sun, D., Zhang, J., ... & Xu, S. (2018). Glucose-bridged silver nanoparticle assemblies for highly sensitive molecular recognition of sialic acid on cancer cells via surface-enhanced raman scattering spectroscopy. *Talanta*, *179*, 200-206. https://doi.org/10.1016/j.talanta.2017.11.006.

[153].Zhang, X., Chen, B., He, M., Zhang, Y., Peng, L., & Hu, B. (2016). Boronic acid recognition based-gold nanoparticle-labeling strategy for the assay of sialic acid expression on cancer cell surface by inductively coupled plasma mass spectrometry. *Analyst*, *141*(4), 1286-1293. https://doi.org/10.1039/C5AN02402A.

[154].Deshayes, S., Cabral, H., Ishii, T., Miura, Y., Kobayashi, S., Yamashita, T., ... & Kataoka, K. (2013). Phenylboronic acid-installed polymeric micelles for targeting sialylated epitopes in solid tumors. *Journal of the American Chemical Society*, *135*(41), 15501-15507. https://doi.org/10.1021/ja406406h.

[155].Zhao, D., Xu, J. Q., Yi, X. Q., Zhang, Q., Cheng, S. X., Zhuo, R. X., & Li, F. (2016). pH-activated targeting drug delivery system based on the selective binding of phenylboronic acid. *ACS Applied Materials & Interfaces*, *8*(23), 14845-14854. https://doi.org/10.1021/acsami.6b04737.

[156].Lee, J. Y., Chung, S. J., Cho, H. J., & Kim, D. D. (2015). Phenylboronic acid-decorated chondroitin sulfate A-based theranostic nanoparticles for enhanced tumor targeting and penetration. Advanced Functional Materials, 25(24), 3705-3717. https://doi.org/10.1002/adfm.201500680.

[157].Li, S., Hou, X., Ma, Y., & Wang, Z. (2022). Phenylboronic-acid-based functional chemical materials for fluorescence imaging and tumor therapy. ACS Omega, 7(3), 2520-2532. https://doi.org/10.1021/acsomega.1c06558.

[158].Kim, H., Kang, S. J., & Rhee, W. J. (2021). Phenylboronic acid-conjugated exosomes for enhanced anti-cancer therapeutic effect by increasing doxorubicin loading efficiency. Biotechnology and Bioprocess Engineering, 26(1), 78-85. https://doi.org/10.1007/s12257-020-0107-5.

[159].Gao, W., Liang, Y., Peng, X., Hu, Y., Zhang, L., Wu, H., & He, B. (2016). In situ injection of phenylboronic acid based low molecular weight gels for efficient chemotherapy. Biomaterials, 105, 1-11. https://doi.org/10.1016/j.biomaterials.2016.07.025.

[160].Kim, J., Lee, J., Lee, Y. M., Pramanick, S., Im, S., & Kim, W. J. (2017). Andrographolide-loaded polymerized phenylboronic acid nanoconstruct for stimuli-responsive chemotherapy. Journal of Controlled Release, 259, 203-211. https://doi.org/10.1016/j.jconrel.2016.10.029.

[161].Li, S., Hu, K., Cao, W., Sun, Y., Sheng, W., Li, F., ... & Liang, X. J. (2014). pH-responsive biocompatible fluorescent polymer nanoparticles based on phenylboronic acid for intracellular imaging and drug delivery. Nanoscale, 6(22), 13701-13709. https://doi.org/10.1039/C4NR04054F.

[162].Zhang, L., Wang, Y., Zhang, X., Wei, X., Xiong, X., & Zhou, S. (2017). Enzyme and redox dual-triggered intracellular release from actively targeted polymeric micelles. ACS Applied Materials & Interfaces, 9(4), 3388-3399. https://doi.org/10.1021/acsami.6b14078.

[163].Xu, Y., Huang, Y., Lu, W., Liu, S., Xiao, Y., & Yu, J. (2019). 4-Carboxyphenylboronic acid-decorated, redox-sensitive rod-shaped nano-micelles fabricated through co-assembling strategy for active targeting and synergistic co-delivery of camptothecin and gemcitabine. European Journal of Pharmaceutics and Biopharmaceutics, 144, 193-206. https://doi.org/10.1016/j.ejpb.2019.09.019.

[164].Ji, M., Li, P., Sheng, N., Liu, L., Pan, H., Wang, C., ... & Ma, Y. (2016). Sialic acid-targeted nanovectors with

phenylboronic acid-grafted polyethylenimine robustly enhance siRNA-based cancer therapy. ACS Applied Materials & Interfaces, 8(15), 9565-9576. https://doi.org/10.1021/acsami.5b11866.

[165]. Naito, M., Ishii, T., Matsumoto, A., Miyata, K., Miyahara, Y., & Kataoka, K. (2012). A phenylboronate-functionalized polyion complex micelle for ATP-triggered release of siRNA. Angewandte Chemie, 43(124), 10909-10913. https://doi.org/10.1002/ange.201203360.

[166]. Yin, D., Li, X., Ma, Y., & Liu, Z. (2017). Targeted cancer imaging and photothermal therapy via monosaccharide-imprinted gold nanorods. Chemical Communications, 53(50), 6716-6719. https://doi.org/10.1039/C7CC02247F.

[167]. Liu, M., Zhang, J., Li, X., Cai, C., Cao, X., Shi, X., & Guo, R. (2019). A polydopamine-coated LAPONITE®-stabilized iron oxide nanoplatform for targeted multimodal imaging-guided photothermal cancer therapy. Journal of Materials Chemistry B, 7(24), 3856-3864. https://doi.org/10.1039/C9TB00398C.

[168]. Lei, L., Xu, Z., Hu, X., Lai, Y., Xu, J., Hou, B., ... & Zhang, W. (2019). Bioinspired multivalent peptide nanotubes for sialic acid targeting and imaging-guided treatment of metastatic melanoma. Small, 15(22), 1900157. https://doi.org/10.1002/smll.201900157.

[169]. Wang, X., Yang, C. X., Chen, J. T., & Yan, X. P. (2014). A dual-targeting upconversion nanoplatform for two-color fluorescence imaging-guided photodynamic therapy. Analytical Chemistry, 86(7), 3263-3267. https://doi.org/10.1021/ac500060c.

[170]. Atlamazoglou, V., Yova, D. M., Kavantzas, N., & Loukas, S. (1999). Fluorescence diagnosis of colon cancer using two novel Rhodamine B derivatives. In I. J. Bigio, H. Schneckenburger, J. Slavik, K. Svanberg, & P. M. Viallet (Eds.), Optical biopsies and microscopic techniques III (pp. 2-10). SPIE. https://doi.org/10.1117/12.336828.

[171]. Peng, N., Xu, R., Si, M., Victorious, A., Ha, E., Chang, C. Y., & Xu, X. D. (2017). Fluorescent probe with aggregation-induced emission characteristics for targeted labelling and imaging of cancer cells. RSC Advances, 7(19), 11282-11285. https://doi.org/10.1039/C6RA25674K.

[172]. Cheng, L., Zhang, X., Zhang, Z., Chen, H., Zhang, S., & Kong, J. (2013). Multifunctional phenylboronic acid-tagged fluorescent silica nanoparticles via thiol-ene click reaction for imaging sialic acid expressed on living cells. Talanta, 115, 823-829. https://doi.org/10.1016/j.talanta.2013.06.060.

[173]. Qian, R., Ding, L., Yan, L., & Ju, H. (2015). Fluorescence imaging for in situ detection of cell surface sialic acid by competitive binding of 3-(dansylamino) phenylboronic acid. Analytica Chimica Acta, 894, 85-90. https://doi.org/10.1016/j.aca.2015.08.054.

[174]. Weng, Q., Wang, X., Wang, X., Bando, Y., & Golberg, D. (2016). Functionalized hexagonal boron nitride nanomaterials: emerging properties and applications. Chemical Society Reviews, 45(14), 3989-4012. https://doi.org/10.1039/C5CS00869G.

[175]. Ciofani, M. E., Şen, Ö., & Çulha, M. (2020). Hexagonal boron nitride nanoparticles for prostate cancer treatment. ACS Applied Nano Materials, 3(3), 2364-2372. https://doi.org/10.1021/acsanm.9b02486.

[176]. Emanet, M., Şen, Ö., & Çulha, M. (2017). Evaluation of boron nitride nanotubes and hexagonal boron nitrides as nanocarriers for cancer drugs. Nanomedicine, 12(7), 797-810. https://doi.org/10.2217/nnm-2016-0322.

[177]. Jedrzejczak-Silicka, M., Trukawka, M., Dudziak, M., Piotrowska, K., & Mijowska, E. (2018). Hexagonal boron nitride functionalized with Au nanoparticles-properties and potential biological applications. Nanomaterials, 8(8), 605. https://doi.org/10.3390/nano8080605.

[178]. Li, X., Wang, X., Zhang, J., Hanagata, N., Wang, X., Weng, Q., ... & Golberg, D. (2017). Hollow boron nitride nanospheres as boron reservoir for prostate cancer treatment. Nature Communications, 8(1), 1-12. https://doi.org/10.1038/ncomms13936.

[179]. Feng, S., Zhang, H., Zhi, C., Gao, X. D., & Nakanishi, H. (2018). pH-responsive charge-reversal polymer-functionalized boron nitride nanospheres for intracellular doxorubicin delivery. International Journal of Nanomedicine, 13, 641. https://doi.org/10.2147/IJN.S153476.

[180]. Zhitnyak, I. Y., Bychkov, I. N., Sukhorukova, I. V., Kovalskii, A. M., Firestein, K. L., Golberg, D., ... & Shtansky, D. V. (2017). Effect of BN nanoparticles loaded with doxorubicin on tumor cells with multiple drug resistance. ACS Applied Materials & Interfaces, 9(38), 32498-32508. https://doi.org/10.1021/acsami.7b08713.

[181]. Sukhorukova, I. V., Zhitnyak, I. Y., Kovalskii, A. M., Matveev, A. T., Lebedev, O. I., Li, X., ... & Shtansky, D. V. (2015). Boron nitride nanoparticles with a petal-like surface as anti-cancer drug-delivery systems. ACS Applied Materials & Interfaces, 7(31), 17217-17225. https://doi.org/10.1021/acsami.5b04101.

[182]. Feng, S., Zhang, H., Xu, S., Zhi, C., Nakanishi, H., & Gao, X. D. (2019). Folate-conjugated, mesoporous silica functionalized boron nitride nanospheres for targeted delivery of doxorubicin. Materials Science and Engineering: C, 96, 552-560. https://doi.org/10.1016/j.msec.2018.11.063.

[183]. Dhanavel, S., Sivaranjani, T., Sivakumar, K., Palani, P., Gupta, V. K., Narayanan, V., & Stephen, A. (2021). Cross-linked chitosan/hydroxylated boron nitride nanocomposites for co-delivery of curcumin and 5-fluorouracil towards human colon cancer cells. Journal of the Iranian Chemical Society, 18(2), 317-329. https://doi.org/10.1007/s13738-020-02031-9.

[184]. Lee, M. H., Sharma, A., Chang, M. J., Lee, J., Son, S., Sessler, J. L., ... & Kim, J. S. (2018). Fluorogenic reaction-based prodrug conjugates as targeted cancer theranostics. Chemical Society Reviews, 47(1), 28-52. https://doi.org/10.1039/C7CS00557A.

[185]. Tao, W., & Farokhzad, O. C. (2022). Theranostic nanomedicine in the NIR-II window: Classification, fabrication, and biomedical applications. Chemical Reviews, 122(6), 5405-5407. https://doi.org/10.1021/acs.chemrev.2c00089.

[186].Ji, X., Ge, L., Liu, C., Tang, Z., Xiao, Y., Chen, W., ... & Tao, W. (2021). Capturing functional two-dimensional nanosheets from sandwich-structure vermiculite for cancer theranostics. Nature Communications, 12(1), 1124. https://doi.org/10.1038/s41467-021-21436-5.

[187].Ouyang, J., Xie, A., Zhou, J., Liu, R., Wang, L., Liu, H., ... & Tao, W. (2022). Minimally invasive nanomedicine: nanotechnology in photo-/ultrasound-/radiation-/ magnetism-mediated therapy and imaging. Chemical Society Reviews, 51(12), 4996-5041. https://doi.org/10.1039/D1CS01148K.

[188].Treibs, A., Kreuzer, F. H., & Häberle, N. (1970). Tripyrryl-trismethane (Hexahydro-cyclononatripyrrole). European Journal of Organic Chemistry, 733(1), 37-43. https://doi.org/10.1002/jlac.19707330105.

[189].Sola-Llano, R., & Bañuelos, J. (2018). Introductory Chapter: BODIPY Dye, an All-in-One Molecular Scaffold for (Bio) Photonics. In J. Bañuelos-Prieto, & R. Sola Llano (Eds.), BODIPY dyes-a privilege molecular scaffold with tunable properties. IntechOpen. https://doi.org/10.5772/intechopen.82682.

[190].Mao, Z., Kim, J. H., Lee, J., Xiong, H., Zhang, F., & Kim, J. S. (2023). Engineering of BODIPY-based theranostics for cancer therapy. Coordination Chemistry Reviews, 476, 214908. https://doi.org/10.1016/j.ccr.2022.214908.

[191].Qi, S., Kwon, N., Yim, Y., Nguyen, V. N., & Yoon, J. (2020). Fine-tuning the electronic structure of heavy-atom-free BODIPY photosensitizers for fluorescence imaging and mitochondria-targeted photodynamic therapy. Chemical Science, 11(25), 6479-6484. https://doi.org/10.1039/D0SC01171A.

[192].Turksoy, A., Yildiz, D., & Akkaya, E. U. (2019). Photosensitization and controlled photosensitization with BODIPY dyes. Coordination Chemistry Reviews, 379, 47-64. https://doi.org/10.1016/j.ccr.2017.09.029.

[193].Nguyen, V. N., Ha, J., Koh, C. W., Ryu, B., Kim, G., Park, J. H., ... & Yoon, J. (2021). Access to the triplet excited states of heavy-atom-free boron-dipyrromethene photosensitizers via radical pair intersystem crossing for image-guided tumor-targeted photodynamic therapy. Chemistry of Materials, 33(19), 7889-7896. https://doi.org/10.1021/acs.chemmater.1c02776.

[194].Banuelos, J. (2016). BODIPY dye, the most versatile fluorophore ever?. The Chemical Record, 16(1), 335-348. https://doi.org/10.1002/tcr.201500238.

[195].Shi, Z., Han, X., Hu, W., Bai, H., Peng, B., Ji, L., ... & Huang, W. (2020). Bioapplications of small molecule Aza-BODIPY: from rational structural design to in vivo investigations. Chemical Society Reviews, 49(21), 7533-7567. https://doi.org/10.1039/D0CS00234H.

[196].Xu, C., Ye, R., Shen, H., Lam, J. W., Zhao, Z., & Zhong Tang, B. (2022). Molecular motion and nonradiative decay: Towards efficient photothermal and photoacoustic systems. Angewandte Chemie, 134(30), e202204604. https://doi.org/10.1002/ange.202204604.

[197].Feng, G., Zhang, G. Q., & Ding, D. (2020). Design of superior phototheranostic agents guided by Jablonski diagrams. Chemical Society Reviews, 49(22), 8179-8234. https://doi.org/10.1039/D0CS00671H.

YAZAR KILAVUZU

GENEL BİLGİLER

• Makale başvurusu için Makale Metni Dosyası, Telif Hakkı Devir Dosyası ve Benzerlik Oran Dosyası olmak üzere üç ayrı formun doldurulması ve sisteme yüklenmesi gerekmektedir.
• Başvurularda iletişimde bulunulacak yazar ve diğer yazarların iletişim bilgileri bulunmalıdır.
• Makale metni içerisindeki makale kontrol listesi ve kapak sayfası eksiksiz olarak doldurulmalıdır.
• Makale metni dosyası içerisinde bulunan makale kontrol listesi ve kapak sayfası eksiksiz doldurulmalıdır.
• Derleme makalelerde başka yayınlara ait şekil ve tablolar kullanılacaksa, kaynak gösterilecek makalenin yayıncısından izin alınmalıdır. Yayıncıdan izin alındığı ve şekillerin uyarlanıp uyarlanmadığı veya doğrudan kullanılıp kullanılmadığı bilgisi şekil başlığında belirtilmelidir. İlgili izin yazısının journalofboron@tenmak.gov.tr adresine gönderilmesi gerekmektedir.
• Her makale, konusu ile ilgili en az iki hakeme gönderilerek şekil, içerik, özgün değer, uluslararası literatüre katkısı bakımından incelettirilir. Hakem görüşlerinde belirtilen eksikler tamamlandıktan sonra, son baskı formatına getirilir ve yazarlardan makalenin son halinin onayı alınır. Dergide basıldığı haliyle makale içinde bulunabilecek hataların sorumluluğu yazarlara aittir.

MAKALE METNİ DOSYASI

• Makale metninin yazımında yazım kurallarına uyulması gerekmektedir.
• Makale metninde kapsayıcı ve bilimsel bir dil kullanılmalıdır.
• Makale metni referanslar dahil araştırma makaleleri için 14.000 kelimeyi tarama makaleleri için ise 22.000 kelimeyi geçmemelidir.
• Makalenin metni, Times New Roman 12 punto ile Makale Metni Dosyası'nın sayfa düzeni değiştirilmeden yazılmalıdır.
• Makale metninin Microsoft Office Word 2010 ve üzeri bir kelime işlemci ile hazırlanması ve yazım hatalarının kontrol edilmesi ve düzeltilmesi gerekmektedir.
• Eğer makale Türkçe ise, Türkçe başlıklarla bire bir uyumlu olacak şekilde oluşturulmuş İngilizce başlıklar parantez içerisinde yazılmalıdır.
• Makale içerisinde kullanılan kısaltma ve sembollerin anlamları ilk kullanıldıklarında açıklanmalıdır.
• Makale metni içerisindeki alt başlıklar numaralandırılmalıdır. Numaralandırma işlemleri ana bölümler için 1.'den başlamalı ve tüm ana başlıklar (Özet, Teşekkür ve Kaynaklar ve Ekler bölümleri hariç) için devam etmelidir. İkincil başlıklar ana bölüm numaralandırmasına uygun olarak 1.1., 1.2., 1.3., ... şeklinde devam etmelidir. Üçüncü başlıklar ikinci başlıklara uygun olarak 1.1.1., 1.1.2., 1.1.3., ... şeklinde devam etmelidir.

TELİF HAKKI DEVİR DOSYASI

• İmzalı Telif Hakkı Devir Dosyası taranarak sisteme yüklenmelidir.
• İmzalı Telif Hakkı Devir Dosyası'nı göndermeyen yazarların başvuruları değerlendirmeye alınmaz.

BENZERLİK ORAN DOSYASI

• Makalenin referanslar bölümü hariç metni "iThenticate" veya "Turnitin" programları ile taranmalıdır.
• Benzerlik oranı raporunun PDF formatında sisteme yüklenmelidir.
• Benzerlik oranı %15'in üzerinde olmamalıdır.

GİZLİLİK POLİTİKASI

Journal of Boron gizliliğe saygı duymaktadır. Kişisel bilgiler, sadece derginin belirtilen amaçları doğrultusunda kullanılacak ve üçüncü kişilerle paylaşılmayacaktır.

YAZIM KURALLARI

MAKALE BAŞLIĞI
• Makale başlığı standart kısaltmalarla birlikte en çok 15 kelimeden oluşmalıdır.
• Eğer makale Türkçe ise, İngilizce başlıkla bire bir uyumlu olacak şekilde Türkçe makale başlığı da oluşturulmalıdır.

ÖZET
• Özet, 250 kelimeyi geçmemelidir.
• Standart olmayan kısaltmalar ilk kullanıldığında tam açıklamalarından sonra parantez içerisinde yazılmalıdır.
• Eğer makale Türkçe ise, İngilizce özetle bire bir uyumlu olacak şekilde Türkçe özet de oluşturulmalıdır.

ANAHTAR KELİMELER
• En fazla 5 anahtar kelime, alfabetik sıraya göre yazılmalıdır.
• Kısaltmalar anahtar kelime olarak kullanılmamalıdır.
• Eğer makale Türkçe ise, İngilizce anahtar kelimelerle bire bir uyumlu olacak şekilde Türkçe anahtar kelimelere de oluşturulmalıdır.

GİRİŞ
• İlgili literatürün özeti, çalışmanın amacı ve özgün değeri ve kurulmuş olan hipotezi içermelidir.
• Kaynaklar, toplu olarak ve aralıklı verilmemeli (örnek [1-5] veya [1, 2, 3, 5, 8]), her kaynağın çalışmaya katkısı irdelenmeli ve metin içerisinde belirtilmelidir.

MALZEMELER VE YÖNTEMLER
• Yürütülmüş olan çalışma deneysel bir çalışma ise deney prosedürü/metodu anlaşılır bir şekilde açıklanmalıdır.
• Teorik bir çalışma yürütülmüşse teorik metodu detaylı bir şekilde verilmelidir.
• Yapılan çalışmada kullanılan metot daha önce yayınlanmış bir metot ise diğer çalışmaya atıf yapılarak bu çalışmanın diğer çalışmadan farklı belirtilmelidir.

SONUÇLAR VE TARTIŞMA
• Elde edilen sonuçlar açık ve öz bir şekilde verilmelidir.
• Elde edilen tüm sonuçlar atıf yapılarak literatür ile karşılaştırılmalıdır.
• Tablolar numaralandırılmalıdır ve düzenlenebilir formatta olmalıdır. Eğer makale Türkçe ise, tablo üst yazılarının bire bir İngilizce çevirileri parantez içerisinde verilmelidir.
• Makale içerisindeki şekiller numaralandırılmalıdır ve en az 300 dpi çözünürlükte olmalıdır. Şekillerin üzerindeki yazılar okunabilir büyüklükte ve yazı tipinde olmalıdır. Kabul edilen şekil formatları TIFF, JPG ve JPEG'dir. Eğer makale Türkçe ise, şekil alt yazılarının bire bir İngilizce çevirileri parantez içerisinde verilmelidir.

SONUÇLAR
• Çalışmadan elde edilen ana sonuçlar ve çıkarımlar kısa ve öz bir şekilde verilmelidir.
• Çalışmaya ait gelecek perspektifleri bu bölümde verilir.

TEŞEKKÜRLER
• Çalışmanın gerçekleşmesi için sağlanan maddi kaynaklar ve kullanılan altyapı bu bölümde belirtilir.
Yazar Katkıları
• Her yazarın katkıları belirtilmelidir.
• Katkı rolleri şu şekildedir: kavramsallaştırma, veri analizi, veri iyileştirme, finansman sağlama, metodoloji, proje yönetimi, kaynak sağlama, yazılım analizi, denetim, doğrulama, görselleştirme, orijinal taslak yazma, inceleme yazma ve düzenleme.

KAYNAKLAR
• Basılmış kaynakların DOI ve ISBN numarası belirtilmelidir.
• İnternet sitesi adresleri (URL) kaynak olarak verilmemelidir. Ancak metin içerisinde istatistiksel bir verinin geçtiği yerde veriden sonra belirtilebilir.
• Kaynaklar listesi metin içerisinden kullanılma sırasına uygun olarak numaralandırılmalıdır.
• Kaynaklar, "APA Publication Manual, Seventh Edition" kurallarına uygun olarak hazırlanmalıdır.
• Kaynaklar İngilizce olarak hazırlanmalıdır. Türkçe kaynakların İngilizce karşılıkları köşeli parantez içerisinde belirtilmelidir.
• APA formatı ve örneklere aşağıdaki bağlantıdan ulaşılabilir.
https://apastyle.apa.org/style-grammar-guidelines/references/examples

EKLER
• Makaledeki ekler EK A (Appendix A), EK B (Appendix B) ve EK C (Appendix C) vb. olarak adlandırılmalıdır.
• Ekler içerisindeki denklemler A1, A2, A3 vb. olarak adlandırılmalıdır, tablo ve şekiller Tablo A1, Tablo A2, Şekil A1, Şekil A2 vb. olarak adlandırılmalıdır.

AUTHOR'S GUIDE

GENERAL INFORMATION

• For article application, 3 individual files which are Manuscript File, Copyright Transfer File and Similarity Ratio File, must be filled in and uploaded to the system.
• Applications should include the contact information of the author and other authors to be contacted.
• The article checklist and cover page in the Manuscript File should be filled in completely.
• Each article is sent to at least two referees related to its subject and examined in terms of format, content, novelty, contribution to literature.
• If figures and tables from other publications are to be used in review articles, permission must be obtained from the publisher of the article to be cited. The information that permission has been granted from the publisher and whether the figures have been adapted or used directly should be mentioned in the figure caption. The relevant permission letter should be sent to journalofboron@tenmak.gov.tr.
• After the deficiencies stated in the referee's comments are completed, it is brought to the final print format and the approval of the final version of the article is obtained from the authors. The responsibility of errors that may be found in the article as it is published in the journal belongs to the authors.

MANUSCRIPT

• Writing rules must be followed, during writing of the manuscript.
• Inclusive and scientific language must be used in the manuscript.
• Manuscript should not exceed 14,000 words for research articles and 22,000 words for review articles, including references.
• The manuscript should be written in Times New Roman 12 points without changing the page layout of the Manuscript File.
• The manuscript should be prepared with a word processor of Microsoft Office Word 2010 and above, and spelling errors should be checked and corrected.
• Abbreviations and symbols used in the manuscript must be explained when used fort he first time.
• Subheadings in the article should be numbered. Numbering should start at 1 for the main section and continue for all main headings (except the Summary, Acknowledgments and References and Appendices sections). Secondary titles continue as 1.1., 1.2., 1.3., ... in accordance with the main chapter numbering. The third headings continue as 1.1.1., 1.1.2., 1.1.3., ... in accordance with the second headings.

COPYRIGHT TRANSFER FILE

• Signed Copyright Transfer File should be scanned and uploaded to the system.
• Applications of the authors who do not send the signed Copyright Transfer File will not be evaluated.

SIMILARITY RATIO FILE

• The manuscript should be scanned with "iThenticate" or "Turnitin" programs, except for the references section.
• The similarity ratio report should be uploaded to the system in PDF format.
• The similarity ratio should not exceed 15%.

PRIVACY POLICY

Journal of Boron respects privacy. Any personal information will only be used in line with the stated purposes of the journal and will not be shared with third parties.

WRITING RULES

TITLE
• The title of the manuscript should consist of a maximum of 15 words with standard abbreviations.

ABSTRACT
• The abstract should not exceed 250 words.
• Non-standard abbreviations should be written in parentheses after their full explanation, when they are used for the first time.

KEYWORDS
• A maximum of 5 keywords should be written in alphabetical order.
• Abbreviations should not be used as keywords.

INTRODUCTION
• The summary of the relevant literature, aim and novelty of the study, and the established hypothesis should be included.
• References should not be given in bulk and in intervals (example [1-5] or [1, 2, 3, 5, 8]), the contribution of each source to the study should be examined and stated in the text.

MATERIALS AND METHODS
• If the study carried out is an experimental study, the test procedure/method should be clearly explained.
• If a theoretical study has been carried out, the theoretical method should be given in detail.
• If the method used in the study is a previously published method, the other study should be mentioned by citing.

RESULTS AND DISCUSSION
• Obtained results should be given in a clear and concise manner.
• All of the results should be compared with the literature by citing.
• Tables should be numbered and in editable format.
• Figures in the manuscript should be numbered and have at least 300 dpi resolution. The texts on the figures should be in legible size and font. Accepted figure formats are TIFF, JPG, and JPEG.

CONCLUSIONS
• Main conclusions and inferences obtained from the study should be given concisely.
• Future perspectives of the study are given in this section.

ACKNOWLEDGEMENTS
• The financial resources provided and the infrastructure used during the study are specified in this section.

AUTHOR CONTRIBUTIONS
• Contributions of each author must be stated.
• Contribution roles are as follows: conceptualization, data analysis, data curation, funding acquisition, methodology, project administration, sourcing, software analysis, supervision, validation, visualization, writing original draft, writing review and editing.

REFERENCES
• DOI and ISBN numbers of printed sources should be specified.
• Website addresses (URLs) should not be given as a source. However, it can be specified after the data where a statistical data is mentioned in the text.
• The list of references should be numbered according to the order in which they are used in the text.
• References should be prepared in accordance with the rules of “APA Publication Manual, Seventh Edition”.
• References should be prepared in English. English equivalents of sources should be indicated in square brackets.
• APA format and examples can be found at the link below.
https://apastyle.apa.org/style-grammar-guidelines/references/examples

APPENDICES
• Appendices in the manuscript must be named as Appendix A (Appendix A), Appendix B (Appendix B) and Appendix C (Appendix C) etc.
• Equations in the appendices must be named as A1, A2, A3, etc., and table and figures numberings must be named as Table A1, Table A2, Figure A1, Figure A2 etc.

TENMAK BOREN
BOR ARAŞTIRMA ENSTİTÜSÜ

BOR DERGİSİ
JOURNAL OF BORON
https://dergipark.org.tr/boron

İÇİNDEKİLER/CONTENTS

TENMAK Bor Araştırma Enstitüsü

Dumlupınar Bulvarı (Eskişehir Yolu 7. km), No:166, D Blok, 06530, Ankara
Tel: (0312) 201 36 00
Faks: (0312) 219 80 55
e-mail: boren.journal@tenmak.gov.tr
web:https://dergipark.org.tr/boron